FINAL TECHNICAL REPORT

AECOM Imagine it. Delivered.

ESTIMATING SHALLOW SHEAR-WAVE VELOCITY PROFILES IN ALASKA USING THE INITIAL PORTION OF P-WAVES FROM LOCAL EARTHQUAKES

U.S. Geological Survey
Award Number G18AP00091
09/01/2018 – 04/30/2020

April 30, 2020

ESTIMATING SHALLOW SHEAR-WAVE VELOCITY PROFILES IN ALASKA USING THE INITIAL PORTION OF P-WAVES FROM LOCAL EARTHQUAKES

FINAL TECHNICAL REPORT

“This material is based upon work supported by the U.S. Geological Survey under Grant No.G18AP00091. The views and conclusions contained in this document are those of the authors and should not be interpreted as representing the opinions or policies of the U.S. Geological Survey. Mention of trade names or commercial products does not constitute their endorsement by the U.S. Geological Survey.

FINAL TECHNICAL REPORT

Prepared for:

US. Geological Survey
905 National Center, 12201 Sunrise Valley Drive,
Reston, VA 20192

Prepared by:

Andreas Skarlatoudis
Principal Seismologist
T: 213.996.2313
E: andreas.skarlatoudis@aecom.com

Paul Somerville
Principal Seismologist
T: 213.996.2200
E: paul.somerville@aecom.com

Hong Kie Thio
Principal Seismologist
T: 213.996.2250
E: hong.kie.thio@aecom.com

AECOM
One California Plaza
300 South Grand Avenue
Los Angeles, CA 90071

T: +1 (213) 593 8100
F: +1 (213) 593 8178
www.aecom.com

Table of Contents

Figures

Tables

Executive Summary

The Alaska Regional Network and Transportable Array provide an invaluable waveform dataset for studying ground motions in Alaska. However, the dataset is useful only after the site effects at each station are well understood. Considering the large number of stations associated with these networks, it would be costly to measure the sub-surface velocity structure beneath every station using geophysical exploration techniques involving arrays, such as ReMi and SASW. Instead, it is more economical to estimate the site conditions using waveforms recorded at the seismic stations.

Most of the methods for estimating site response from recorded earthquake waveforms use the frequency dependent ratio between the horizontal and vertical component of either ambient noise or S waves from earthquakes. We instead use the horizontal and vertical component of P waves to infer the sub-surface velocity structure. It has been demonstrated that the ratio of radial to vertical P waves is mostly sensitive to sub-surface shear velocity, so the radial/vertical ratio of the P wave is a good indicator of subsurface shear velocity. Therefore, the subsurface velocity structure can be estimated using an approach similar to teleseismic P receiver functions, but at much smaller scale and higher frequency, whose results are in good agreement with results from ReMi and Refraction/Reflection techniques (Ni et al., 2013; Kim et al., 2016). This method has been widely used in the Central Eastern United States by Ni and Somerville (2013) and Hosseini et al. (2016) where a rich database of local earthquakes from 2009 to 2013 recorded at ~560 seismic stations was analyzed and associated receiver functions were inverted.

The Alaska Regional Network and Transportable Array have recorded numerous earthquakes in the magnitude range of interest (**M**2.5-4.5) and at shallow depth, which provides an ideal opportunity for this study. V_{S30} is used to represent the site amplification of ground motions in all ground motion models that are used by the USGS in generating the National Seismic Hazard Maps, as well as in the professional practice of seismic hazard analysis in the United States.

This method was successfully used in our previous USGS project (Hosseini et al., 2016). USGS colleagues including Alan Yong from the USGS Pasadena office are interested to use the results of such studies to diversify the USGS database of shear-wave velocities across the United States (Herrick, Hosseini and Yong 2017). The results of this work will provide a basis for improved site-specific hazard estimates in Alaska.

1. Introduction

The value of adopting (making permanent) selected Earthscope TA stations for improving our understanding of earthquake hazards in Alaska was documented by the Alaska Earthquake Monitoring Working Group (Crouse et al., 2016), which included two AECOM investigators (Crouse and Somerville). This Working Group emphasized that an improved monitoring network will result in a more confident understanding of the seismic risk to population, infra-structure, and services. Specifically, a better understanding of shear wave structure in the recording seismic stations will help to (1) reduce the epistemic uncertainties in the Alaska Seismic Hazard Maps, (2) improve engineering design using earthquake recordings, and (3) improve earthquake source characterization.

The geology and shear wave velocity at multiple sites in the Anchorage region were studied by Nath et al. (1997), and Dutta et al. (2001). Generalized inversion and H/V spectral ratios were used in the estimation of shear wave velocity at numerous temporary sensors and permanent strong motion stations (Martirosyan et al., 2002 and Dutta et al., 2003). Specifically, weak- and strong- motion recordings were used to estimate the amplification by comparing the response of basin sites in Anchorage to a reference site in the nearby Chugach Mountains, where significant frequency-dependent site amplification was observed (Boore, 2004). The objective of this project is to expand the analysis of shear wave velocity profiles to the vast area outside the Anchorage basin (Figure 1-1), using Earthscope TA, ANSS and Alaska Regional Network stations, making use of the abundant earthquake data (Figure 1-1).

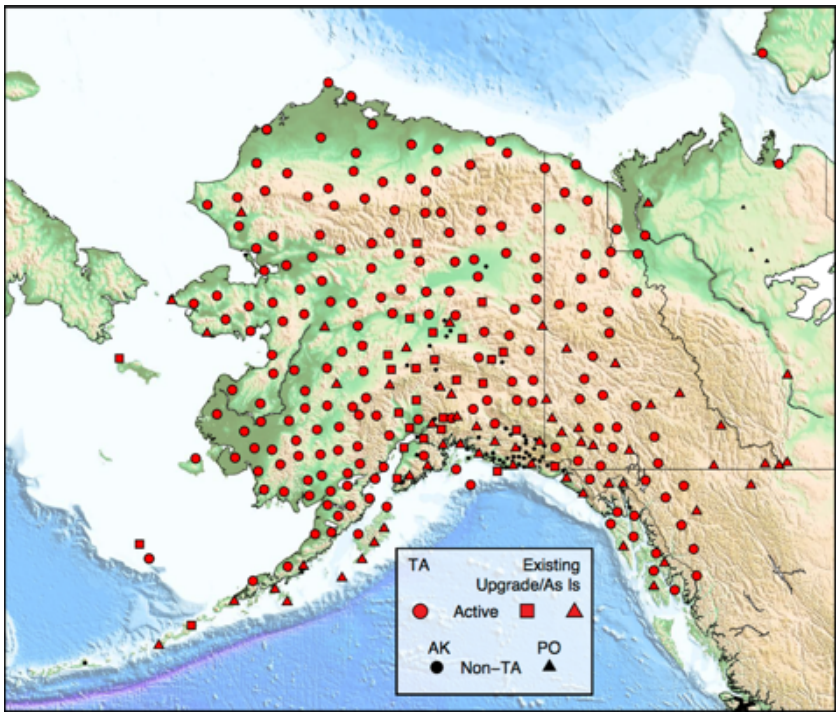

Figure 1-1. Transportable Array (TA) station installation plan and location in Alaska.

Source: USArray website, version 10/25/2018.

The products of this project are:

I. Mean shear-wave velocity over depth of resolution
II. A database of processed ground motions recorded at these stations from 2000 to 2019
III. Estimates of V_{S30} and uncertainty in the shear wave velocity profiles at each station

We expect that these products will be used to improve ground motion estimates in the Alaska portion of the National Seismic Hazard Map, and will provide more reliable estimates of seismic hazards and site response throughout Alaska.

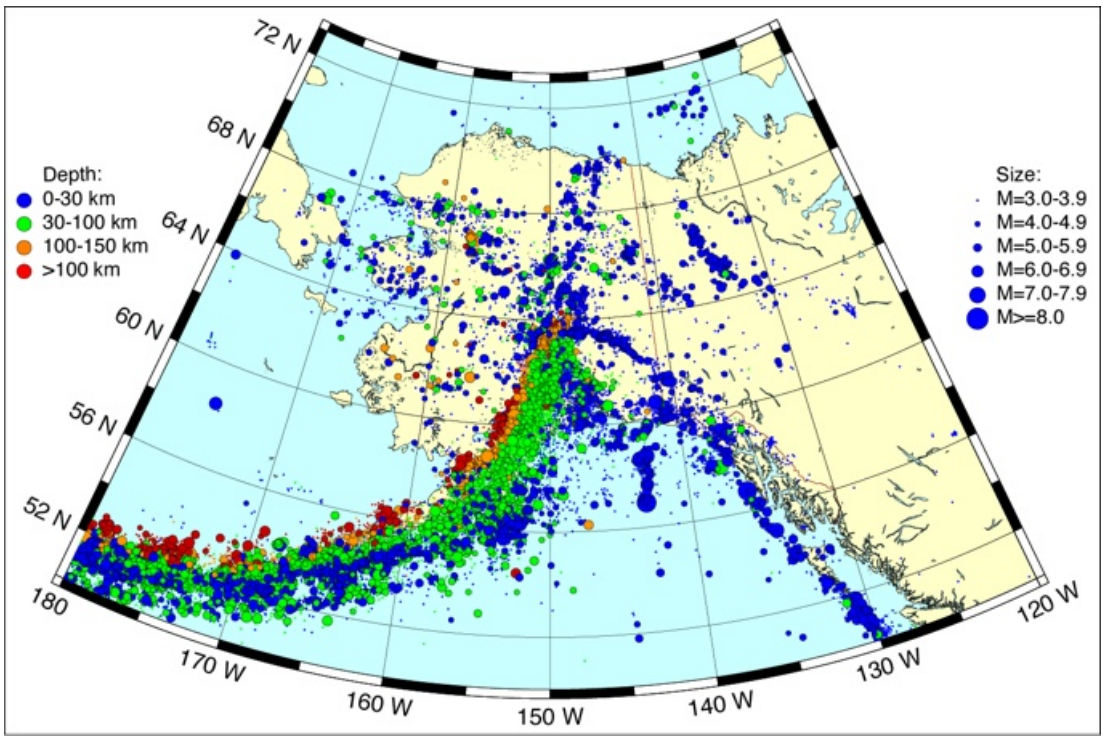

Figure 1-2. Seismicity from 1970-2012 for Alaska and vicinity from the Alaska Earthquake Center (AEC) and USGS PDE catalogs.

Source: Natasha Ruppert (AEC)

1.1 Theory of estimating shallow shear velocity from local P waveforms

Ni et al. (2013) originally developed the method of characterizing site effects by modeling the H/V ratio of the initial portion of local *P* waves. Kim et al. (2016) applied the same principles to estimate the subsurface S wave velocities for seismic stations in CENA. In this method the conversion of the incident *S* wave, at an interface, to *P* waves can be used to model near-surface structure (tens to hundreds of meters), when the first tenths of a second of the *P* waveforms are examined.

As most earthquakes occur in crystalline basement where seismic velocities are high, and most seismic stations are located on lower velocity material, the incidence angles of *P* and *PS* near the seismic station are typically much smaller than the takeoff angle at the earthquake. Therefore, the *P* wave is weaker on the radial component than on the vertical component

because of the steeper ray path of the *P* wave, and *PS* is stronger on the radial component because its polarization is perpendicular to the ray path and almost horizontal.

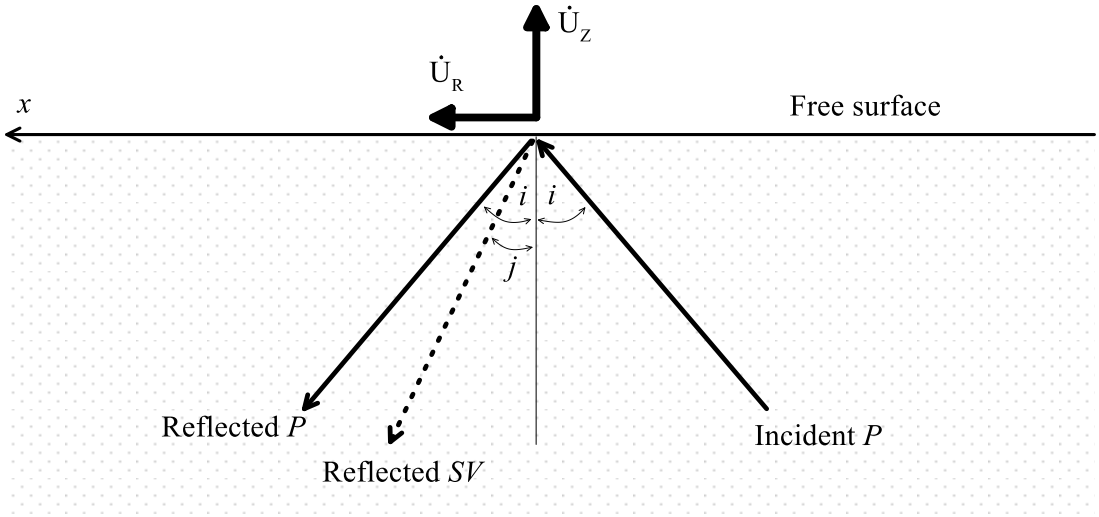

Figure 1-3. Schematic representation of incident *P* wave and reflected *P* and S_V waves. U_R and *Uz* are the radial and vertical components of particle velocity.

Source: Kim et al. (2016)

From Aki and Richards (2002), the particle motions of incoming *P* and *S* waves are described by equations (1) in which U_R, U_T, U_Z are radial, tangential, and vertical components of the particle velocity at the free surface; V_P is the subsurface P velocity; V_S is the subsurface shear velocity; *p* is the ray parameter (horizontal slowness); *i* is the angle between the *P* rays and the vertical axis; and *j* is the angle between the *S* ray and the vertical axis (Figure 1-3).

$$[U_R, U_T, U_z] = \frac{\bar{P} \cdot [R, T, Z] exp\,[(i\omega(px - t)]}{\left(\frac{1}{V_S^2} - 2p^2\right)^2 + 4p^2 \frac{cos\, i}{V_P} \frac{cos\, j}{V_S}} \quad (1a)$$

$$R = \frac{4V_P p}{V_S^2} \frac{cos\, i}{V_P} \frac{cos\, j}{V_S} \quad (1b)$$

$$T = 0 \quad (1c)$$

$$Z = \frac{-2V_P}{V_S^2} \frac{cos\, i}{V_P} \left(\frac{1}{V_S^2} - 2p^2\right) \quad (1d)$$

The ratio of the radial to the vertical component of the initial amplitude of the velocity time series associated with the *P* wave (shown in Figure 1-3) can be estimated from equation (2):

$$\frac{\dot{U}_R}{\dot{U}_Z} = \frac{-2V_S p \cos j}{1 - 2p^2 V_S^2} \quad (2)$$

Solving equation (2) for the shear wave velocity of the subsurface soil (V_S) results in equation (3):

$$V_S = \frac{cos\, j \pm \sqrt{cos^2 j + 2\left(\frac{\dot{U}_R}{\dot{U}_Z}\right)^2}}{2p\left(\frac{\dot{U}_R}{\dot{U}_Z}\right)} \quad (3)$$

For plane waves, the ray parameter *p* is given as (Aki and Richards, 2002):

$$p = \frac{\sin i}{V_P} = \frac{\sin j}{V_S} \quad (4)$$

The angle *j* is related to V_S and the ray parameter, *p*, as shown in Equation (5):

$$j = \sin^{-1}(pV_S) \quad (5)$$

Given that the ray parameter is known, V_S can be derived by iteratively solving equations 3 and 5, until they converge to an acceptable tolerance (Kim et al., 2016). Kim et al. (2016) proposed a way to estimate the ray parameter assuming a simplified, two-layered, subsurface structure and by brute-forcing a solution of Snell's law for the two layers. We follow a different approach

that involves an analytical calculation of the ray parameter along the ray-path between earthquake hypocenter and the recording station, which is described in the next sections.

The resulting V_S from this procedure is considered to be equivalent to the time-averaged shear wave velocity from the surface to a depth z (V_{SZ}), at which we assume that the subsurface structure is resolvable. This depth can be estimated as the product of the pulse duration of the earthquake source time function and the shear wave velocity V_{SZ}, which is equivalent to the minimum wavelength of the *S*-wave. For small events (**M** < 5) a value of 0.1s for the source time function duration is considered typical based on various studies (Kikuchi and Ishida, 1993, Singh et al., 2000, Kanamori and Brodsky, 2004 and Harrington and Brodsky, 2009).

The final product of this analysis is the estimated V_{S30} value for each site. For correlating the V_{SZ} values with the corresponding V_{S30} we use the Boore et al. (2011) results.

2. Data Collection and Processing

2.1 Database description

We collected our dataset from IRIS using the following criteria:

- Events spanning the time period from 2000 to 2019.
- Events within about 200 km epicentral distance, to limit as much as possible the first seismic wave arrival to P_g phases.
- Events with magnitudes less or equal to **M**5, for the following reasons:
    - subsurface velocity structure can be resolved at frequencies as high as 10 Hz (for **M**3 events) or 20 Hz (for **M**2 events) because of their short source duration,
    - 3D crustal heterogeneity is less of a problem because only tens of meters to hundreds of meters in the region near the site are involved.
- Events with hypocentral depth down to 35km, to limit the analysis to crustal events.

These criteria result in 704 events listed in Table A-1 in Appendix A. The recording sites with at least 3 usable recordings from these events are listed in Table B-1 in Appendix B. The map in Figure 2-1 shows the spatial distribution of the event and station databases used in the analysis.

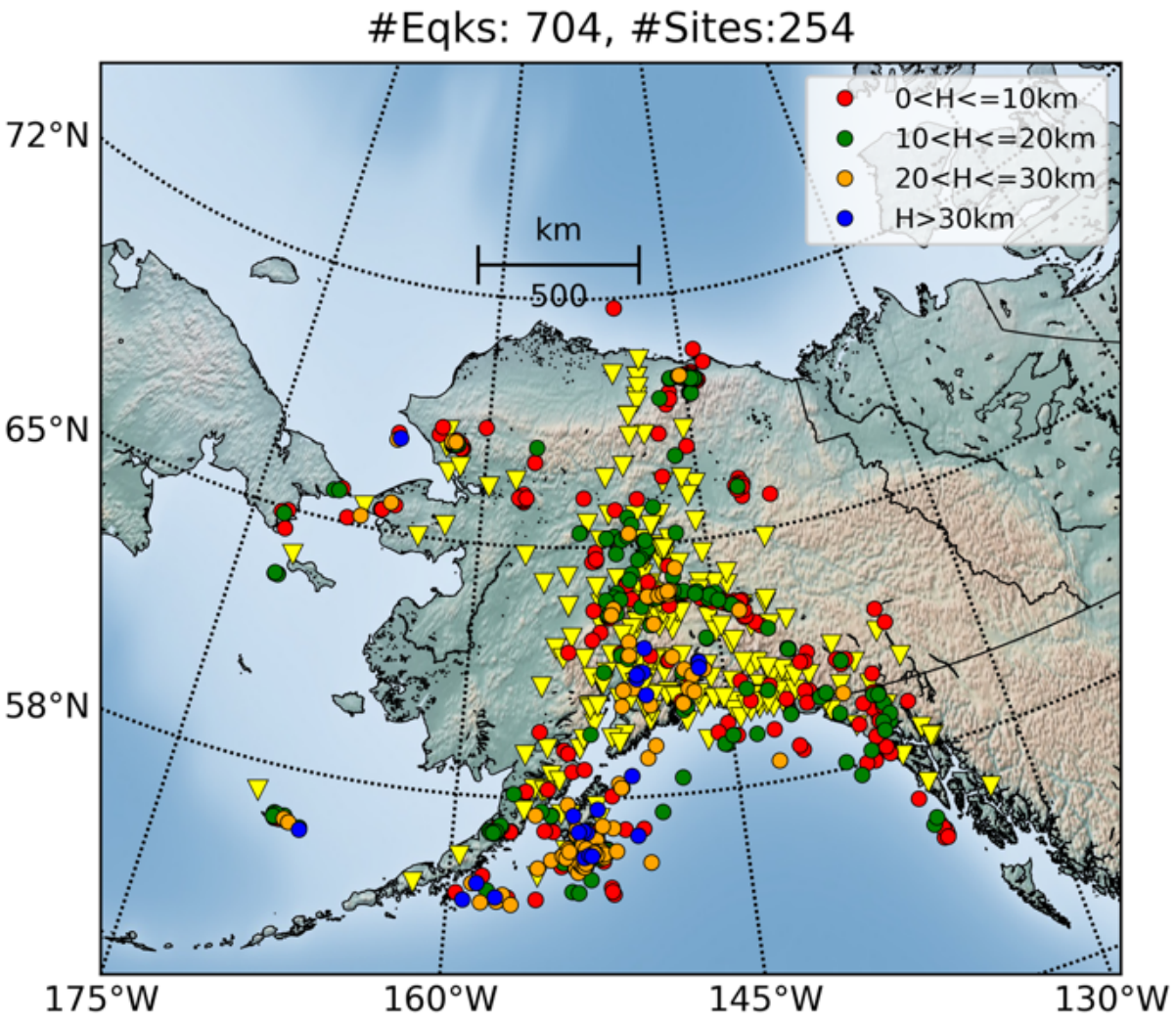

Figure 2-1. Map showing the spatial distribution of epicenters (circles) and recording stations (triangles) following the criteria described in Section 2.1. The total number of events in the database is 704 and the total number of recording sites is 254. The circles are color coded based on the hypocentral depth of the event.

In Figure 2-2 we show for the site with the largest usable number of recordings the spatial distribution of the corresponding events.

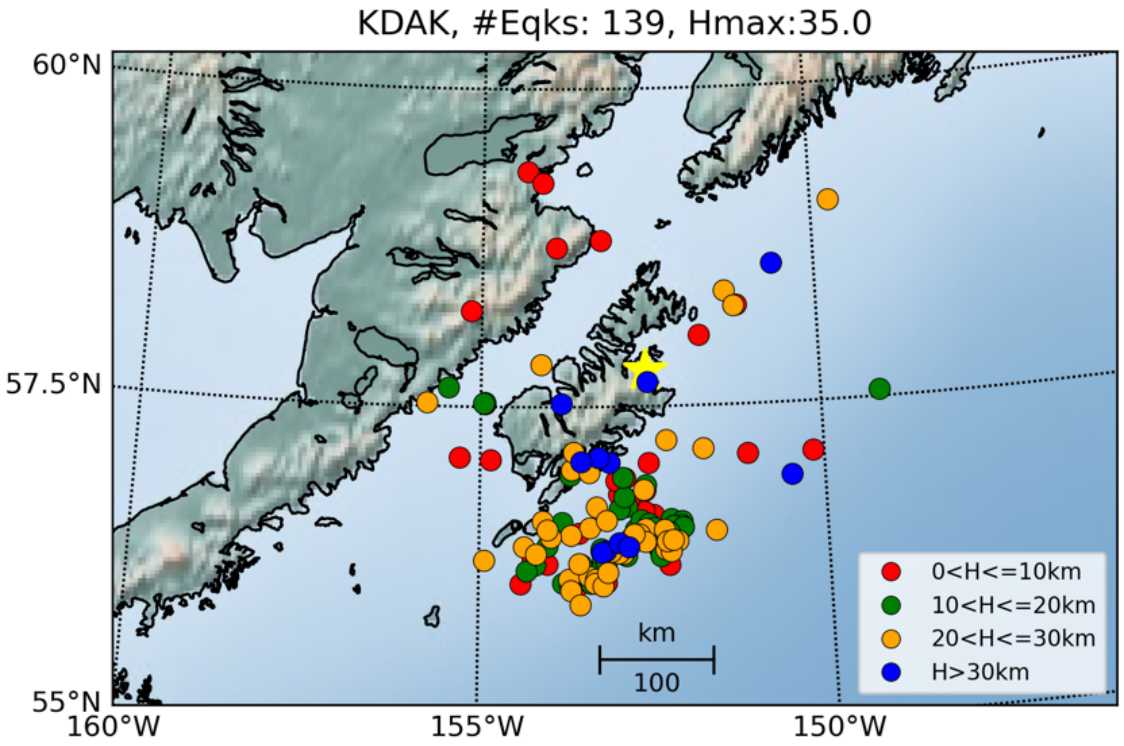

Figure 2-2. Map showing the spatial distribution of epicenters (circles) for site KDAK. The site location is denoted with the yellow star. The number of events that produced the recordings used in the analysis is 139. The circles are color coded based on the hypocentral depth of the event.

2.2 Data Processing

SAC2000 software (Goldstein et al., 2003, Goldstein and Snoke, 2005) and ObsPy (Beyreuther et al., 2010, Megies et al., 2011, Krischer et al., 2015) have been used to perform the following processing steps:

2.2.1 Instrument Correction

We used the instrument response distributed by IRIS together with the available recordings. Recorded ground motions are corrected for the instrument response by performing de-convolution in the frequency domain. The corrected recorded ground motions are converted to velocity.

2.2.2 Automatic Arrival Time Detection

The algorithm that we use picks onset times using an Auto Regression - Akaike Information Criterion (AR-AIC) method. The detection intervals are successively narrowed down with the help of STA/LTA ratios as well as STA-LTA difference calculations. This technique picks the onset times, employing full power of the AR-AIC algorithm and the STA/LTA ratio (Akazawa, 2004).

We manually inspect every recording for correct *P* wave arrival time detection and manually pick the *P* wave arrival time in the case of a picker failure. Figure 2-3 shows examples of identification of *P*-arrival time using the AR-AIC algorithm.

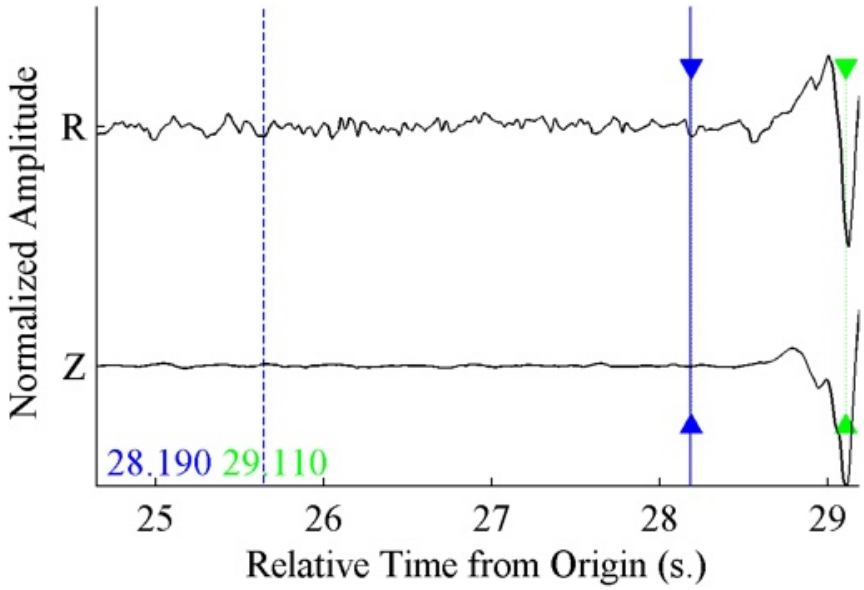

Figure 2-3. Radial and vertical components of ground motion from a recording from our database. The initial arrival time predicted by the non-AR AIC picker is shown with the dashed blue line. Theoretical arrivals of various P phases predicted using Taup toolbox are shown with the green line. The manual pick is shown with the solid blue line.

2.2.3 Visual Inspection

After removing the instrument response, corrected ground motions are rotated to the great circle path to give radial, traverse, and vertical components prior to performing the next step.

Visual inspection is performed to make sure that the automatic *P* wave arrival time is detected correctly. A large number of the recordings needed revisions of their *P* wave arrival times. To make sure that we are picking the correct arrival time, we calculate the theoretical travel time for various phases of compressional waves which helps detect P wave arrivals robustly. Theoretical arrival times are calculated using the Taup toolkit implementation in ObsPy, using the Ak135 earth model (Kennet et al., 1995). An example of this step is shown in Figure 2-3.

Noisy seismograms were filtered (high pass and/or low pass) with an eight-pole, Butterworth, acausal filter to remove noise.

Finally, the initial portions of the radial and vertical components of the corrected velocity time series ($\dot{U}_R$ and $\dot{U}_Z$, respectively) are automatically marked. A visual inspection is then performed to revise the automatic marks when needed.

The resulting number of radial and vertical component ground motions after processing and visual inspection is 3876.

3. Calculation of V_{SZ}

3.1 Regional Velocity model

We employed the 3D shear-wave velocity model of the Alaskan Cordillera developed from the joint inversion of ambient noise tomography and receiver functions as distributed by IRIS (Ward and Lin, 2018). The model incorporates seismic data from an earlier ambient noise tomography study (Ward, 2015) along with Transportable Array data to image the shear wave velocity structure of the Alaskan Cordillera from the joint inversion of surface wave dispersion and receiver functions. The figure shows the shear-wave velocity results for 1, 5, 10 and 25 km depth. The site locations are shown with the white triangles.

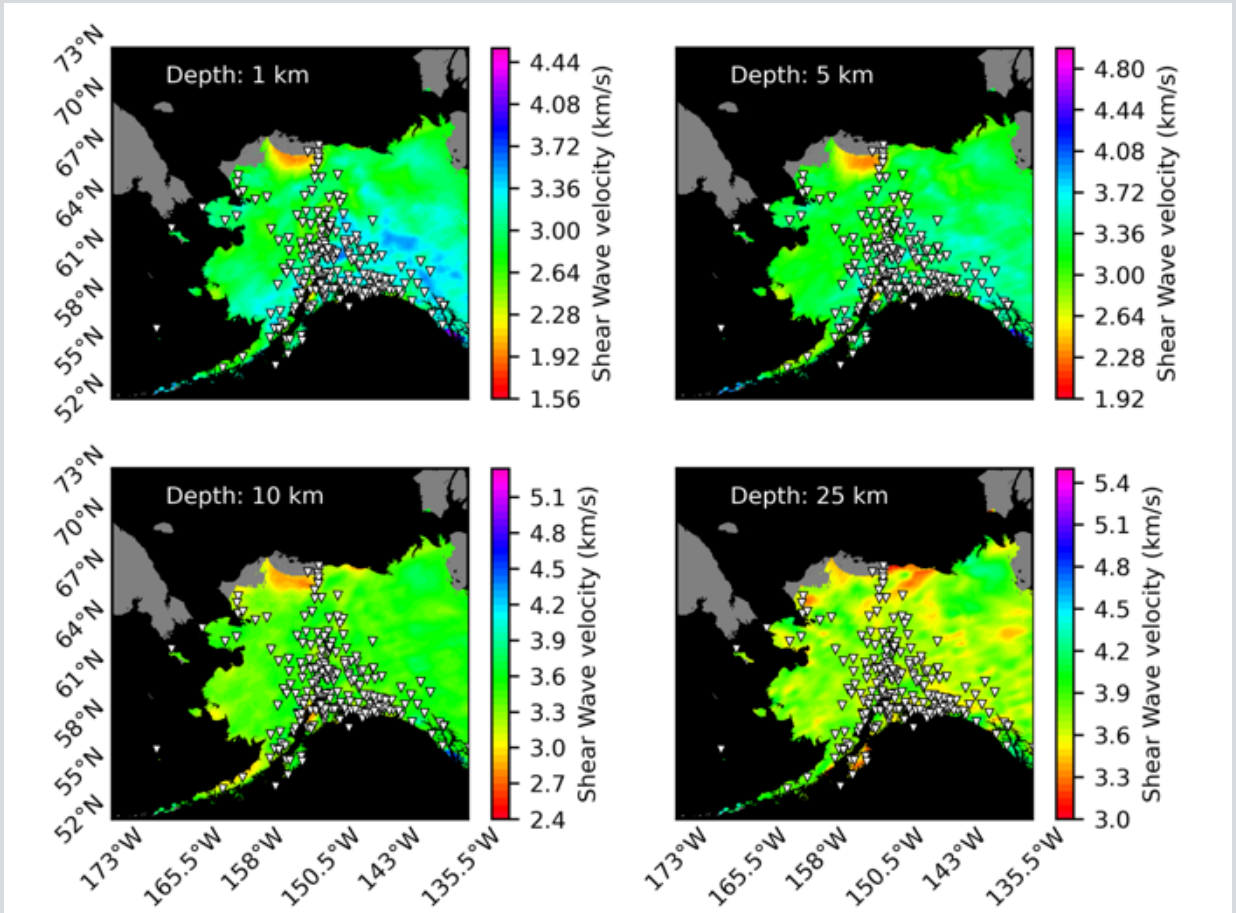

Figure 3-1. Maps showing the Ward and Lin (2018), shear wave velocity model for AK for four depths, 1km, 5km, 10km and 25km. The recording sites used in the analysis are depicted with the white triangles.

For the analysis, the compressional wave velocity V_P is required. We use the Brocher (2005) work to convert V_S to V_P (Equation 6). This relation is applicable for V_S between 0 and 4.5 km/sec.

$$V_P = 0.9409 + 2.0947V_S - 0.8206V_S^2 + 0.2683V_S^3 - 0.0251V_S^4 \quad (6)$$

For each event – recording site pair we sample each layer of the 3D velocity model to the depth of 35km, at several locations along the travel path, to create 1D velocity models. The final 1D model that is used to estimate the ray parameter for the specific path is the average of these local 1D models, supplemented for layers deeper than 35km by the Ak135 reference global velocity model (Kennet et al., 1995).

3.2 Calculation of the ray parameter

The TauP Toolkit is a seismic travel time calculator. In addition to travel times, it can calculate derivative information such as ray paths through the earth, pierce and turning points. It handles many types of velocity models and can calculate times for virtually any seismic phase with a phase parser. We use the TauP Toolkit to compute the ray parameter. In the cases where there is more than one possible ray parameters, we select the one that corresponds to the shortest travel time, since we have picked only the first *P*-wave arrivals. The calculated ray parameters for the recordings used in the analysis are shown in Figure 3-2 plotted against epicentral distance. The histograms showing the distribution of the ray parameter and the epicentral distance values are also shown in the figure.

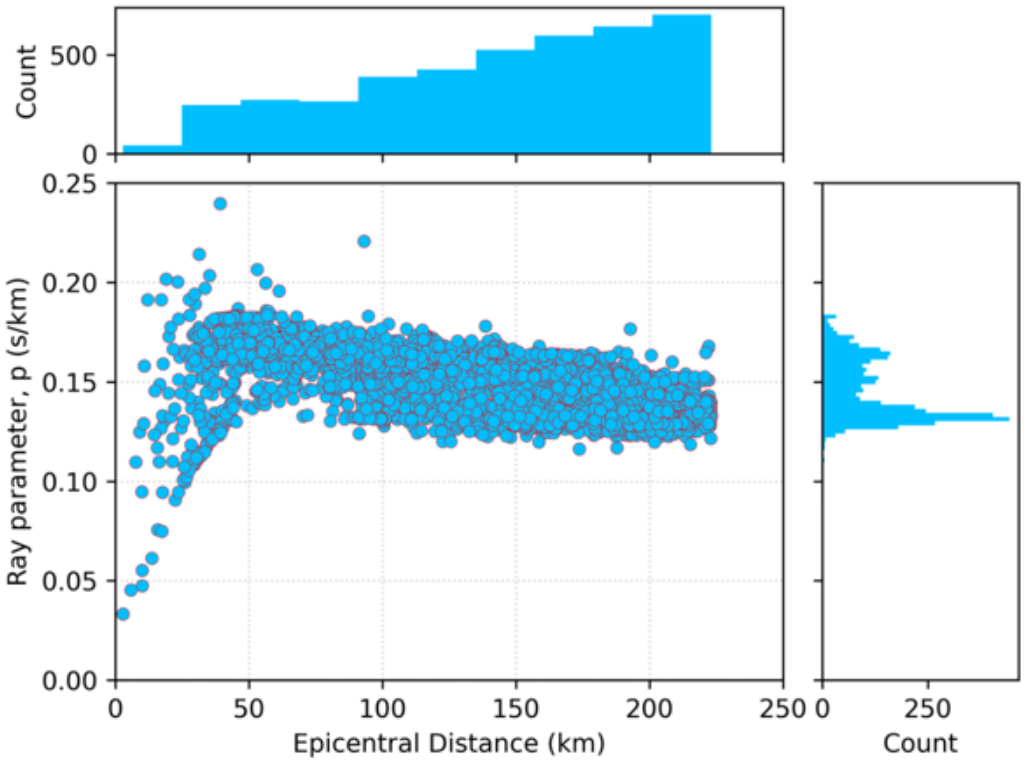

Figure 3-2. Calculated ray parameters for the recordings used in the analysis plotted against epicentral distance. The histograms showing the distribution of the ray parameter and the epicentral distance values are also plotted.

We follow the Kim et al. (2016) approach to calculate the *Vsz* for each site. Given that the ray parameter is estimated, V_{SZ} can be derived by iteratively solving Equations (3) and (5), until they converge to an acceptable tolerance (typically within 10% of a degree for angle *j*). An example of the results of the analysis for a subset of sites is presented in Figures 3-3. The full set of figures is shown in Appendix B.

For each site, the box extends from the lower to upper quartile values of the V_{SZ} estimates resulting from n different earthquakes recorded at the site, with the orange line depicting the median. The whiskers extend from the box to show the range of the estimates. The mean value is shown with the red star. The mean and the +/- 1 standard deviation values of the estimated V_{S30} (described in detail in Section 4) are shown with the green x and arrows. The mean value is also listed in parenthesis next to the station name. Measured V_{S30} values, for those sites that are available, are shown with the open circles.

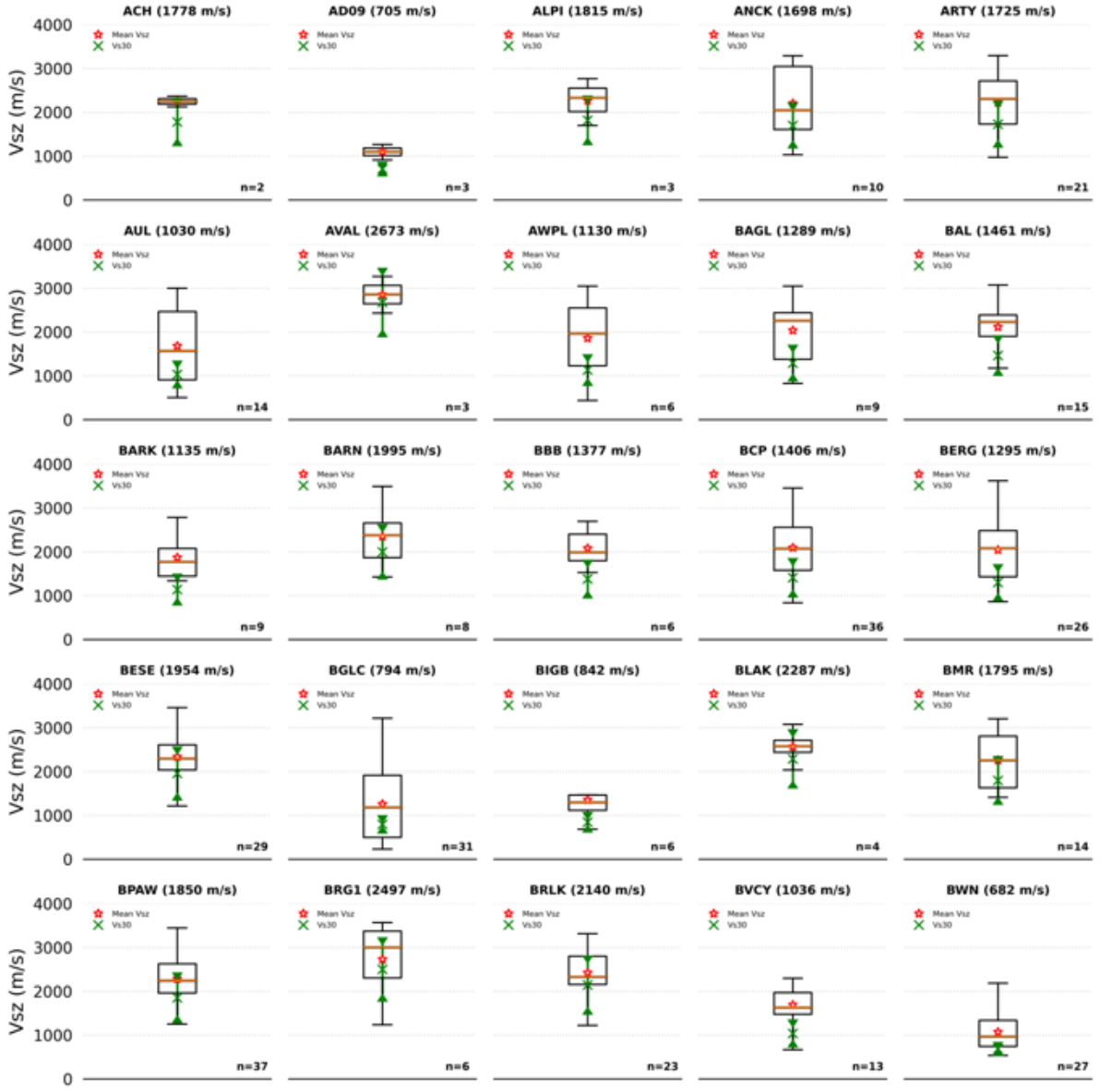

Figure 3-3. V_{SZ} results for the first set of recording sites. For each site the box extends from the lower to upper quartile values of the data, with the orange line depicting the median. The whiskers extend from the box to show the range of the data. The mean value is shown with the red star. The mean and the +/- 1 standard deviation values of the estimated V_{S30} are shown with the green x and arrows. The mean value is also listed in the parenthesis next to the station name. The measured V_{S30} values, for those sites where they are available, are shown with the open circles.

4. Evaluation of the derived V_{S30}

The final product of this analysis is the estimated V_{S30} value for each site. For correlating the V_{SZ} values with the corresponding V_{S30} we use the Boore et al. (2011) results. Boore et al (2011) used V_S profiles from sites in Japan, California, Turkey, and Europe, and demonstrated that there is a strong correlation between V_{S30} and V_{SZ}. These correlations may not be directly applicable to AK sites due to significantly different geological settings and the presence of glacial deposits in many areas of AK, but the lack of available V_S measurements at sites in AK dictates the use of these correlations. A scatter plot of the V_{SZ} and the corresponding V_{S30} values is shown in Figure 4-1. The horizontal error bars correspond to +/- 1 standard deviation of the conversion relation. The vertical error bars correspond to +/- 1 standard deviation of the V_{SZ} estimates at the site.

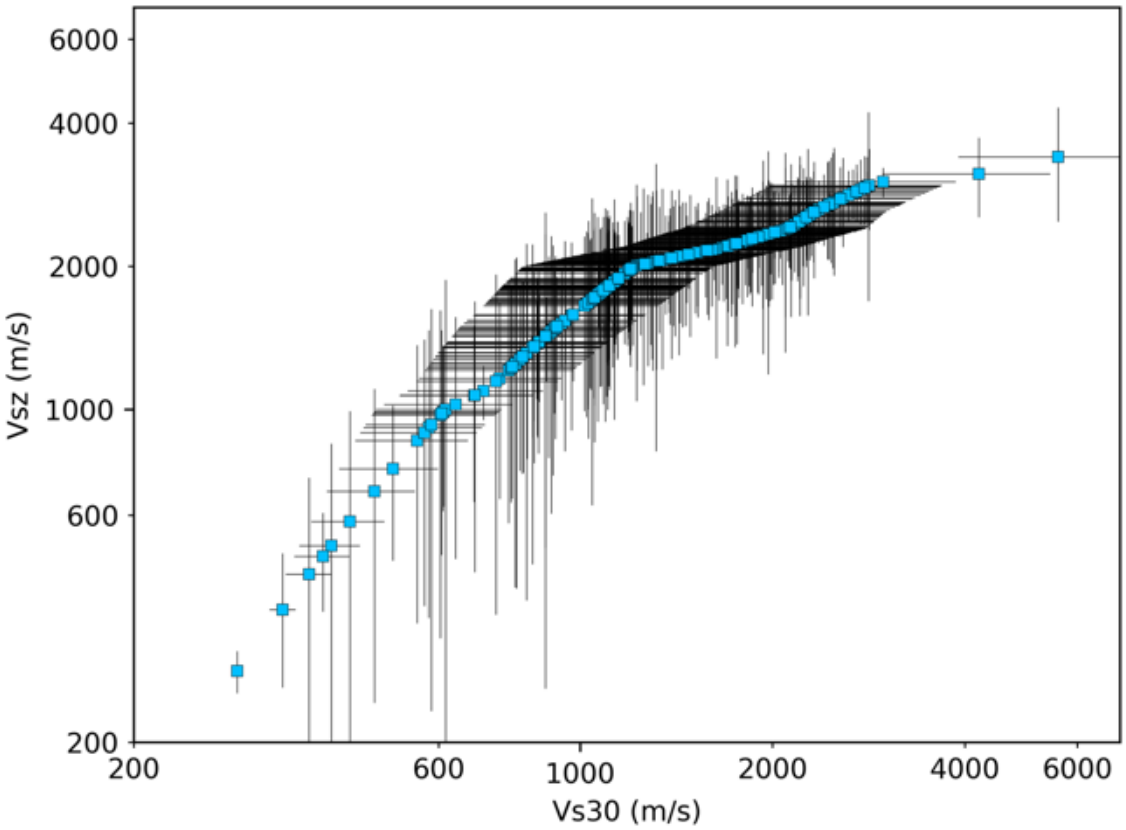

Figure 4-1. Estimated V_{SZ} (m/s) with the corresponding V_{S30} (m/s) values based on the Boore et al., (2011) correlations. The depth (z) that corresponds to each V_{SZ} value is estimated as z = 0.1 (s) * V_{SZ} (m/s). The horizontal error bars correspond to +/- 1 standard deviation of the conversion relation. The vertical error bars correspond to +/- 1 standard deviation of the V_{SZ} estimates at the site.

As can be seen from the leftmost histogram in Figure 4-2, the distribution of the V_{SZ} values has a mean of about 2000 m/s. The corresponding V_{S30} histogram (rightmost panel) exhibits a

bimodal distribution with the first peak at values around 1000 m/s and the second around 2000 m/s. This effect is the combination of the distribution of the V_{SZ} values in our database and the Boore et al. (2011) correlation relations that were used to estimate the V_{S30}.

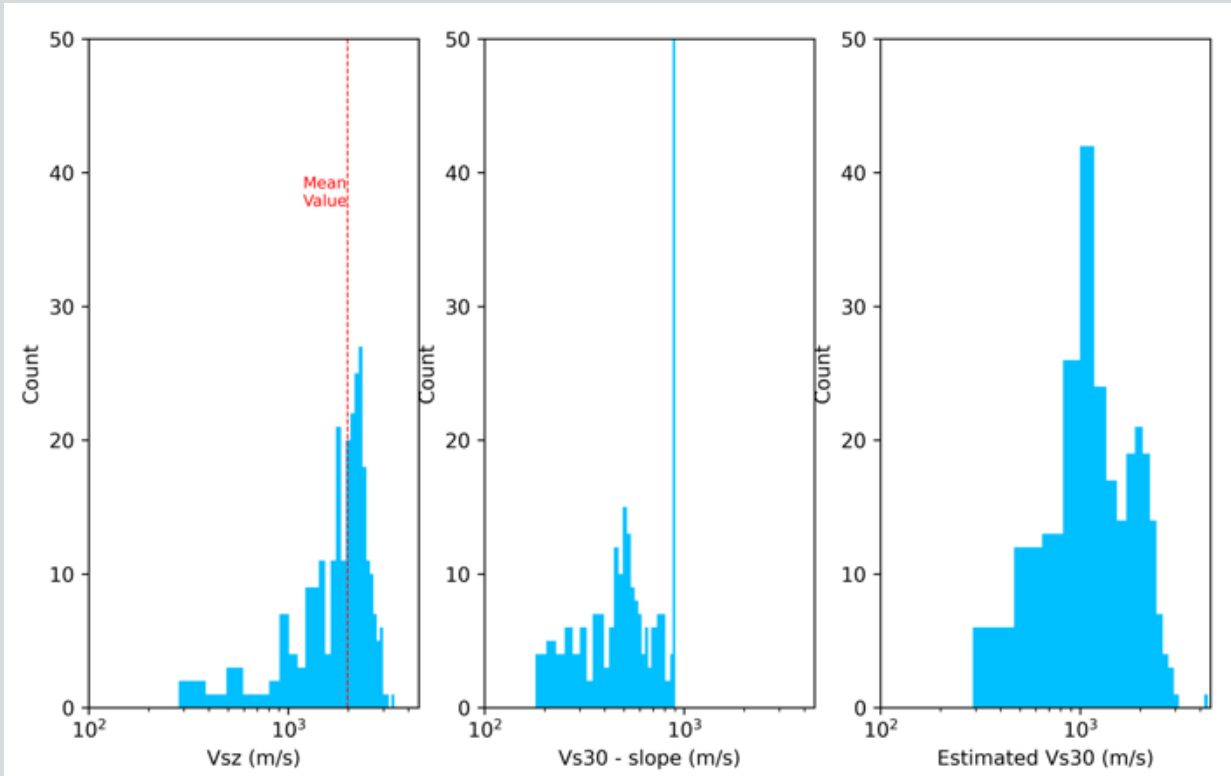

Figure 4-2. Histograms showing the V_{SZ}, V_{S30} from slope and Estimated V_{S30} distribution. Note the cap at the highest V_{S30} in the middle panel (V_{S30} from slope); 62 of the 254 stations have V_{S30} of 900 m/s.

USGS has been compiling maps with V_{S30} estimates approximated via correlation to topographic slope and direct measurements for the last several years (Wald and Allen, 2007, Allen and Wald, 2009, Worden et al., 2015, Yong et al., 2015). The slope-based V_{S30} map for AK from Wald and Allen, (2007) is shown in Figure 4-3.

In a more recent communication with USGS (Eric Thompson, personal communication, 2020) we have obtained the latest iteration of the slope-based V_{S30} estimates for the Alaska region. The histogram of these values (Figure 4-2) shows that there is a cap at the highest V_{S30}, of 900 m/s; 62 of the 254 stations, 24.4% of them, have V_{S30} of 900 m/s. This is a limitation of the topographic slope proxy method that affects the characterization of hard rock sites with very high V_{S30} values.

z values are calculated as the product of the source time function duration and the V_{SZ} measurements. We assumed 0.1s as a typical duration of the source time function for small events, following Ni et al (2013) and Kim et al. (2016). A histogram of the z values of the V_{SZ} measurements is shown in Figure 4-4. Table A-2 in Appendix A lists the mean V_{SZ}, the slope-based V_{S30}, the measured V_{S30} for the sites where this is available and the estimated V_{S30} from our analysis.

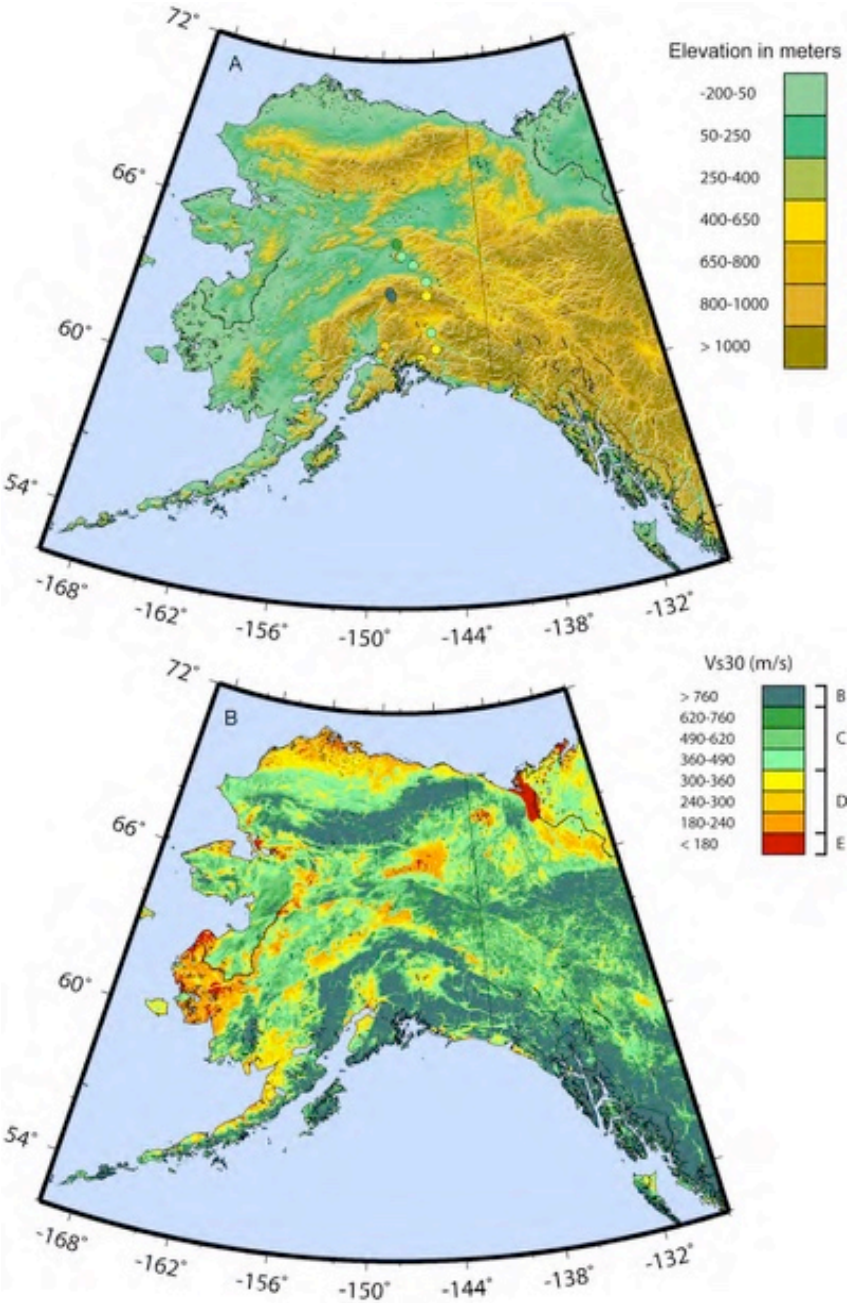

Figure 4-3. A. The topographic relief map for the State of Alaska. B, Site-condition map derived from topographic slope.

Source: Allen and Wald (2007)

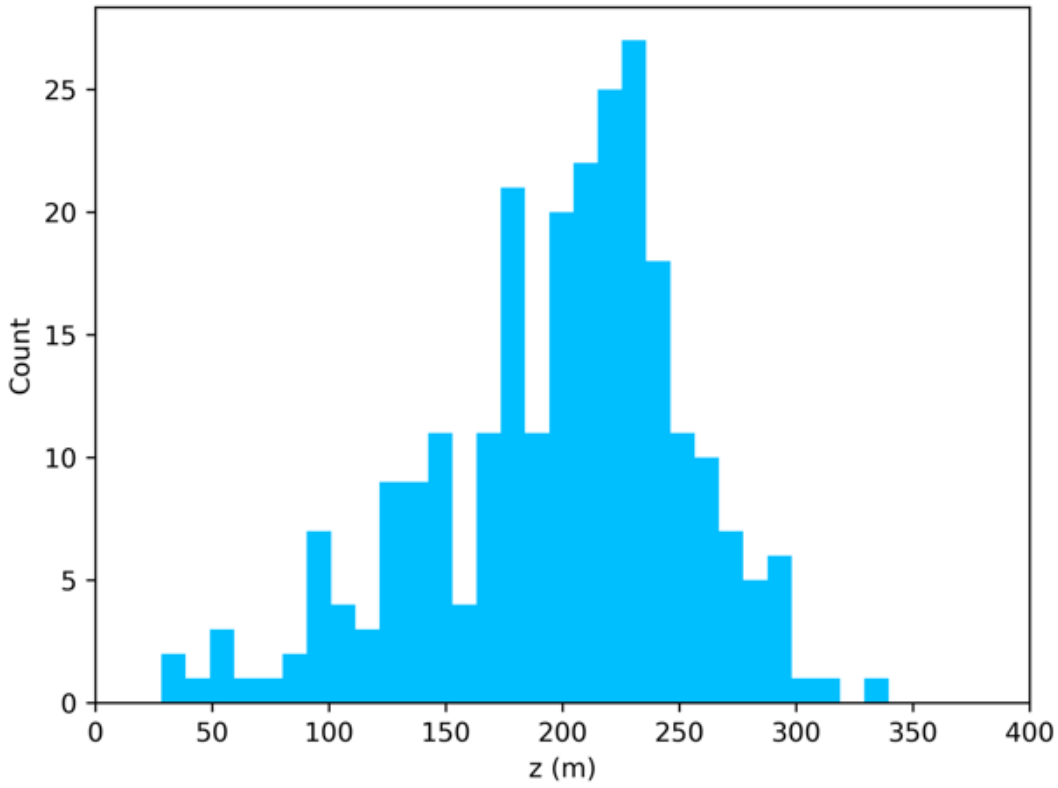

Figure 4-4. Histogram of the depth (*z*) that corresponds to each V_{SZ}. Each value is estimated as $z = 0.1 * V_{SZ}$.

The V_{SZ}/V_{S30} ratio is plotted against *z* for all sites in Figure 4-5. V_{SZ} is about 60% higher than V_{S30} for z values between about 100 and 200. This percentage decreases for z values outside of this depth range. For the largest z values of our dataset, we see that the V_{SZ}/V_{S30} ratio drops below unity (as low as 0.6).

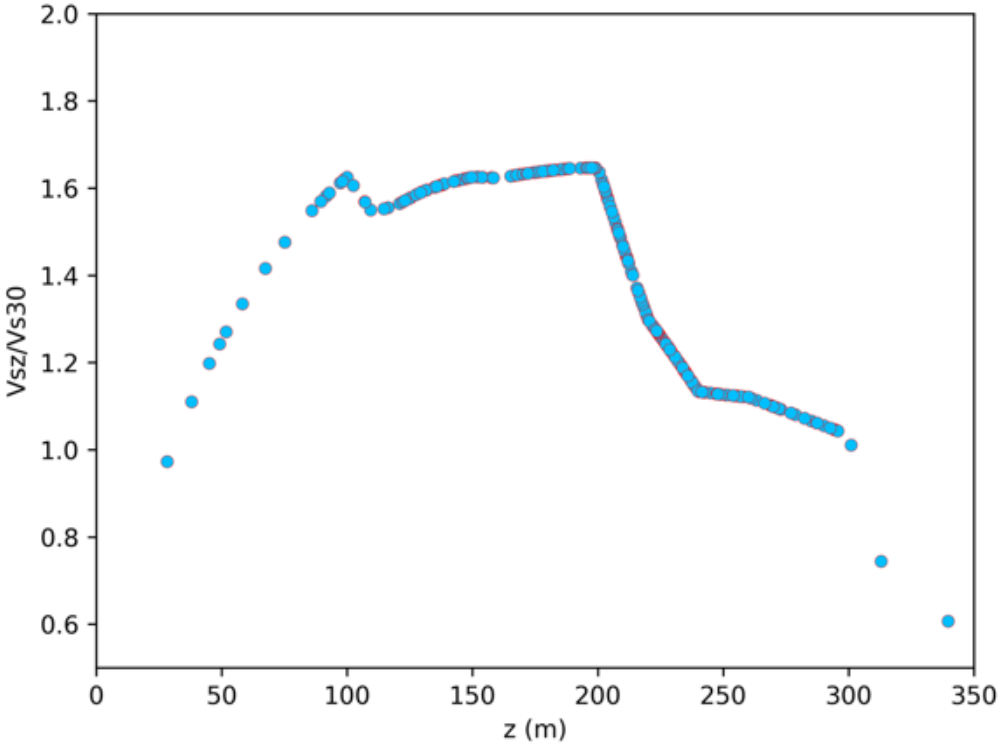

Figure 4-5. V_{SZ} /V_{S30} ratio plotted against depth (z) for all sites.

4.1 Comparison and validation of the V_{S30} results.

Dutta et al. (2000) estimated the shear wave velocity profiles at 36 sites in Anchorage, AK using surface waves inversion. Our database includes usable recordings for four of those sites and we use them as reference sites to validate our estimated V_{S30} results. These sites are shown in Figure 4-6 with the orange circles and again separately in Figure 4-7.

In Figure 4-6 we compare the estimated V_{S30} values from this study with the V_{S30} values estimated from the topographic slope proxy. Figure 4-6 (top) shows that for sites with slope-based V_{S30} less than about 900 m/s, our estimated values are higher than the ones from the topographic slope proxy. It seems possible that glaciation may have caused Alaskan sites to have relatively high V_{S30} even where the slope is low; the high V_S of glaciated rocks are documented in Motadezian et al. (2011). Also, due to the fact that the highest V_{S30} estimated from the topographic slope proxy is about 900 m/s, the comparison for the sites with V_{S30} higher than that is not meaningful (Figure 4-6, bottom). For the four sites with measured V_{S30} (orange circles) there's a fairly good agreement between the estimated and the slope-based V_{S30}. Cannon and Dutta (2015) came to a similar conclusion after improving the correlation between measured V_{S30} values and the slope-based V_{S30} values, by incorporating geologic-based coefficients for Anchorage.

The comparison between the estimated and measured V_{S30} values is shown in Figure 4-7. The horizontal error bars correspond to +/- 1 standard deviation of the conversion relation. Table 4-1 is an excerpt of Table A-2 listing the corresponding values for the sites shown in Figure 4-7. The numbers in parenthesis, next to the slope-based and estimated V_{S30} values, show the % difference from the measured V_{S30}.

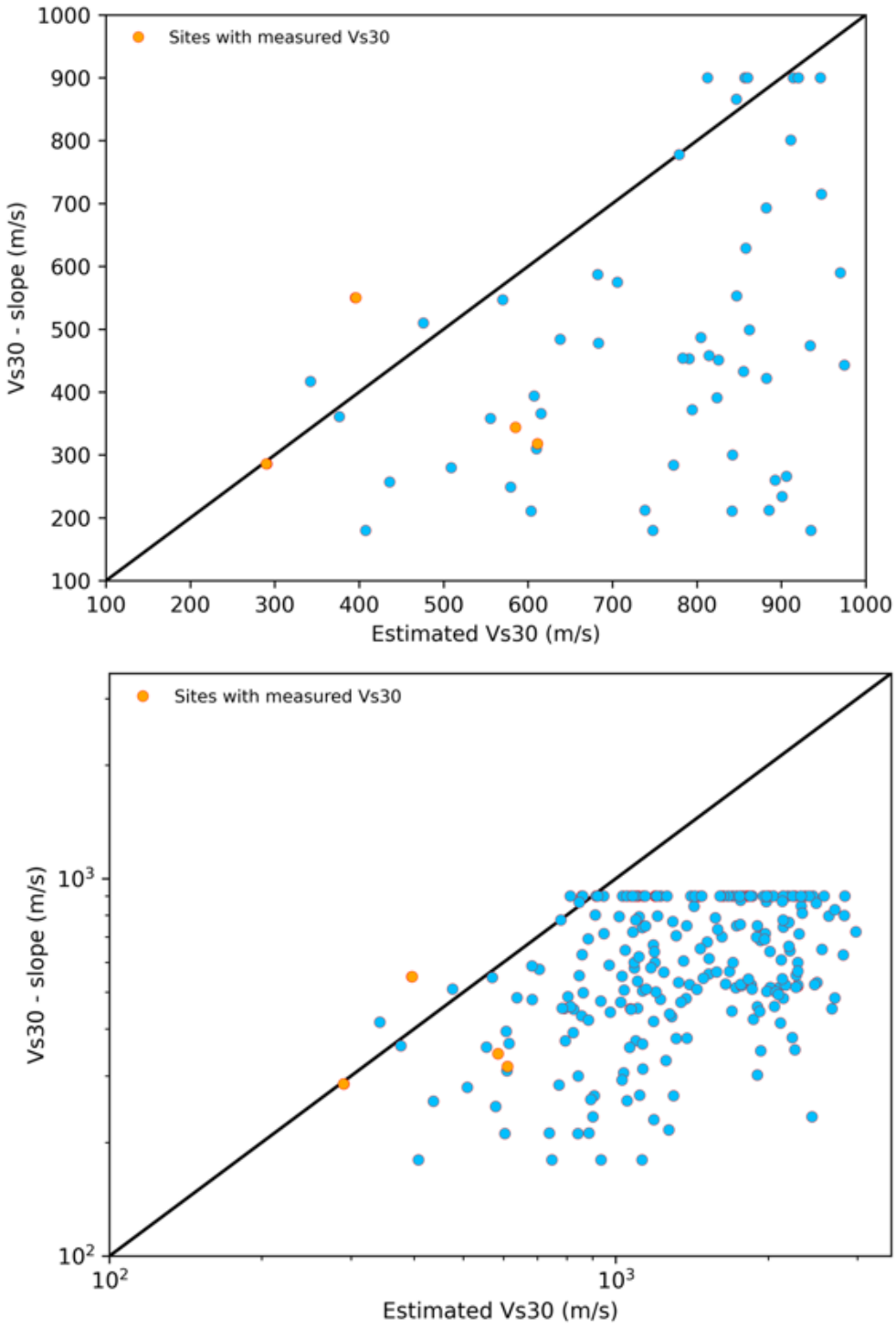

Figure 4-6. Scatter plot of the estimated V_{S30} against the slope-based V_{S30} for V_{S30} values up to 1000 m/s (top). Same plot for all estimated V_{S30} values.

Table 4-1. Mean V_{SZ} derived from the analysis, topographic slope proxy V_{S30} (Slope V_{S30}), measured V_{S30} and estimated V_{S30} correlated to the mean V_{SZ} for the sites used in the analysis. The station coordinates and the depth extent resolvable z(m) from the analysis are also provided. The numbers in parenthesis show the % difference from the measured value.

Site	Latitude	Longitude	z (m)	Mean V_{SZ} (m/s)	Slope V_{S30} (m/s)	Measured V_{S30} (m/s)	Estimated V_{S30} (m/s)
K211	-149.8580	61.1491	28	282	286 (27%)	394	290 $\pm$ 4 (26%)
K212	-149.7930	61.1556	99	990	318 (38%)	514	611 $\pm$ 135 (19%)
K213	-149.8590	61.1128	93	930	344 (3%)	354	585 $\pm$ 124 (65%)
K215	-149.7520	61.0862	49	492	550 (33%)	412	396 $\pm$ 39 (4%)

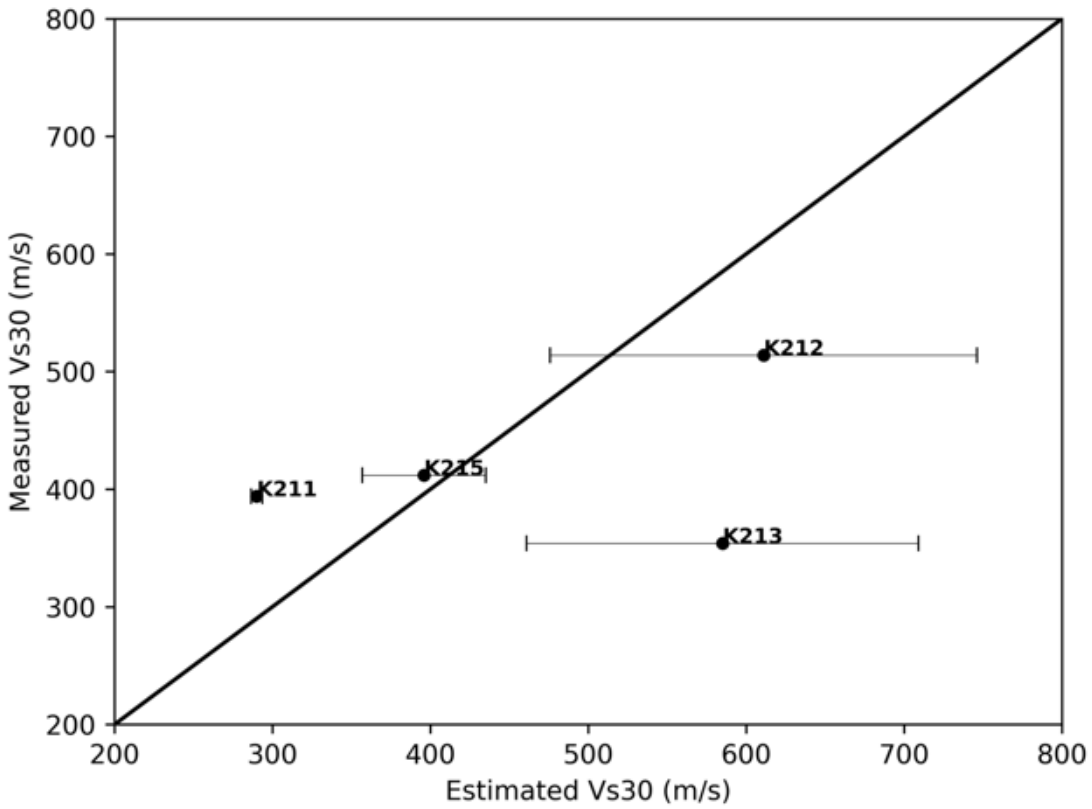

Figure 4-7. Scatter plot of the estimated against the measured V_{S30}. The horizontal error bars correspond to +/- 1 standard deviation of the conversion relation.

In Figure 4-8 the spatial distribution of the estimated V_{S30} is shown. Each symbol, which corresponds to a recording site, is color coded using the NEHRP site category definitions (shown in Figure 4-9). In Figure 4-10 symbols are color coded with a color pallet which is a continuous function of the estimated V_{S30} value. The basemap in both figures corresponds to the most recent slope-based V_{S30} values from USGS, as provided to us by Eric Thompson (personal communication, 2020).

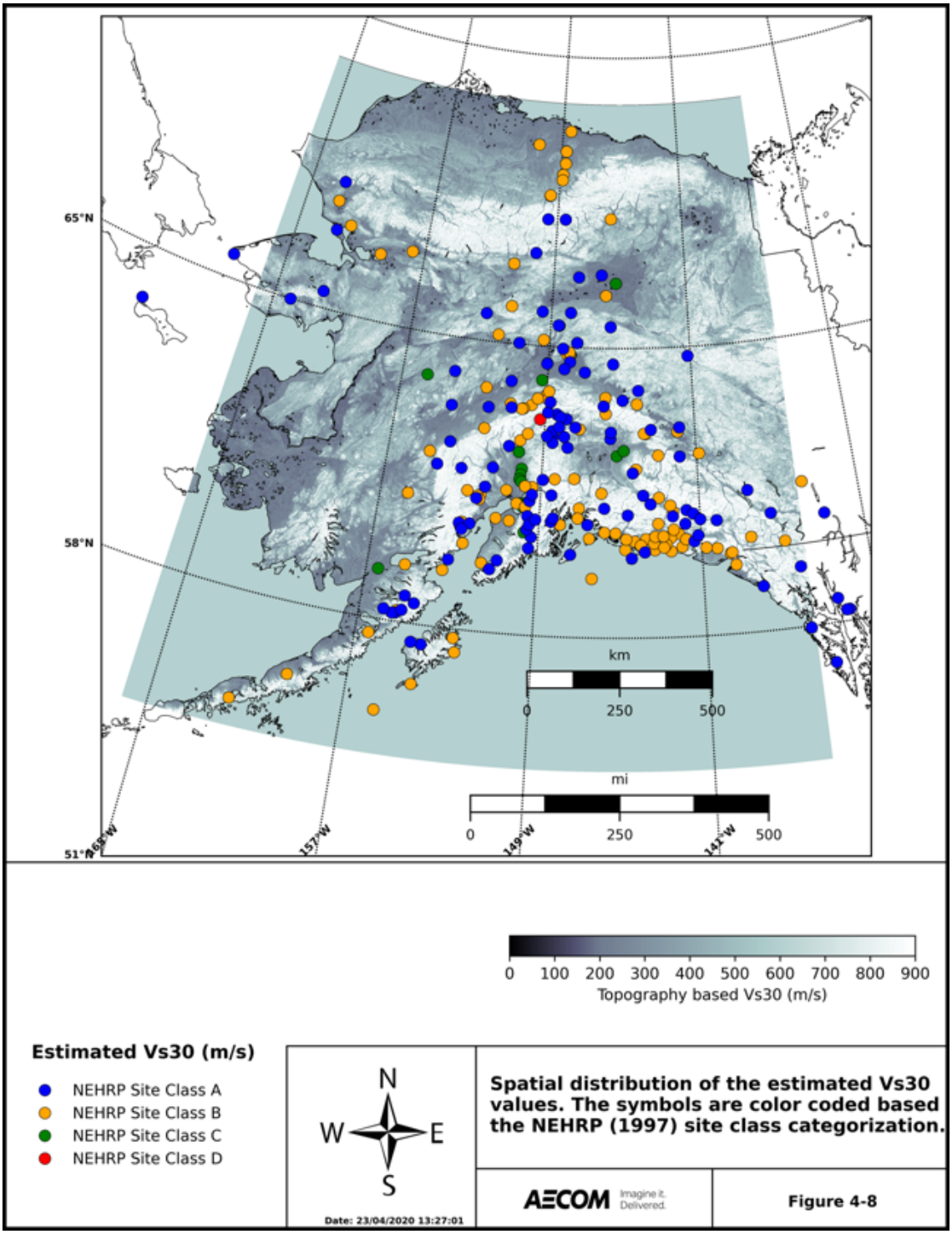

Figure 4-8. Spatial distribution of the estimated V_{S30} values. The symbols are color coded based on the NEHRP (1997) site class categorization.

Site Class	Description	Average Properties in top 30m		
		Shear-wave velocity, V_{S30} (m/s)	SPT N (Blows/300mm)	Undrained shear strength, S_U (kPa)
A	Hard Rock	> 1500	Not applicable	Not applicable
B	Rock	760 - 1500	Not applicable	Not applicable
C	Very dense soil and soft rock	360 - 760	> 50	> 100
D	Stiff soil	180 – 360	15 – 50	50 – 100
E	Soft soil	< 180	< 15	< 50
		Plus any profile with more than 3m of soil having the following characteristics: Plasticity index, PI > 20% Moisture content, w ≥ 40% Undrained shear strength, S_U < 25kPa		
F*	-	Any profile containing soils with one ore more of the following characteristics: Soil vulnerable to potential collapse under seismic loading, e.g. liquefiable soils, quick and highly sensitive clays, collapsible weakly cemented soils. Peats and/or highly organic clays (H>8m of peat and/or highly organic clay) Very high plasticity clays (H>8m with PI>75%) Very thick soft/medium stiff clays (H>36m)		

Figure 4-9. Site class categories according to NEHRP (1997).

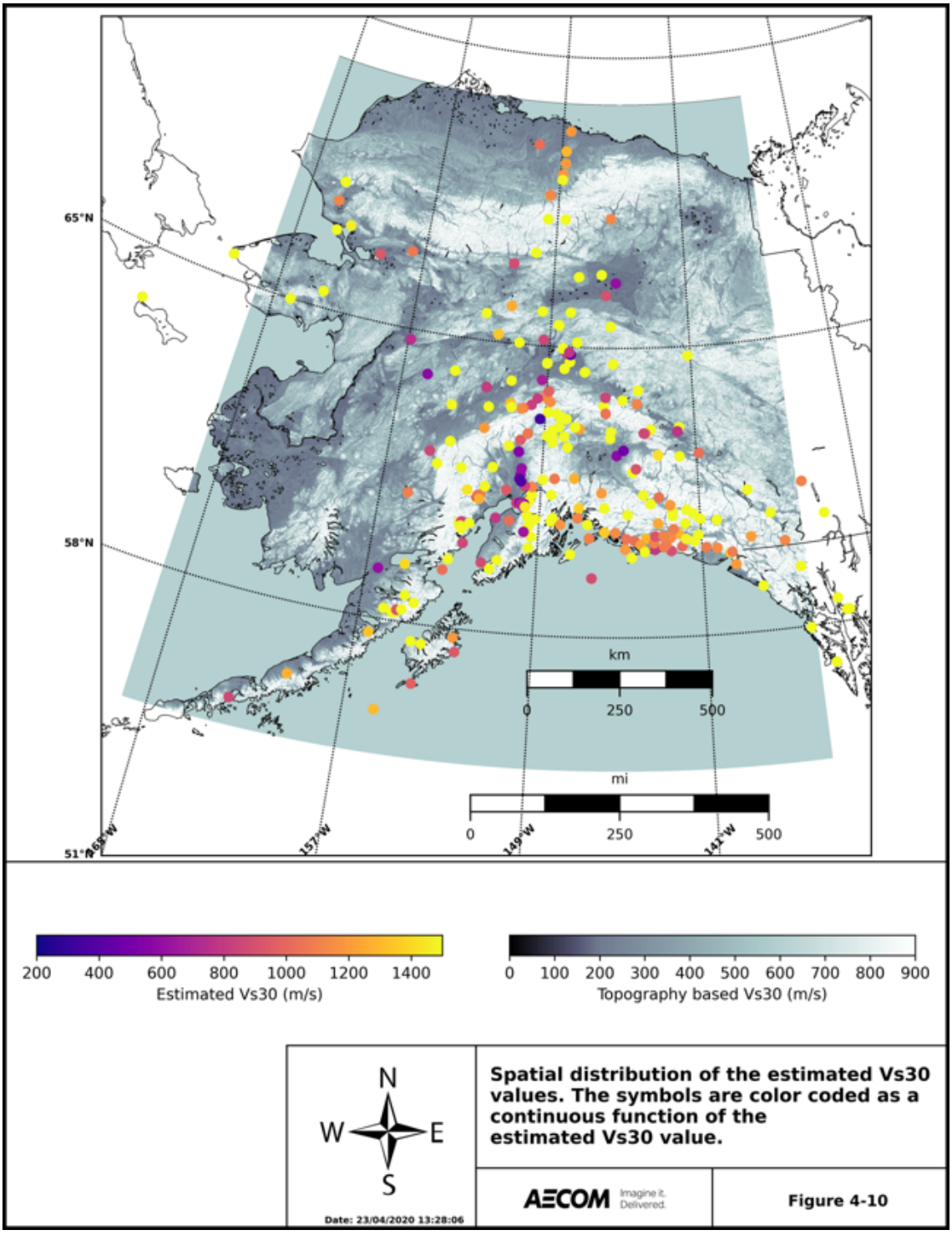

Figure 4-10. Spatial distribution of the estimated V_{S30} values. The symbols are color coded as a continuous function of the estimated V_{S30} value.

4.2 Comparison with local geology

We compared the estimated V_{S30} values with the geologic map of Alaska. The map and associated digital databases are the result of compilation and interpretation of published and unpublished 1:250,000-scale and limited 1:500,000- to 1:63,360-scale maps (Willson et al., 2015).

We used the geologic formation on which each recording site is situated and assigned a NEHRP site class based on the work of Wills and Clahan (2006) for California, adapting it to the Alaska geologic conditions. Generally, the site classes we assigned are one unit lower (i.e. faster) than what is used in California by Wills and Clahan (2006), because California rocks are known to have low seismic velocities due to weathering. Most of Alaska was glaciated so we expect bedrock to be less weathered and Quaternary formations to be gravels instead of sands and soils. Wills and Clahan (2006) might be representative of Anchorage but not most of the rest of the state.

We classified Quaternary as NEHRP Site Class C (instead of D in Wills and Clahan, 2006) because we expect the seismic stations would be on gravels, not soils or sands. Most Tertiary (T) sites were classified as NEHRP Site Class B (instead of C in Wills and Clahan, 2006). We classified most Cretaceous (K) sites as NEHRP Site Class A (instead of B in Wills and Clahan, 2006). Finally, we classified crystalline rocks as NEHRP Site Class A. The description of the geologic formation as well as the corresponding NEHRP Site Class classification for all sites are given in Appendix A (Table 2).

For sites with the same assigned NEHRP site class, we plot the histogram of the estimated V_{S30} values (Figure 4-11). The vertical red lines show the site class boundaries. The percentage of sites that fall within the site class boundaries is also shown in each panel. For site classes A and B, a very large percentage of the estimated V_{S30} values is falling within the site class boundaries, suggesting that the estimated V_{S30} values are representative of the local site geology. This number is dropping significantly for Site Class C (20%). Accounting for the uncertainty in our estimates results are improved (see also Figure 4-14). Moreover, some of the volcanic formations that were assigned to Site Class C could potentially be classified under Site Class B under certain conditions but still the majority of our estimates exhibit higher V_{S30} values than the upper boundary of Site Class C (760 m/s).

Figures 4-12 through 4-14 summarize the results of our analysis for each Site Class. For each site, we show the estimated V_{S30} with the corresponding uncertainty (black squares and green lines). We also show the slope based V_{S30} (open diamonds) and the measured V_{S30} value (red circles) for the sites where that is available. The vertical red lines show the site class boundaries. These figures depict the same pattern as the histograms in Figure 4-11:good agreement for Site Classes A and B and poorer agreement for Site Class C. The comparison of the estimated with the slope-based V_{S30} for the Site Class A and B sites is characterized by the highest slope-based V_{S30} capped at about 900 m/s, as described in the previous section. For Site Class C, the estimated V_{S30} values are generally higher than the slope-based ones. Despite the fact that a higher number of slope-based V_{S30} values (compared to the estimated V_{S30} values) are within the Site Class boundaries, slope-based V_{S30} estimates for several sites fall below the lower boundary of Site Class C (360 m/s) which is not what would be expected based on the general geology of Alaska as well as the fact that seismological stations (the majority of the sites in our database) are usually located on hard soil/bedrock site conditions to reduce background noise in the recordings.

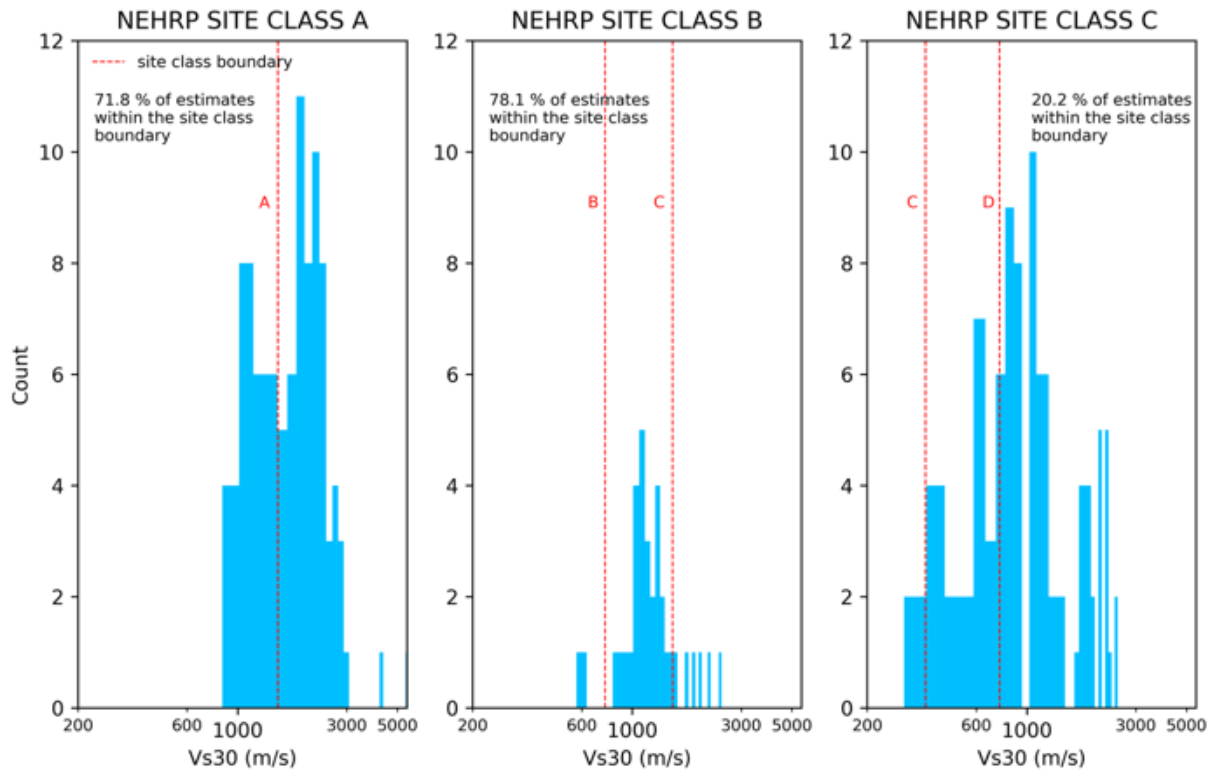

Figure 4-11. Histograms of the estimated V_{S30} for sites within the same NEHRP Site Class category. The Site Class boundaries are denoted with the vertical red lines. The percentage of the sites within the Site Class boundary is also shown.

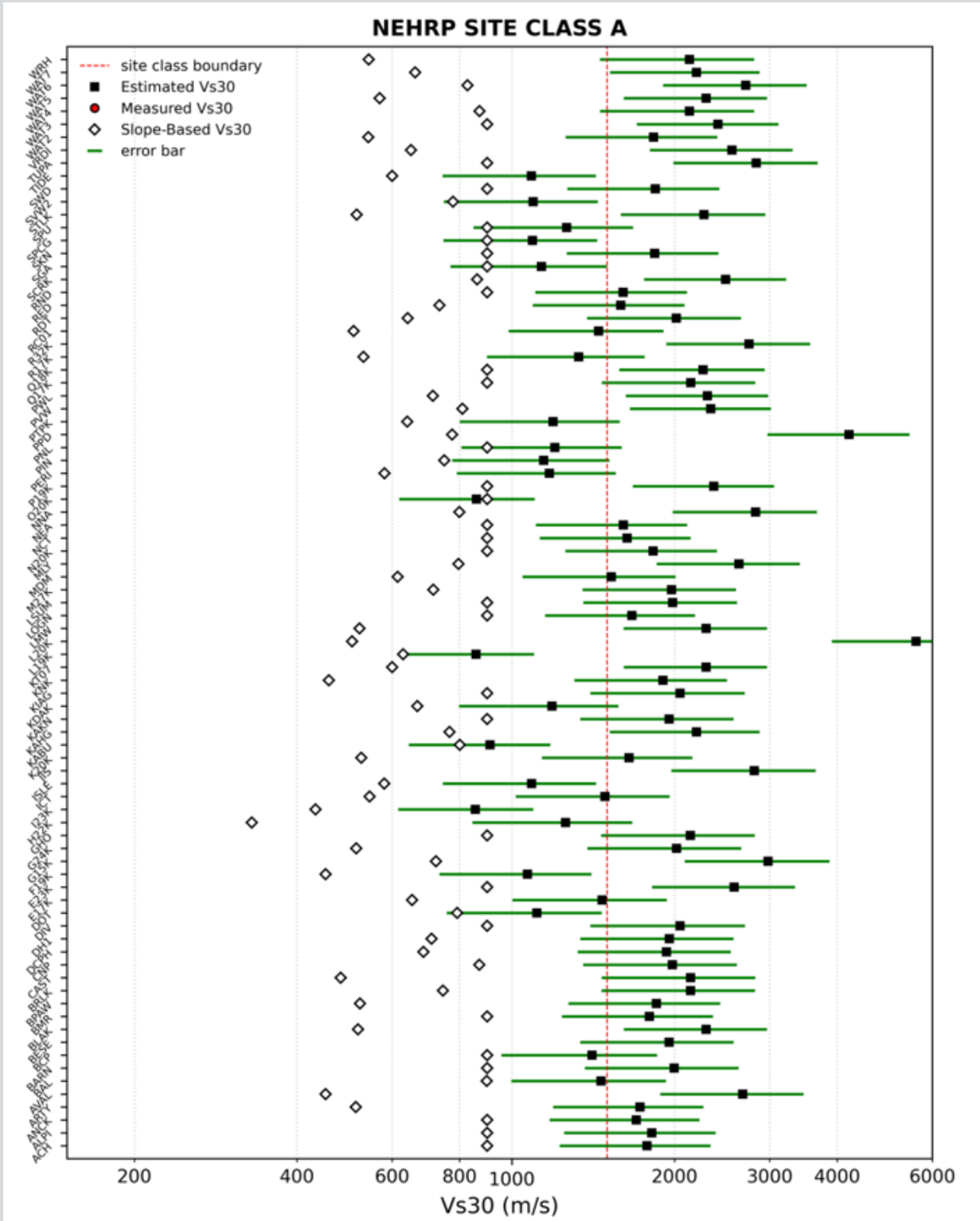

Figure 4-12. Estimated V_{S30} and the corresponding uncertainty from the correlation (+/- 1 standard deviation), shown with black squares and green lines, respectively for all sites in NEHRP Site Class A. The slope- based V_{S30} (open diamonds) and the measured V_{S30} (red circles) are also shown. The vertical red line shows the Site Class A boundary.

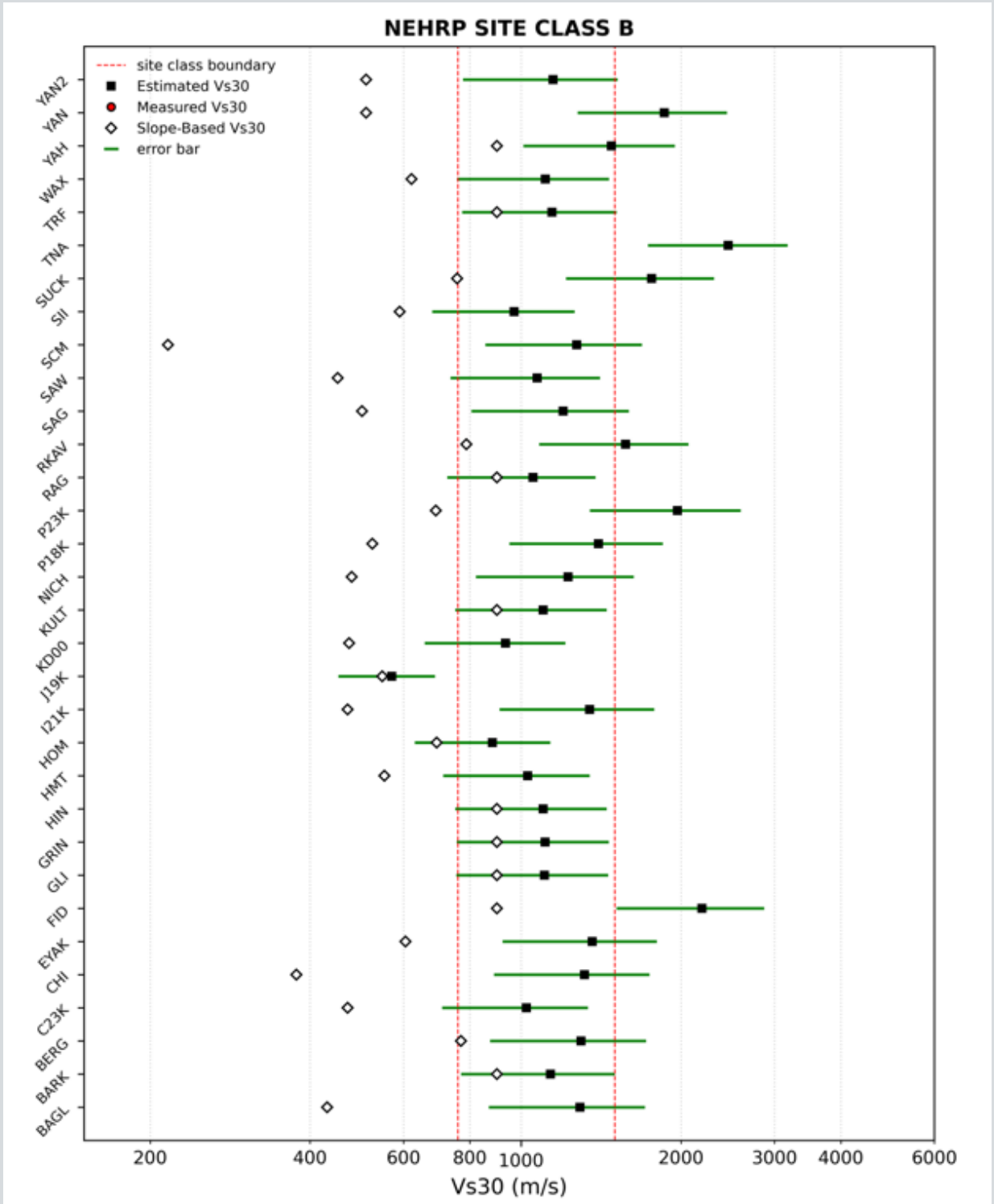

Figure 4-13. Estimated V_{S30} and the corresponding uncertainty from the correlation (+/- 1 standard deviation), shown with black squares and green lines, respectively for all sites in NEHRP Site Class B. The slope- based V_{S30} (open diamonds) and the measured V_{S30} (red circles) are also shown. The vertical red lines show the Site Class B boundaries.

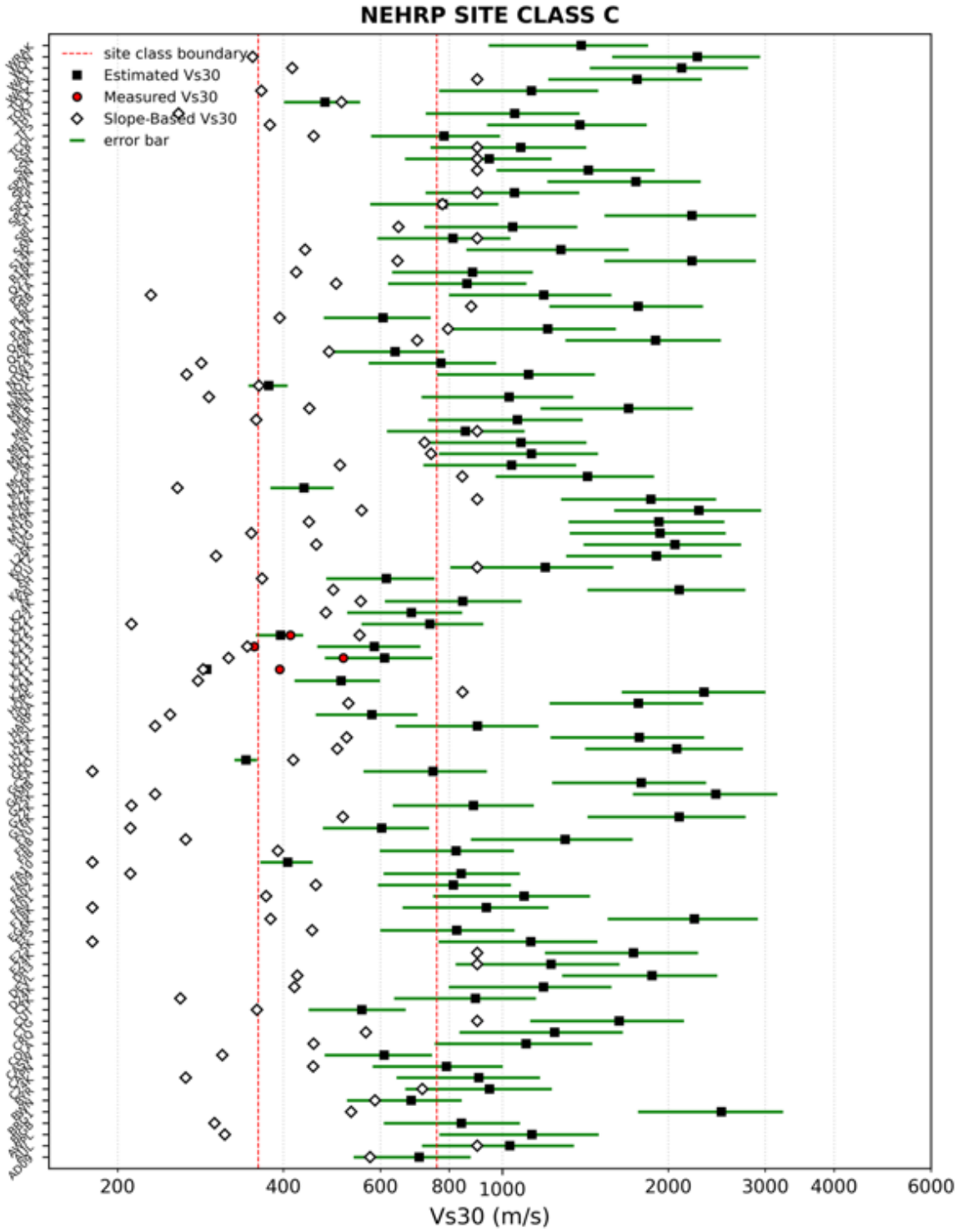

Figure 4-14. Estimated V_{S30} and the corresponding uncertainty from the correlation (+/- 1 standard deviation), shown with black squares and green lines, respectively for all sites in NEHRP Site Class C. The slope- based V_{S30} (open diamonds) and the measured V_{S30} (red circles) are also shown. The vertical red lines show the Site Class C boundaries.

5. Conclusions

We employ the method of receiver functions, at much smaller scale and higher frequency, as introduced by Ni et al. (2013) to estimate the time averaged velocity over the top 30m (V_{S30}) in the state of Alaska.

We have used data from the AK permanent seismological network as well as the Transportable Array to perform our analysis. In total we have identified 704 events that meet the criteria for this type of analysis. The corresponding waveforms have been downloaded from IRIS and have been processed using automated routines and manual inspection procedures. The processing of the waveform database resulted in 3876 single component recordings from 254 recording sites.

The results strongly depend on the quality of the data as well as on the accuracy of the picks in the seismic waveforms, therefore the analysis was performed with focus on quality, with manual inspection and picking of phases being the most critical step in estimating the final V_{S30} values.

The high V_{SZ} values estimated using this method show that the majority of the recording stations are situated in stiff soil/rock site conditions. This does not come as a surprise since seismological network sites are typically installed at stiff soil/rock sites, distant from urban environment to minimize the background noise. The estimated V_{S30} values from the correlation with V_{SZ} also support this observation. For a small number of sites in our database, the estimated V_{S30} values exhibit high values (> 3000 m/s). These very high V_{S30} values are a result of the analysis as well as of the correlation functions used to estimate the V_{S30}. However, these results do not practically impact the site characterization and the use of the data from those sites in ground motion and hazard studies.

There is a very limited number of sites with measured V_{S30} and for those sites, the quality of the available recordings was average. In addition, the small number of recordings per site did not allow for robust statistical evaluation of the estimated V_{S30}. Nevertheless, the comparison of the estimated with the measured V_{S30} at those sites shows that the application of the receiver function method in Alaska can detect the differences between stiff soil/rock and soft soil sites and can predict with fairly good accuracy the V_{S30} for all types of site conditions.

The comparison with the slope-based V_{S30} estimates is relatively good for V_{S30} values below 900 m/s. The inherent limitation of the topographic slope proxy method for the characterization of hard rock sites with very high V_{S30} values (62 of the 254 stations, 24.4% of them, have slope based V_{S30} of 900 m/s), does not allow a direct comparison for these 62 sites in our database.

We used local site geology to assign a NEHRP Site Class to the sites of our database as an alternative method to evaluate the estimated V_{S30} values. For site classes A and B, a very large percentage (almost 80%) of the estimated V_{S30} values falls within the site class boundaries, suggesting that the estimated V_{S30} values are representative of the local site geology. However, for Site Class C, only 20% of the sites fall within the Site Class boundaries, while the majority of our estimates exhibit higher V_{S30} values than the upper boundary of Site Class C (760 m/s).

Local site geology is another proxy method for estimating the V_{S30} at a site and as such the result may not be representative of the actual V_{S30} at that site. This could be a possible explanation for the poorer comparison with the estimated V_{S30} values for the Site Class C sites. These results could also mean that the application of the method has failed at these sites,

although the results for Site Class A and B as well as the comparison at the sites with measured V_{S30} suggest otherwise. Looking at the comparison of the estimated with the slope-based V_{S30} values, a higher number of sites (for the slope-based V_{S30} values) falls within the Site Class boundaries but several sites fall below the lower boundary of Site Class C (360 m/s). These low slope-based V_{S30} values are not supported by the general geology of Alaska or the fact that the majority of the sites in our database are seismological stations (installed at stiff-soil/rock sites and distant from urban environment to minimize the background noise).

There are several sources of uncertainty that impact our final V_{S30} estimates such as, the acceptable tolerance adopted when iteratively solving Equations (3) and (5), the assumption of a fixed source time function duration for all events in our database, the uncertainty associated with the Brocher (2005) V_S to V_P conversion relationship etc. However, we believe that the highest sources of uncertainty in our results are described below (ranked from the highest to the lowest based on the compiled database for Alaska), which alternatively can be also seen as fields for further research and improvement in the next years.

- The computed V_{SZ} values are sensitive to the estimation of the $\dot{U}_R/\dot{U}_Z$ ratio. The accuracy of the *P*-wave arrival pick as well as the selection of the initial amplitude of the $\dot{U}_R$ and $\dot{U}_Z$ components are critical steps in the methodology that can be affected by the quality of the recordings (background noise, baseline issues etc.). Moreover it is important to correctly identify the type of the *P*-wave that is marked as the first arrival, since beyond the critical distance P_n waves are arriving ahead of P_g. The correct identification is important for selecting the appropriate ray parameter and corresponding travel time.

- The regional velocity model for Alaska from Ward and Lin (2018) that we used in our analysis is a great improvement over the previous ones and it incorporates results from the most recent non-invasive geophysical methods. The intended use of this model probably does not include the one used in this report. Moreover, inherent limitations of the geophysical methods used result in a lower resolution at the very top layers (<3km) which are the most critical for this method. A further improvement of the regional velocity model focused at the shallower layers would greatly benefit the use of the local receiver function method.

- The estimated V_{SZ} values for Alaska correspond generally to depths larger than 30m. This results in higher variability in the estimated V_{S30}, since the uncertainty in the correlations is typically higher for z > 30 m. Moreover, the lack of Alaska specific V_{SZ} - V_{S30} relationships adds to this uncertainty. A better calibrated and regionalized V_{SZ} - V_{S30} relationships can lower the uncertainty in the V_{S30} estimation.

- The estimation of the ray parameter, following the Kim et al. (2016) approach, assumes a very simplified velocity structure (layer over half-space). We followed a different approach using the regional 3D model to create an average 1D velocity model over the source-site path and calculated the ray parameter for that model. Although the velocity layers near the surface are the ones that practically control the resulting V_{SZ}, a more elaborate calculation of the ray parameter could improve the overall analysis.

Future Research

1. We plan to incorporate in the dataset sites from Alaskan strong motion networks that have available data for these events. Working with the strong motion network sites, which are typically installed in urban areas and in a variety of site conditions, will be

more challenging due to the higher background noise but will allow further testing of the method in AK at sites with lower V_{S30}.

2. Application of methods like the one followed in this report is of most potential value in areas with a very small number or no sites with measured V_{S30}. However, the combination of the small number of sites with measured V_{S30} in Alaska and the limited number of available recordings at these sites hinders a more detailed and robust validation of the results. Validation of the method against more sites with measured V_{S30} will allow the use of results with higher confidence.
3. Improvement of the regional model by incorporating measurements that would allow the description of the top layers of the upper crust in more detail and incorporate local features (e.g. basins).
4. Include additional evaluation methodologies such as residual analysis using Ground Motion Prediction Equation models.

6. Data and Resources

Seismic data were downloaded from the IRIS data services.

The slope based Vs30 for AK were downloaded from: https://usgs.maps.arcgis.com/apps/webappviewer/index.html?id=8ac19bc334f747e486550f32837578e1), Eric Thompson, personal communication, 2020)

All data will be made available upon email request to the authors of the report.

7. Acknowledgments

We would like to thank Prof. C.B. Papazachos for his valuable comments and suggestions. We also thank Dr D. M. Boore for sharing with us the coefficients for correlations of V_{SZ} with V_{S30}.

8. References

Akazawa, T. (2004). A technique for automatic detection of onset time of P-and S-Phases in strong motion records, 13th World Conference on Earthquake Engineering.

Aki, K. and P. G. Richards (2002). Quantitative Seismology. J. Ellis. Sausalito, CA. University Science Books. 700 pages.

Allen, T. and D. Wald (2007). Topographic Slope as a Proxy for Seismic Site-Conditions (Vs30) and Amplification Around the Globe. USGS Open-File Report 2007-1357.

Berg, E. (1973). Crustal Structure in Alaska, *Tectonophysics*, **20**, 165-182.

Beyreuther M., R. Barsch, L. Krischer, T. Megies, Y. Behr and J. Wassermann (2010). ObsPy: A Python Toolbox for Seismology. *Seism. Res. Lett.*, **81**, 530-533.

Boore, D. (2004). Ground Motion in Anchorage, Alaska, from the 2002 Denali Fault Earthquake: Site Response and Displacement Pulses, *Bull. Seismol. Soc. Am.*, **94**. S72–S8.

Boore, D. M., E. M. Thompson, and H. Cadet (2011). Regional correlations of VS30 and velocities averaged over depths less than and greater than 30 m, *Bull. Seism. Soc. Am.,* **101**, 3046-3059.

Brocher, T. M. (2005). Empirical relations between elastic wavespeeds and density in the Earth's crust, *Bull. Seismol. Soc. Am.*, **95**, 2081–2092.

Cannon, E.C. and U. Dutta (2015). Evaluating Topographically-Derived Vs30 Values for Seismic Site Class Characterization in Anchorage, Alaska, USA. 6th International Conference on Earthquake Geotechnical Engineering, 1-4 November 2015, Christchurch, New Zealand

Crotwell, H. P., T. J. Owens, and J. Ritsema (1999). The TauP Toolkit: Flexible seismic travel-time and ray-path utilities, *Seism. Res. Lett.*, **70**, 154–160.

Crouse, C.B., J. Freymueller, D. Given, P. Haeussler, S. Masterman, M. O'Hare, D. Oppenheimer, S. Schwartz, P. Somerville, P. Whitmore, D. Wilson (2016). Analysis of the Benefits and Costs for the Adoption of EarthScope Stations in Alaska, Alaska Earthquake Monitoring Working Group.

Dutta U., N. Biswas, A. Martirosyan, S. Nath, M. Dravinski, A. Papageorgiou and R. Combellick (2000). Delineation of spatial variation of shear wave velocity with high-frequency Rayleigh waves in Anchorage, Alaska. *Geophys. J. Int.*, **143**, 365-375.

Dutta, U., A. Martirosyan, N. Biswas, A. Papageorgiou, and R. Combellick (2001). Estimation of S-wave site response in Anchorage, Alaska, from weak-motion data using Generalized Inversion Method, *Bull. Seismol. Soc. Am.*, **91**, 335-346.

Dutta, U., N. Biswas, A. Martirosyan, A. Papageorgiou, and S. Kinoshita (2003). Estimation of earthquake source parameters and site response in Anchorage, Alaska, from strong-motion network data using generalized inversion method, *Phys. Earth Planet. Interiors* **137**, 13–29.

Feng L. and M.H. Ritzwoller (2019). A 3-D Shear Velocity Model of the Crust and Uppermost Mantle Beneath Alaska Including Apparent Radial Anisotropy, *J. Geophys. Res. Solid Earth*, 10.1029/2019JB018122.

Goldstein, P., A. Snoke. (2005). SAC Availability for the IRIS Community, Incorporated Institutions for Seismology Data Management Center Electronic Newsletter.

Goldstein, P., D. Dodge, M. Firpo, Lee Minner (2003) SAC2000: Signal processing and analysis tools for seismologists and engineers, Invited contribution to The IASPEI International Handbook of Earthquake and Engineering Seismology, Edited by WHK Lee, H. Kanamori, P.C. Jennings, and C. Kisslinger, Academic Press, London.

Harrington, R. M. and E. E. Brodsky (2009). Source duration scales with magnitude differently for earthquakes on the San Andreas fault and on secondary faults in Parkfield, California. *Bull. Seismol. Soc. Am.*, **99**, 2323-2334.

Hosseini M., P. Somerville, A. Skarlatoudis, H. K. Thio, and J. Bayless (2016). Constraining shallow subsurface S wave velocities with the initial portion of local P waves recorded at multiple seismic networks including ANSS and EarthScope Transportable Array in the CEUS. Final Technical Report, Award G14AP00110, 58pp.

Kanamori, H. and E. E. Brodsky (2004). The physics of earthquakes. *Reports on Progress in Physics*, **67**, 1429-1496.

Kennett, B.L.N. Engdahl, E.R. & Buland R. (1995). Constraints on seismic velocities in the Earth from travel times, *Geophys. J. Int.*, **122**, 108-124.

Kikuchi, M. and M. Ishida (1993). Source retrieval for deep local earthquakes with broadband records. *Bull. Seismol. Soc. Am.*, **83**, 1855-1870.

Kim B., Y. M. A. Hashash, E. M. Rathje, J.P. Stewart, S. Ni, P.G. Somerville, A.R. Kotke, W.J. Silva, K.W. Campbell (2016). Subsurface Shear Wave Velocity Characterization Using P-Wave Seismograms in Central and Eastern North America. *Earthquake Spectra*, **2**, 143-169.

Krischer L., T. Megies, R. Barsch, M. Beyreuther, T. Lecocq, C. Caudron, J. Wassermann (2015). ObsPy: a bridge for seismology into the scientific Python ecosystem Computational Science & Discovery, **8**, 014003.

Martirosyan, A., and N. Biswas (2002). Site response at a rock site in Anchorage, Alaska from borehole strong-motion records, *Seism. Res. Lett.*, **73**, 267.

Motazedian, D., J.A. Hunter, A. Pugin, and H. Crow (2011). Development of a Vs30 (NEHRP) map for the city of Ottawa, Ontario, Canada. Can. Geotech. J. 48: 458–472 (2011).

Megies T., M. Beyreuther, R. Barsch, L. Krischer, J. Wassermann (2011). ObsPy – What can it do for data centers and observatories?. *Annals Of Geophysics*, **54**, 47-58.

Miller M.S., L. J. O'Driscoll, R.W. Porritt and S.M. Roeske (2018). Multiscale crustal architecture of Alaska inferred from P receiver functions, *Lithosphere*, **10**, 267-278.

Nath, S. K., N. N. Biswas, M. Dravinski, and A. S. Papageorgiou (2002). Determination of S-wave site response in Anchorage, Alaska, in the 1–9 Hz frequency band, *Pure Appl. Geophys.* **159**, 2673–2698.

NEHRP Recommended Provisions for Seismic Regulations for New Buildings", FEMA 273, 1997, Federal Emergency Management Agency, Washington DC.

Ni, S., Z. Li and P. G. Somerville (2013). Estimating shallow shear wave profiles for site response estimation using local P-wave seismograms, and application in the Central United States. *Seism. Res. Lett.*, **85**, 82-90.

Singh, S. K., J. Pacheco, M. Ordaz and V. Kostoglodov (2000). Source time function and duration of Mexican earthquakes. *Seismol. Soc. Am.,* **90**, 468-482.

Torne M., I. Jiménez–Munt, J. Vergés, M. Fernàndez, A. Carballo and M. Jadamec (2019). Regional Crustal and Lithospheric Thickness Model for Alaska, the Chukchi Shelf, and the Inner and Outer Bering Shelves, *Geophysical Journal International*, **220**, 522–540.

Trabant, C., A. R. Hutko, M. Bahavar, R. Karstens, T. Ahern, and R. Aster (2012). Data Products at the IRIS DMC: Stepping Stones for Research and Other Applications. *Seism. Res. Lett.*, **83**, 846–854.

Wald, D. J., and Allen, T. I.,2007, Topographic slope as a proxy for seismic site conditions and amplification. *Bull. Seismol. Soc. Am.,* **97**, 1379-1395.

Wang Y. and C. Tape (2014). Seismic Velocity Structure and Anistoropy of the Alaska Subduction Zone based on Surface Wave Tomography, *J. Geophys. Res. Solid Earth*, **119**, 8845–8865.

Ward, K. M., & Lin, F.-C. (2018). Lithospheric structure across the Alaskan cordillera from the joint inversion of surface waves and receiver functions. *J. Geophys. Res. Solid Earth*, **123**, 8780– 8797.

Wills, CJ, and KB Clahan (2006). Developing a map of geologically defined site-condition categories for California. *Bull. Seismol. Soc. Am.,* **96**,1483–1501.

Wilson, F.H., Hults, C.P., Mull, C.G, and Karl, S.M, comps., 2015, Geologic map of Alaska: U.S. Geological Survey Scientific Investigations Map 3340, pamphlet 196 p., 2 sheets, scale 1:1,584,000, http://dx.doi.org/10.3133/sim3340.

Worden, C. B., D. J. Wald, J. Sanborn, and E. M. Thompson, 2015, Development of an open-source hybrid global Vs30 model, Seismological Society of America Annual Meeting, 21-23 April, Pasadena, California.

Yong, A., Thompson, E.M., Wald, D., Knudsen, K.L., Odum, J.K., Stephenson, W.J., and Haefner, S. (2016). Compilation of VS30 Data for the United States: U*.S. Geological Survey Data Series* 978, 8 p.,http://dx.doi.org/10.3133/ds978.

Zhang Y., A. Li, and H. Hu (2018). Crustal Structure in Alaska From Receiver Function Analysis, *GRL*, 10.1029/2018GL081011.

Appendix A

Table A-1. Events used in the analysis.

a/a	YYYYMMDD	HHMMSS.FF	Longitude	Latitude	Depth (km)	Magnitude
1	20000315	091008.35	-151.0550	63.5940	11.4	4.2
2	20000509	113857.50	-153.1890	56.3660	33.0	4.3
3	20000510	105223.16	-152.8670	56.3970	33.0	4.3
4	20000803	131258.24	-136.6690	60.4030	1.0	4.2
5	20001012	172956.18	-152.9990	56.4280	33.0	4.5
6	20001109	162514.18	-152.3110	64.6120	10.0	4.4
7	20001129	103545.37	-150.3870	63.9230	6.8	5.4
8	20001206	184024.76	-150.4450	63.9410	6.5	5.0
9	20010110	202553.93	-153.5380	57.0710	33.0	4.2
10	20010110	201222.81	-153.6920	56.9640	19.6	5.3
11	20010114	145731.33	-153.3230	56.7130	24.6	4.7
12	20010211	215031.30	-153.6450	57.1450	25.8	5.2
13	20010325	113449.78	-149.4020	64.6430	18.0	4.4
14	20010403	202723.38	-150.0880	65.7930	11.1	4.1
15	20010516	225845.88	-147.2360	64.2880	23.8	4.1
16	20010604	184234.91	-152.2980	64.6630	10.0	5.1
17	20010607	062832.29	-150.9110	66.0210	10.0	4.2
18	20010619	124209.97	-147.4120	64.0650	17.2	4.1
19	20010619	192617.46	-146.2080	61.3970	6.4	4.2
20	20010630	094141.92	-150.1880	64.0560	15.3	4.4
21	20011121	170112.82	-152.8850	56.7120	16.3	4.6
22	20020203	205826.88	-153.4020	56.1110	18.1	4.2
23	20020705	164137.44	-147.5050	63.6430	0.0	4.9
24	20020711	233743.17	-153.2320	56.0940	8.3	4.1
25	20021103	184713.65	-147.5038	63.6141	0.7	4.7
26	20021103	233721.24	-147.6400	63.4729	4.3	4.1
27	20021103	231956.61	-147.4511	63.6546	6.9	4.7
28	20021103	234418.78	-147.4012	63.6081	6.4	4.2
29	20021103	221841.88	-147.8001	63.2601	5.0	5.4

a/a	YYYYMMDD	HHMMSS.FF	Longitude	Latitude	Depth (km)	Magnitude
30	20021103	224416.26	-145.8630	63.3830	5.7	4.1
31	20021104	003736.57	-147.4398	63.6022	7.5	4.4
32	20021104	153441.99	-145.1094	63.3304	7.4	4.4
33	20021104	015337.95	-147.4787	63.6621	12.8	4.6
34	20021104	035525.15	-147.5438	63.5647	8.8	4.1
35	20021104	001730.66	-147.3464	63.5139	4.8	4.1
36	20021104	095559.29	-147.4274	63.6403	10.0	4.5
37	20021104	074024.11	-145.0393	63.3190	6.7	4.2
38	20021104	000156.91	-147.3229	63.6328	15.0	4.6
39	20021104	093501.85	-145.2449	63.3693	9.5	4.6
40	20021104	115231.38	-144.4346	63.1983	9.9	4.6
41	20021104	191954.93	-147.6286	63.5058	3.1	4.2
42	20021104	074326.84	-144.0974	63.1085	3.1	4.2
43	20021104	050001.20	-144.8903	63.3214	5.3	4.2
44	20021104	150611.99	-147.6806	63.6224	5.0	4.3
45	20021104	163953.72	-147.3873	63.6644	5.0	4.3
46	20021104	065018.87	-144.7460	63.2625	11.9	4.5
47	20021105	013329.93	-143.5651	62.9163	6.5	4.6
48	20021105	072752.01	-147.8378	63.6692	29.2	4.6
49	20021105	201339.19	-146.9284	63.5694	3.8	4.1
50	20021105	075046.96	-145.4875	63.4372	4.7	4.8
51	20021105	231401.45	-143.7870	63.1437	0.8	4.5
52	20021105	122329.27	-145.2500	63.4341	10.9	4.3
53	20021105	172242.13	-145.1362	63.3661	9.8	4.7
54	20021106	022536.89	-143.7676	63.1753	1.9	4.1
55	20021107	041903.10	-147.5548	63.5564	6.0	4.3
56	20021108	202903.32	-143.5587	62.8982	26.5	4.8
57	20021108	175423.05	-143.6590	62.9669	1.0	4.5
58	20021108	142447.59	-147.1060	63.6058	1.4	4.6
59	20021108	173453.02	-148.4513	63.5666	23.7	5.3
60	20021108	144658.62	-144.4784	63.1646	3.4	4.7
61	20021108	040419.50	-142.0297	62.2645	20.0	5.2
62	20021109	100001.69	-147.7345	63.6507	24.4	4.2

a/a	YYYYMMDD	HHMMSS.FF	Longitude	Latitude	Depth (km)	Magnitude
63	20021109	011402.74	-147.4556	63.6375	0.8	4.1
64	20021109	110311.94	-147.4334	63.6229	5.9	4.6
65	20021110	214941.94	-147.8767	63.6269	10.0	4.5
66	20021110	053555.22	-147.5750	63.6102	5.0	4.2
67	20021111	220756.07	-147.7854	63.5856	7.9	4.1
68	20021111	200952.65	-147.2398	63.5665	5.1	4.1
69	20021112	002415.72	-144.8395	63.3913	5.0	4.2
70	20021113	083913.99	-147.0124	63.6129	2.9	4.2
71	20021114	143724.00	-146.1175	63.5118	17.3	4.6
72	20021115	220540.35	-147.8555	63.5218	9.3	4.2
73	20021117	092257.45	-145.1700	63.3843	11.0	4.2
74	20021118	202132.19	-147.5378	63.6189	0.9	4.1
75	20021124	132955.75	-144.1411	63.0927	5.0	4.5
76	20021126	160617.93	-145.4037	63.3154	7.6	4.2
77	20021127	052039.10	-143.2597	62.8676	5.0	4.2
78	20021201	071756.49	-145.4309	63.4174	19.2	4.6
79	20021206	030013.45	-144.7660	63.3701	5.0	4.7
80	20021213	231413.37	-143.2164	62.7033	7.0	4.5
81	20021214	162731.84	-144.8917	63.4752	13.9	4.1
82	20021214	195118.11	-135.5369	62.1165	5.0	4.4
83	20021217	095818.23	-151.0256	63.7088	14.5	4.2
84	20021227	211159.28	-143.3123	63.1624	1.0	4.1
85	20021227	050217.98	-148.4705	63.6543	2.3	4.6
86	20030106	105339.33	-147.1428	63.5569	8.9	4.9
87	20030116	001917.60	-153.1254	57.0596	32.3	5.2
88	20030124	045210.83	-145.3433	63.3477	16.5	5.0
89	20030309	101741.86	-147.6935	63.6788	20.1	4.1
90	20030323	092229.10	-146.0012	63.5817	10.1	4.1
91	20030330	134123.11	-148.1383	63.6026	24.4	4.7
92	20030402	063938.56	-150.1622	65.2680	16.5	4.5
93	20030402	064736.67	-150.0662	65.3519	22.2	4.1
94	20030530	125342.28	-147.4755	63.6445	0.1	4.1
95	20030621	034312.06	-153.2850	57.0994	33.0	4.4

a/a	YYYYMMDD	HHMMSS.FF	Longitude	Latitude	Depth (km)	Magnitude
96	20030621	074749.61	-153.8148	57.5273	30.6	4.1
97	20030621	115857.85	-153.2673	57.0946	4.4	4.5
98	20030725	082943.95	-148.3027	63.5868	3.0	4.2
99	20030803	041049.84	-153.5456	56.2597	17.2	5.2
100	20030910	073426.55	-147.1973	63.5373	4.8	4.1
101	20030920	213515.35	-147.7234	63.5726	1.0	4.4
102	20031003	182640.55	-152.6489	56.4991	10.0	4.7
103	20040125	105458.26	-147.1932	63.5831	10.2	4.4
104	20040127	182600.79	-147.2564	63.6175	11.9	4.4
105	20040130	195152.95	-154.9248	56.2875	28.1	4.5
106	20040223	050347.63	-142.4668	62.3806	1.9	4.5
107	20040319	123510.03	-155.7892	57.5274	29.3	4.3
108	20040727	211837.62	-152.9889	56.6909	19.0	4.1
109	20040804	011352.39	-136.5527	59.4460	5.0	4.5
110	20040925	161140.51	-151.2944	63.2580	24.4	4.2
111	20040925	191818.06	-143.3422	62.6802	10.0	4.1
112	20041027	160307.57	-153.3794	56.2034	3.5	4.6
113	20041027	163816.78	-153.2527	56.3549	33.0	4.5
114	20041027	100939.39	-153.1880	56.1134	9.6	4.2
115	20041103	020839.86	-153.1863	56.2668	15.1	4.6
116	20041108	062111.06	-151.4477	63.0947	23.7	4.8
117	20041118	120528.31	-146.8403	63.6289	17.4	4.6
118	20041122	044407.93	-153.0106	56.3487	25.3	4.5
119	20041122	133604.87	-153.1088	56.3617	22.0	4.6
120	20041204	210435.80	-149.1275	63.5598	21.7	4.6
121	20041223	051252.96	-151.4391	63.2980	15.0	4.4
122	20050113	173632.91	-147.5411	60.5082	29.5	4.5
123	20050123	072631.47	-153.5759	56.2677	24.0	4.6
124	20050129	194634.92	-143.9881	63.0821	13.1	4.1
125	20050211	212933.20	-139.5049	60.1354	11.7	4.7
126	20050211	210022.47	-139.4573	60.1779	14.8	5.2
127	20050216	191913.23	-152.6355	56.6716	6.1	4.1
128	20050220	183635.55	-153.2372	56.0876	25.0	4.6

a/a	YYYYMMDD	HHMMSS.FF	Longitude	Latitude	Depth (km)	Magnitude
129	20050406	224851.64	-147.4429	63.6487	6.0	4.2
130	20050406	224206.55	-146.4217	61.4540	33.0	4.3
131	20050409	190331.09	-154.4056	56.1051	10.0	4.1
132	20050426	203650.12	-153.6921	56.4875	28.0	4.5
133	20050521	081637.22	-148.3145	66.0435	15.0	4.1
134	20050707	231650.49	-150.4275	62.3248	28.8	4.1
135	20050830	042403.21	-143.4292	63.1436	6.2	4.9
136	20050914	200007.74	-144.1283	60.9441	10.0	4.4
137	20051001	221633.66	-142.5056	60.6902	10.0	4.2
138	20051004	125215.34	-145.2270	63.2680	3.9	4.4
139	20051108	024720.36	-150.9342	63.5957	18.5	4.6
140	20051109	071707.94	-147.5035	63.5588	8.0	4.6
141	20051224	234918.92	-150.1885	71.7232	10.0	4.3
142	20051229	205744.78	-137.3488	58.6745	10.0	4.2
143	20060130	123421.09	-151.6057	63.1133	14.2	4.4
144	20060215	131725.25	-153.7228	56.1449	21.3	4.2
145	20060220	014001.55	-146.1281	69.5998	10.5	4.7
146	20060312	042901.12	-146.1466	69.5726	4.2	4.5
147	20060322	212716.74	-145.8394	69.5963	10.0	4.1
148	20060329	141358.49	-149.5498	63.2816	14.1	4.1
149	20060428	181645.70	-149.1059	63.5477	13.8	4.1
150	20060522	142020.48	-143.3433	69.9438	1.0	4.4
151	20060527	180452.69	-151.2145	63.5795	10.2	4.4
152	20060611	082555.65	-147.4641	66.8727	10.0	4.2
153	20060708	090527.14	-169.6392	65.9134	10.0	4.4
154	20060710	153029.81	-169.8226	65.8491	13.6	5.0
155	20060804	041319.86	-147.4127	68.0725	10.0	4.3
156	20060814	184823.47	-152.5504	57.6943	34.4	4.1
157	20060822	035517.06	-138.1438	58.0184	10.0	4.1
158	20060826	005005.09	-142.0349	66.2716	10.0	4.2
159	20060901	234452.13	-142.3209	66.3095	10.1	4.3
160	20060922	130119.27	-143.7170	60.3515	10.0	4.1
161	20061028	221802.72	-144.1284	63.1660	1.0	4.5

a/a	YYYYMMDD	HHMMSS.FF	Longitude	Latitude	Depth (km)	Magnitude
162	20061108	021434.02	-149.5991	60.8253	33.6	4.3
163	20061114	175808.85	-140.2284	65.9307	10.0	4.1
164	20061126	064916.20	-170.1828	65.8235	16.5	4.3
165	20070109	154932.53	-137.1314	59.4522	3.1	5.3
166	20070217	145140.16	-147.6543	64.3571	5.3	4.7
167	20070408	220943.53	-144.9478	59.4687	17.9	4.5
168	20070410	163423.46	-144.4504	69.6340	10.0	4.3
169	20070420	205410.88	-144.9299	69.5713	5.3	4.3
170	20070420	150648.13	-145.4071	69.6283	10.0	4.3
171	20070428	052032.55	-144.9638	69.5886	10.0	4.5
172	20070521	122432.79	-143.9708	70.3293	10.0	4.1
173	20070610	180608.53	-142.3844	66.2301	10.0	4.2
174	20070704	174913.46	-141.4573	58.8892	10.0	4.6
175	20070709	042750.56	-138.5183	60.0629	25.0	4.1
176	20070713	053853.19	-155.6883	59.8559	10.0	4.3
177	20070903	010152.41	-154.8534	57.0815	6.6	4.8
178	20070919	112225.65	-146.1460	61.4097	28.2	4.4
179	20071010	062314.69	-152.9787	56.3641	14.6	4.6
180	20071011	221855.47	-153.1690	56.1955	23.6	4.7
181	20071013	073909.11	-152.8935	56.3233	12.2	4.3
182	20071103	195505.39	-142.1528	66.0296	10.0	4.6
183	20071129	222744.12	-142.4936	66.3456	10.0	4.7
184	20071215	224538.64	-141.9751	66.3623	10.0	4.1
185	20080103	135308.72	-142.2389	66.3986	10.0	4.1
186	20080110	014037.25	-145.0990	63.2300	6.6	4.3
187	20080423	050200.27	-150.8297	63.6517	9.6	4.1
188	20080426	040539.94	-151.6035	63.0788	13.1	4.5
189	20080511	040304.13	-145.1551	59.8292	4.8	4.6
190	20080512	125035.68	-153.1707	56.6062	25.8	5.2
191	20080517	092002.64	-142.1825	66.5325	10.0	4.5
192	20080525	211424.32	-153.7140	56.1011	10.3	4.3
193	20080525	191824.77	-153.8043	56.1137	14.1	5.4
194	20080605	050146.52	-153.5580	56.1551	13.2	4.1

a/a	YYYYMMDD	HHMMSS.FF	Longitude	Latitude	Depth (km)	Magnitude
195	20080605	093935.50	-153.5809	56.1333	3.0	4.2
196	20080605	095945.13	-153.5933	56.0881	3.6	4.1
197	20080609	111147.85	-153.2863	56.1994	15.4	4.1
198	20080716	101159.45	-149.5652	64.5961	13.9	4.2
199	20080924	121952.76	-150.1249	63.5102	0.0	4.5
200	20080925	193410.05	-149.0356	63.9605	10.0	4.2
201	20081008	095303.13	-143.8555	60.7032	15.1	5.3
202	20081126	072914.87	-151.4778	63.2182	10.1	4.4
203	20081203	024730.22	-137.9464	60.9707	10.0	4.4
204	20090117	135641.95	-151.0348	63.5982	12.8	4.4
205	20090215	193457.93	-146.4178	61.6447	29.6	4.5
206	20090317	073304.72	-149.8320	65.5858	13.7	4.1
207	20090327	025838.92	-138.4182	61.0289	9.7	5.1
208	20090328	141122.22	-138.4901	61.0222	9.3	4.3
209	20090330	042833.29	-152.6636	56.5456	20.0	4.1
210	20090330	074033.01	-152.5634	56.5785	20.0	4.1
211	20090330	112950.40	-152.6827	56.6030	20.0	4.7
212	20090330	120909.04	-152.6397	56.4716	20.0	4.7
213	20090330	173814.49	-152.8350	56.4621	22.3	5.2
214	20090330	034248.87	-152.7844	56.4936	26.0	5.2
215	20090330	110434.18	-152.4982	56.6461	0.0	4.2
216	20090331	032733.49	-152.5946	56.4568	9.7	4.3
217	20090410	055011.44	-151.7383	63.5085	16.6	4.7
218	20090502	215043.44	-153.5707	56.5042	9.3	4.3
219	20090503	050951.74	-152.2184	56.4914	5.2	4.1
220	20090515	192315.85	-152.2633	56.5217	13.7	5.2
221	20090515	184149.13	-152.3405	56.5063	20.0	4.4
222	20090515	182417.70	-152.3475	56.5287	27.2	5.2
223	20090515	195943.02	-152.2882	56.4717	14.5	4.6
224	20090515	173818.52	-152.2262	56.4444	28.5	4.9
225	20090515	184412.20	-152.1071	56.5616	18.0	4.2
226	20090515	204724.05	-152.2439	56.6123	18.0	4.3
227	20090516	191704.90	-152.3654	56.4498	20.0	4.1

a/a	YYYYMMDD	HHMMSS.FF	Longitude	Latitude	Depth (km)	Magnitude
228	20090516	192003.38	-152.5998	56.4500	20.0	4.4
229	20090516	182226.02	-152.5038	56.5469	20.0	5.3
230	20090516	182120.83	-152.3346	56.3977	15.2	4.9
231	20090516	182231.61	-152.5461	56.4348	15.2	5.5
232	20090516	100112.77	-152.2597	56.3532	29.0	4.3
233	20090516	212927.46	-152.2828	56.5120	19.9	4.6
234	20090516	013521.84	-152.0794	56.5465	18.0	4.5
235	20090517	003024.90	-152.3107	56.4355	20.9	4.4
236	20090517	095837.72	-152.3308	56.3734	21.0	4.3
237	20090518	115739.24	-152.0894	56.5899	18.0	4.1
238	20090607	232435.16	-136.7805	58.7760	11.1	5.1
239	20090725	014342.54	-143.6365	59.4138	14.9	5.1
240	20090725	074605.60	-147.4295	61.3811	17.4	4.3
241	20090814	035601.63	-151.1131	57.1120	6.8	4.3
242	20090904	093036.93	-153.4367	56.1652	27.1	4.8
243	20090921	104125.16	-147.1576	60.9076	23.1	4.6
244	20091108	100312.94	-138.5572	57.7209	19.6	4.3
245	20091227	031244.90	-152.7641	56.5341	18.1	5.3
246	20091228	151407.82	-152.6174	56.5380	22.6	4.6
247	20100212	032252.27	-152.1937	56.5277	19.4	4.8
248	20100219	051246.09	-153.5640	55.9423	23.0	4.1
249	20100219	071804.15	-142.1787	66.2391	10.0	4.1
250	20100219	010420.92	-153.6893	56.0529	23.0	4.1
251	20100222	232942.58	-153.6752	57.0077	25.1	4.9
252	20100314	073801.49	-152.2874	56.2486	10.0	4.2
253	20100314	073810.81	-152.8526	56.7686	10.0	4.4
254	20100323	091546.37	-152.4072	56.3199	20.0	4.2
255	20100513	183054.89	-166.7050	65.5673	10.0	4.3
256	20100531	161938.71	-152.6245	56.4323	23.3	4.4
257	20100613	134305.95	-156.9606	58.0990	15.3	5.3
258	20100616	033357.69	-139.2098	58.1708	14.0	4.7
259	20100620	172808.31	-146.8482	60.8118	24.4	4.6
260	20100708	031549.26	-150.5273	61.8567	16.0	5.0

a/a	YYYYMMDD	HHMMSS.FF	Longitude	Latitude	Depth (km)	Magnitude
261	20100808	211224.49	-149.2204	61.8995	6.5	4.2
262	20100819	000441.87	-154.2406	56.3064	10.0	4.2
263	20100905	104125.83	-145.0828	63.3969	4.0	4.1
264	20100907	055406.22	-151.7533	57.1611	23.4	4.3
265	20100917	204313.33	-149.7241	59.0705	27.0	4.1
266	20101014	125926.89	-140.5991	60.3624	2.2	4.2
267	20101115	182440.39	-149.4091	60.5345	26.0	4.7
268	20101117	195032.47	-152.9221	56.7872	15.1	4.1
269	20101210	054235.94	-135.1625	59.3882	10.0	4.6
270	20101217	120155.16	-151.4067	63.3308	8.4	4.2
271	20110118	151707.87	-151.0237	60.5414	28.7	4.2
272	20110119	024840.07	-152.7068	56.4919	22.0	4.3
273	20110123	025005.52	-150.8229	63.5129	14.0	5.1
274	20110123	233750.56	-150.8786	63.5367	14.5	5.0
275	20110301	103639.77	-149.2521	59.4057	23.6	4.1
276	20110317	170516.63	-137.7561	58.3255	16.5	4.2
277	20110526	084842.04	-154.1914	56.3424	24.0	4.8
278	20110528	134401.42	-151.2547	63.3954	10.0	4.2
279	20110822	113119.84	-154.3630	56.3995	27.0	4.3
280	20110826	044550.30	-152.2241	56.5590	18.0	4.5
281	20110831	213755.15	-151.3732	58.3960	28.0	4.3
282	20110915	020648.66	-138.0609	59.1075	9.4	4.6
283	20110916	140009.70	-147.0816	61.2446	6.2	4.1
284	20110924	105254.09	-152.5178	63.2343	2.8	4.4
285	20111014	130305.82	-145.3581	59.2476	16.2	4.1
286	20111017	061440.91	-167.7583	56.3621	32.3	4.6
287	20111022	143221.46	-152.0113	61.5118	15.7	4.3
288	20111105	204643.38	-136.0260	56.6812	1.1	4.4
289	20111115	074949.07	-150.3443	61.0296	27.6	4.1
290	20111203	093357.19	-150.9720	62.0184	7.9	4.5
291	20111209	012542.36	-145.7531	62.2414	12.7	4.4
292	20120113	013831.27	-149.1404	57.5508	19.4	4.8
293	20120128	181137.42	-147.4825	63.6023	1.1	4.3

a/a	YYYYMMDD	HHMMSS.FF	Longitude	Latitude	Depth (km)	Magnitude
294	20120221	135044.10	-166.5612	67.5811	22.0	5.3
295	20120222	143229.94	-166.4687	67.7210	10.0	4.4
296	20120226	234222.34	-145.7760	62.2593	10.9	4.3
297	20120308	105742.33	-150.9233	60.9935	14.5	4.3
298	20120402	175247.00	-160.2122	68.2547	10.0	4.2
299	20120407	032646.09	-166.5128	67.7271	10.0	4.3
300	20120501	173843.73	-153.3756	56.1174	19.7	4.5
301	20120505	023051.21	-166.5392	67.7693	10.0	4.2
302	20120605	111937.00	-152.6494	62.4059	10.0	4.1
303	20120612	181703.30	-168.3529	56.5109	25.1	4.4
304	20120622	075017.37	-152.9323	56.9417	17.4	4.7
305	20120719	170211.06	-154.3180	59.3518	6.7	4.2
306	20120720	185411.57	-153.4192	56.5484	20.5	5.2
307	20120724	060538.35	-152.9380	56.3446	22.0	4.4
308	20120803	190253.92	-157.6296	57.1521	8.9	4.5
309	20120803	150144.32	-157.6483	57.1365	16.4	4.2
310	20120803	145801.03	-157.6464	57.1692	10.0	4.7
311	20120809	164322.85	-147.5541	60.3253	10.8	4.9
312	20120828	153459.08	-147.7671	63.5651	23.7	4.6
313	20121001	040550.86	-152.1556	56.4401	20.7	4.1
314	20121022	081912.56	-155.1592	58.2530	10.0	4.2
315	20121212	140040.30	-153.8096	56.5919	10.2	4.1
316	20121217	005300.57	-153.9762	56.4751	29.1	4.3
317	20121225	034329.65	-147.3074	61.4592	20.9	4.7
318	20121231	113828.37	-141.0496	61.6012	10.5	4.2
319	20130105	092721.63	-135.1272	55.5944	10.0	4.7
320	20130105	101121.77	-135.3239	55.8543	10.0	4.9
321	20130105	204319.48	-135.3055	55.4465	10.0	4.3
322	20130105	094126.39	-135.2369	55.7211	4.2	4.1
323	20130105	113935.61	-135.1091	55.5023	9.0	4.3
324	20130106	083729.25	-135.1347	55.6735	7.0	4.5
325	20130108	144636.06	-135.4039	56.0507	14.0	4.1
326	20130120	220303.99	-151.3369	63.3066	6.5	4.1

a/a	YYYYMMDD	HHMMSS.FF	Longitude	Latitude	Depth (km)	Magnitude
327	20130226	223342.47	-142.6748	59.4538	2.0	4.3
328	20130302	110029.14	-166.3547	67.6294	35.0	4.3
329	20130310	171105.22	-154.0909	59.2615	7.1	5.0
330	20130325	200244.41	-155.6047	56.0553	24.1	4.8
331	20130411	170050.39	-153.2113	58.8056	4.5	4.2
332	20130514	023340.24	-153.8813	58.7535	6.8	4.1
333	20130525	082930.30	-149.3571	66.3027	10.0	4.3
334	20130610	080554.35	-167.7772	56.4272	19.7	4.9
335	20130620	230605.25	-145.7561	62.2352	3.9	4.5
336	20130714	160451.95	-141.0724	61.5876	1.5	4.1
337	20130714	081517.06	-141.1082	61.6066	7.2	4.5
338	20130715	131656.53	-141.0417	61.5691	6.7	4.4
339	20130715	165949.42	-141.0496	61.5904	1.6	4.2
340	20130718	035259.86	-156.3745	58.1763	8.9	4.5
341	20130818	211925.09	-152.8999	56.9394	3.0	4.2
342	20130823	212858.62	-141.0650	61.5655	3.3	4.6
343	20130828	192926.92	-156.8760	55.0188	24.0	4.3
344	20130901	225207.09	-144.7620	69.1324	5.3	4.6
345	20130912	044103.37	-152.8301	59.7905	15.2	4.5
346	20130921	184234.11	-156.3409	58.1668	7.1	4.4
347	20130922	181149.96	-156.3168	58.1887	7.8	4.5
348	20130926	023535.35	-135.6129	55.8656	14.0	4.3
349	20131003	074748.95	-137.2550	58.5715	10.0	4.2
350	20131008	061805.88	-154.0283	56.5339	29.9	4.1
351	20131011	133559.28	-150.4787	56.9298	35.0	4.1
352	20131011	202425.25	-158.6115	55.5686	33.0	4.4
353	20131119	144420.99	-138.9502	59.5351	11.7	4.3
354	20131207	164408.82	-158.0780	55.3764	17.1	5.5
355	20131224	205647.73	-141.7151	60.2348	9.3	4.3
356	20140225	202438.91	-138.2345	60.9619	11.0	4.3
357	20140305	031316.69	-149.5373	62.1301	32.4	4.4
358	20140327	072833.23	-163.4417	68.1239	10.0	4.3
359	20140328	113908.86	-142.6626	58.5746	23.0	4.1

a/a	YYYYMMDD	HHMMSS.FF	Longitude	Latitude	Depth (km)	Magnitude
360	20140331	131538.88	-152.4229	56.3684	10.0	4.2
361	20140418	184418.93	-162.3453	67.6773	18.4	5.4
362	20140418	230405.46	-144.9626	63.4246	6.1	4.2
363	20140418	213850.04	-162.2803	67.8211	10.0	4.2
364	20140418	185647.54	-162.5017	67.7056	16.7	5.3
365	20140419	084901.39	-162.3513	67.7153	10.0	4.5
366	20140419	113106.83	-162.2622	67.7781	10.0	4.2
367	20140419	113139.62	-162.2652	67.7665	10.0	4.6
368	20140426	061159.00	-162.5893	67.7664	25.0	4.1
369	20140503	095107.78	-162.2935	67.7009	11.5	4.9
370	20140503	101125.01	-162.2787	67.7957	10.0	4.1
371	20140503	104052.28	-162.0715	67.7146	10.0	4.2
372	20140503	111910.02	-162.1602	67.7384	10.0	4.4
373	20140503	095710.21	-162.3252	67.7664	23.5	4.8
374	20140503	115433.50	-162.3038	67.7679	10.0	4.2
375	20140503	085714.03	-162.2178	67.7247	10.0	5.5
376	20140503	095418.96	-162.2383	67.7232	10.0	4.1
377	20140505	115913.32	-162.5015	67.6878	10.0	4.6
378	20140505	121235.26	-162.4329	67.7428	10.0	4.5
379	20140505	121559.28	-162.4641	67.7542	10.0	4.2
380	20140511	105158.46	-162.3774	67.7452	10.0	4.2
381	20140530	062732.97	-162.0797	67.6974	10.0	4.8
382	20140603	040833.72	-162.1504	67.7330	10.0	4.5
383	20140604	115858.62	-136.7789	59.0281	12.9	5.5
384	20140605	054429.12	-140.3081	61.1759	8.9	5.0
385	20140605	053801.45	-140.3318	61.1929	2.5	4.9
386	20140607	031359.89	-162.1591	67.7289	10.0	4.5
387	20140607	044719.76	-162.3160	67.7774	10.0	4.6
388	20140616	120108.72	-162.1460	67.6948	11.8	5.5
389	20140616	125650.87	-161.9548	67.7349	10.0	4.1
390	20140617	130143.40	-162.1518	67.7406	10.0	4.3
391	20140617	143724.52	-148.2251	63.5569	11.0	4.5
392	20140620	003045.02	-162.2666	67.6874	10.0	4.2

a/a	YYYYMMDD	HHMMSS.FF	Longitude	Latitude	Depth (km)	Magnitude
393	20140629	065844.40	-148.5683	63.4954	14.9	4.7
394	20140630	124937.52	-155.6694	55.1731	10.0	4.6
395	20140712	111532.74	-140.2879	61.1597	3.9	4.5
396	20140717	115302.89	-140.3613	60.3411	10.0	4.7
397	20140718	020145.23	-161.7646	67.6123	10.0	4.4
398	20140718	020316.72	-161.7689	67.6308	10.0	4.3
399	20140718	053326.17	-161.7973	67.5945	10.0	4.8
400	20140720	021545.46	-140.3136	60.2849	10.0	4.6
401	20140725	105406.26	-137.1058	58.3654	10.0	4.7
402	20140725	111935.77	-137.0772	58.2952	10.0	4.5
403	20140811	084655.44	-152.5437	64.5909	10.0	4.1
404	20140827	061019.84	-145.4694	59.2705	14.0	5.0
405	20140828	133311.60	-161.9000	67.6018	10.0	4.3
406	20140831	030656.61	-149.0859	65.1286	6.0	4.8
407	20140910	160148.62	-152.1382	62.6247	7.6	4.3
408	20140916	090520.15	-162.5351	67.6857	10.0	4.1
409	20141018	133331.08	-158.3802	55.0369	30.0	4.6
410	20141021	003658.66	-149.0008	65.1193	5.9	4.7
411	20141023	163025.55	-149.0131	65.1189	12.7	4.8
412	20141105	160352.33	-136.2686	59.2052	10.6	4.9
413	20141114	060432.08	-152.9983	56.8120	10.0	4.1
414	20150101	111734.98	-154.0305	56.4060	10.4	4.1
415	20150105	092318.43	-155.3022	57.1016	5.0	4.2
416	20150131	032456.79	-168.9424	56.6380	6.4	4.9
417	20150131	204710.67	-169.0829	56.5536	6.8	5.1
418	20150131	123831.10	-168.9308	56.6266	8.6	5.2
419	20150131	013928.81	-169.0452	56.5528	10.0	4.5
420	20150131	173912.51	-169.1149	56.6553	10.0	5.3
421	20150131	193310.61	-169.0515	56.6418	10.0	4.3
422	20150131	171616.68	-169.0495	56.6659	12.7	4.8
423	20150131	174930.16	-169.1791	56.5972	11.7	4.6
424	20150131	172131.45	-168.9513	56.6319	10.0	4.5
425	20150131	223305.16	-169.1368	56.6370	10.0	4.5

a/a	YYYYMMDD	HHMMSS.FF	Longitude	Latitude	Depth (km)	Magnitude
426	20150131	223833.58	-169.0446	56.6311	10.0	4.2
427	20150131	174649.64	-169.1540	56.6911	18.1	4.2
428	20150201	174031.66	-169.0612	56.6155	6.9	5.2
429	20150201	114338.56	-169.1281	56.5374	10.0	4.1
430	20150201	203813.11	-169.1721	56.5854	10.0	4.4
431	20150201	112025.87	-169.0802	56.6520	10.4	5.3
432	20150201	200746.19	-168.8609	56.5346	9.6	4.6
433	20150202	021327.29	-169.1637	56.6410	10.0	4.2
434	20150202	042913.21	-169.1667	56.6752	10.0	4.4
435	20150206	120408.46	-157.0420	57.0386	4.8	4.4
436	20150209	153447.67	-168.9965	56.6438	10.0	4.2
437	20150214	122047.05	-163.6056	67.9055	0.0	4.1
438	20150214	121822.29	-162.2476	67.7641	10.0	4.5
439	20150218	221507.29	-136.9334	58.3262	10.0	4.2
440	20150308	194305.24	-148.8309	63.4993	10.3	4.2
441	20150403	082929.97	-145.4651	67.6399	10.0	4.5
442	20150518	154910.23	-150.4714	61.9461	28.6	4.4
443	20150521	165645.12	-136.4849	59.5200	14.4	4.2
444	20150626	043950.71	-154.1159	57.8327	23.7	4.9
445	20150701	232013.30	-154.0946	56.6007	24.0	4.7
446	20150727	022154.28	-150.9143	60.9855	20.8	4.1
447	20150810	075358.79	-138.9724	59.5150	8.0	4.3
448	20150811	184829.98	-139.8272	60.0855	15.0	4.1
449	20150902	083307.13	-151.3697	63.2654	16.4	4.3
450	20150908	113438.87	-157.0204	57.0648	10.0	4.7
451	20151006	000851.41	-157.0373	57.0371	4.4	4.2
452	20160117	145231.11	-153.0357	66.3772	10.0	4.2
453	20160118	040554.78	-150.6586	62.0814	6.5	4.8
454	20160124	104236.42	-153.4230	56.9850	28.7	4.1
455	20160205	182839.11	-145.7411	59.6055	0.0	4.1
456	20160222	023043.90	-144.6754	69.1326	10.0	4.1
457	20160305	040724.04	-162.5724	67.6646	10.0	4.4
458	20160402	151700.11	-157.7312	57.1600	9.3	4.2

a/a	YYYYMMDD	HHMMSS.FF	Longitude	Latitude	Depth (km)	Magnitude
459	20160402	090601.51	-157.6218	57.1204	10.0	4.3
460	20160404	140035.10	-157.9860	57.0009	11.6	4.4
461	20160404	133015.92	-158.0528	56.9871	16.0	4.5
462	20160405	031805.63	-157.9092	57.0029	10.4	4.3
463	20160412	205001.75	-162.5256	67.6797	10.0	4.3
464	20160414	032406.90	-151.6078	56.5154	21.0	4.1
465	20160415	085425.61	-151.4728	63.1540	6.2	4.5
466	20160421	101359.92	-151.6453	63.0379	7.8	4.3
467	20160502	133845.43	-144.7183	59.4575	9.3	5.2
468	20160502	043720.97	-157.7870	57.0289	11.3	4.3
469	20160518	032548.37	-151.0346	65.2766	10.8	4.2
470	20160531	123102.06	-157.9227	56.9986	10.8	4.2
471	20160614	125136.73	-158.1479	57.0508	11.1	4.1
472	20160709	083502.78	-165.9011	65.7562	10.0	4.4
473	20160719	124801.76	-157.7459	57.0046	8.2	4.1
474	20160803	150432.42	-139.5575	60.1724	10.7	4.2
475	20160816	195841.12	-157.8613	56.9590	12.4	4.4
476	20160819	173626.50	-146.3741	61.6151	32.6	4.4
477	20160826	231125.73	-148.0349	63.5600	8.7	4.1
478	20160827	151405.78	-158.3601	55.7823	8.2	4.8
479	20160828	025138.14	-150.1615	57.1114	3.4	4.2
480	20160829	042552.99	-151.5782	63.0138	8.1	4.3
481	20160910	023223.52	-153.2562	56.3830	19.5	4.7
482	20160910	025349.28	-153.2414	56.2912	18.9	4.7
483	20160920	111357.24	-147.9186	58.4612	17.2	4.1
484	20160921	221159.87	-157.6670	55.1930	35.0	4.1
485	20161106	194050.14	-148.2012	61.7329	6.8	4.3
486	20161112	215236.56	-157.7081	57.0943	12.5	5.1
487	20161114	203215.12	-157.7431	57.0856	11.4	4.2
488	20161116	142535.19	-137.5820	59.6525	7.6	4.8
489	20161204	131544.49	-150.9475	61.9631	18.0	4.6
490	20161208	101813.17	-150.0092	64.2201	13.4	4.6
491	20170116	205337.23	-136.8193	58.2000	10.0	4.1

a/a	YYYYMMDD	HHMMSS.FF	Longitude	Latitude	Depth (km)	Magnitude
492	20170116	214009.30	-136.8139	58.1223	1.5	4.5
493	20170202	132142.75	-154.3206	56.2079	19.7	4.2
494	20170213	071713.74	-142.7196	62.4964	9.5	5.2
495	20170305	215311.89	-152.2926	57.2343	29.2	4.3
496	20170322	090452.85	-168.8997	65.1546	10.0	4.4
497	20170324	234949.53	-157.5729	57.2127	16.0	4.8
498	20170325	010038.10	-157.5147	57.1705	5.4	4.3
499	20170427	144430.47	-154.9440	57.5333	11.0	4.5
500	20170427	171032.39	-154.9600	57.5285	10.8	4.1
501	20170429	111548.90	-151.1656	63.1225	11.9	5.2
502	20170430	110356.87	-154.9369	57.5221	9.9	4.2
503	20170501	145949.78	-136.8991	59.8820	0.0	4.1
504	20170501	123658.49	-136.7688	59.7823	3.6	4.3
505	20170501	143540.77	-136.7037	59.7904	1.7	4.2
506	20170501	145920.90	-136.9250	59.8140	16.0	5.0
507	20170501	142024.38	-136.6292	59.7772	4.1	5.5
508	20170501	155031.85	-136.6574	59.7634	4.0	4.1
509	20170501	204846.59	-136.6538	59.8354	4.6	4.1
510	20170501	124918.98	-136.8380	59.8780	8.1	5.2
511	20170501	150120.89	-136.6306	59.8653	10.0	4.1
512	20170501	152147.09	-136.7041	59.8428	10.0	4.1
513	20170501	145922.45	-136.6481	59.7953	12.3	4.9
514	20170502	080929.73	-136.7847	59.7969	1.2	4.1
515	20170502	123645.33	-136.7688	59.7704	10.0	4.1
516	20170502	174642.95	-136.6499	59.8138	10.0	4.2
517	20170502	131354.44	-151.1155	63.1339	11.3	4.2
518	20170504	031345.44	-136.6826	59.8032	10.0	4.4
519	20170505	052130.84	-136.6292	59.8007	3.8	4.3
520	20170508	050902.30	-146.9213	65.2576	10.6	4.1
521	20170511	030624.22	-152.6319	56.8452	20.7	4.2
522	20170511	144109.54	-152.5560	57.0570	5.0	4.1
523	20170511	143631.29	-152.6029	56.8783	19.0	5.4
524	20170512	005457.44	-152.6201	56.8375	4.2	4.3

a/a	YYYYMMDD	HHMMSS.FF	Longitude	Latitude	Depth (km)	Magnitude
525	20170521	193339.56	-136.6721	59.7681	5.0	4.2
526	20170529	081359.41	-147.9303	61.8343	23.2	4.2
527	20170614	205614.23	-168.3804	56.5096	14.3	4.4
528	20170622	152138.45	-146.8540	61.2666	22.5	4.2
529	20170629	200526.24	-168.0421	65.2848	25.6	4.2
530	20170711	093027.41	-147.3348	60.4234	20.0	4.4
531	20170812	144121.11	-151.8735	55.4005	10.0	4.7
532	20170815	014233.35	-151.8134	55.3175	9.1	4.2
533	20170818	044435.69	-136.3941	59.0023	11.6	4.1
534	20170905	082359.12	-152.9205	55.7332	11.8	4.4
535	20170912	064343.34	-157.0626	55.2018	8.4	4.5
536	20170916	233802.21	-136.7936	59.8659	6.5	5.1
537	20170921	221520.97	-148.8756	62.7831	20.3	4.2
538	20171007	160714.52	-151.4919	63.1078	9.3	4.2
539	20171011	060520.58	-141.0809	61.5870	10.3	4.1
540	20171015	065031.45	-168.4448	56.5154	16.6	4.2
541	20171016	135438.36	-172.4798	63.1655	13.5	4.5
542	20171023	185004.77	-172.7624	64.9305	10.0	4.5
543	20171105	173259.37	-173.1714	64.8571	10.0	4.6
544	20171105	222743.41	-140.0544	61.4049	3.8	4.1
545	20171105	232603.79	-172.9831	64.8243	17.1	4.1
546	20171113	160037.57	-142.6560	60.5610	19.1	4.2
547	20171115	115203.65	-159.2482	55.0847	31.8	4.7
548	20171117	160931.71	-157.8048	56.9826	12.8	4.2
549	20171127	221830.47	-147.4303	60.5552	16.6	5.3
550	20171205	144532.46	-149.7029	61.4606	30.8	4.2
551	20171219	001016.33	-136.7334	59.8411	10.0	4.1
552	20171230	114316.28	-149.0240	63.8011	7.1	4.1
553	20180116	044102.89	-172.2967	63.1343	12.5	4.5
554	20180116	044610.35	-172.2829	63.1468	13.4	4.1
555	20180116	105055.08	-172.4926	63.1453	11.7	4.1
556	20180118	024747.70	-136.7916	59.7913	10.0	4.5
557	20180126	211004.67	-148.1374	61.7511	3.5	4.3

a/a	YYYYMMDD	HHMMSS.FF	Longitude	Latitude	Depth (km)	Magnitude
558	20180201	071710.03	-153.0316	56.9181	0.0	4.1
559	20180220	091045.40	-135.1700	61.6800	0.0	4.1
560	20180222	221524.28	-157.3026	55.2760	20.3	4.4
561	20180223	033114.64	-158.8542	55.5542	26.8	5.0
562	20180324	055243.44	-153.3455	56.1123	25.1	4.6
563	20180324	060006.60	-153.3355	56.1403	26.3	4.1
564	20180411	164412.12	-147.6133	60.5790	6.6	4.1
565	20180412	234432.85	-138.2663	60.8665	10.0	4.2
566	20180420	074708.51	-155.4862	57.6491	16.8	4.2
567	20180502	071557.02	-141.3021	58.7642	9.8	4.2
568	20180511	013900.60	-146.3915	67.4173	10.8	4.4
569	20180511	014006.91	-146.3667	67.4203	8.4	4.4
570	20180515	203153.14	-140.5385	61.1665	5.8	4.1
571	20180516	124955.53	-157.5196	66.3494	7.2	4.3
572	20180527	183041.04	-153.5417	55.3675	12.0	4.1
573	20180529	154246.82	-149.0813	62.7579	13.9	4.3
574	20180703	070709.78	-157.9463	57.0387	6.2	4.6
575	20180724	041242.37	-157.5477	55.0931	3.0	4.2
576	20180724	041709.92	-157.5911	55.0870	26.1	4.5
577	20180724	041902.04	-157.5155	55.1127	19.6	4.1
578	20180812	151838.00	-144.6580	69.5268	5.6	4.8
579	20180812	154225.12	-144.3156	69.5500	5.2	4.4
580	20180812	214739.02	-144.1860	69.4506	3.7	4.3
581	20180812	151420.73	-144.7372	69.5722	2.9	5.0
582	20180812	153449.60	-144.6773	69.5262	2.1	4.4
583	20180812	221113.76	-144.1437	69.4212	2.9	4.1
584	20180812	160209.29	-144.9518	69.5493	1.0	5.5
585	20180812	232938.46	-144.1184	69.4182	6.6	4.3
586	20180812	235948.97	-144.1484	69.5289	18.2	4.1
587	20180812	150407.42	-145.1628	69.5641	4.9	4.2
588	20180812	183644.05	-144.7123	69.5347	4.3	5.1
589	20180812	205643.48	-144.3410	69.4504	4.5	4.1
590	20180812	213803.34	-144.1327	69.4577	4.3	4.5

a/a	YYYYMMDD	HHMMSS.FF	Longitude	Latitude	Depth (km)	Magnitude
591	20180812	154206.16	-144.7802	69.5357	2.5	4.1
592	20180812	164439.53	-144.5089	69.4709	0.9	4.2
593	20180812	220016.98	-144.4964	69.4783	1.4	4.6
594	20180812	224625.98	-144.1509	69.4256	7.0	4.4
595	20180812	153337.36	-144.3907	69.5676	9.5	4.1
596	20180813	063725.33	-144.2148	69.4732	10.0	4.3
597	20180813	193608.77	-144.4590	69.5469	17.3	5.0
598	20180813	054147.11	-144.1909	69.4679	12.0	4.2
599	20180813	133543.90	-145.3279	69.6505	22.7	4.3
600	20180813	110512.71	-144.6331	69.5344	15.6	4.4
601	20180813	054356.16	-144.3482	69.5186	8.2	4.3
602	20180813	095555.20	-144.3483	69.4623	10.8	4.5
603	20180813	050018.65	-144.4359	69.5187	13.2	4.1
604	20180813	052232.14	-144.1824	69.4583	7.7	4.1
605	20180813	085311.77	-144.3751	69.4703	7.4	4.3
606	20180813	095658.70	-144.7871	69.5355	7.3	4.5
607	20180814	165311.60	-144.7699	69.5651	10.0	4.6
608	20180814	144957.37	-144.2064	69.4665	6.7	4.2
609	20180816	181409.52	-153.8528	55.4007	14.8	4.4
610	20180816	063230.06	-144.4262	69.4902	6.5	4.3
611	20180816	072239.13	-144.2275	69.5342	11.1	4.5
612	20180818	045257.36	-145.2578	69.6377	14.5	4.1
613	20180818	070601.63	-144.2300	69.5127	12.3	4.2
614	20180818	043936.55	-144.2966	69.4826	15.1	4.5
615	20180819	133223.56	-144.9148	69.5810	18.5	4.4
616	20180819	193007.51	-145.4517	69.6396	21.1	4.2
617	20180820	093347.99	-145.1864	69.5727	8.7	4.4
618	20180821	224733.99	-172.6441	64.4297	10.0	4.2
619	20180823	043038.99	-144.3146	69.4957	11.7	4.5
620	20180828	111321.70	-144.8964	69.5602	18.2	4.1
621	20180828	151843.46	-150.5718	65.1780	16.9	4.7
622	20180830	224951.61	-144.2569	69.5462	4.0	4.1
623	20180901	064119.71	-144.9367	69.5759	19.1	4.8

a/a	YYYYMMDD	HHMMSS.FF	Longitude	Latitude	Depth (km)	Magnitude
624	20180905	040351.28	-144.4289	69.7026	0.0	4.1
625	20180910	233710.62	-144.5924	69.5864	12.4	4.2
626	20180914	050215.51	-147.0843	69.0586	13.2	4.2
627	20180914	172929.45	-150.6420	58.5984	34.6	4.3
628	20180918	124056.96	-144.1598	69.5136	10.8	5.1
629	20180921	042826.31	-143.9369	69.4556	5.0	4.1
630	20181001	005824.95	-146.3174	69.2103	7.3	4.2
631	20181003	032937.54	-148.9191	64.8979	19.7	4.3
632	20181014	235314.77	-156.3956	67.7739	10.5	5.3
633	20181016	112212.81	-146.3975	61.5360	30.1	4.3
634	20181016	164516.74	-145.0505	69.5833	16.4	4.1
635	20181018	001710.97	-146.3403	69.0211	7.4	4.1
636	20181027	165728.35	-151.5744	65.2283	14.8	5.3
637	20181113	152642.06	-150.9489	64.7981	19.2	4.1
638	20181116	012649.16	-166.7790	65.5676	10.0	4.2
639	20181116	010530.19	-166.8070	65.5781	8.9	4.6
640	20181116	235603.25	-168.5851	56.5647	18.8	4.3
641	20181116	033115.09	-144.3921	69.5355	7.9	4.1
642	20181117	095701.61	-168.6224	56.5760	20.5	4.2
643	20181117	172243.70	-168.6276	56.6546	18.2	4.2
644	20181201	124453.69	-149.8976	61.4731	34.4	4.5
645	20181201	135250.09	-150.0782	61.4012	34.0	4.1
646	20181201	070728.39	-150.0560	61.4030	22.8	4.5
647	20181207	152257.64	-144.9470	69.5942	6.9	4.5
648	20181208	163615.58	-149.9191	61.4704	29.5	4.1
649	20181218	023143.87	-144.7349	69.6662	10.0	4.7
650	20181227	142113.00	-150.1027	61.2900	35.0	4.9
651	20181230	071411.89	-144.9437	69.6613	10.0	4.6
652	20190106	034534.53	-153.2799	65.4070	17.1	5.1
653	20190109	065139.56	-144.6726	69.1016	14.6	4.5
654	20190110	193638.17	-144.7034	69.1454	11.0	4.1
655	20190112	171406.99	-144.6465	69.1308	12.9	4.2
656	20190114	142314.12	-145.0837	69.6092	2.9	4.2

a/a	YYYYMMDD	HHMMSS.FF	Longitude	Latitude	Depth (km)	Magnitude
657	20190114	004119.26	-145.0273	69.6240	5.6	4.9
658	20190115	164444.66	-144.1801	69.5414	10.0	4.2
659	20190201	150938.66	-157.7269	57.0426	13.2	4.4
660	20190203	174030.06	-144.3773	69.5001	6.3	4.2
661	20190206	200446.04	-150.0298	61.4085	34.3	4.1
662	20190210	133548.27	-157.2255	66.3077	7.7	4.8
663	20190306	213313.99	-157.2186	66.3108	9.1	5.4
664	20190310	040747.19	-145.4573	69.6304	13.1	4.2
665	20190310	224010.80	-141.6003	59.8048	0.6	4.2
666	20190311	000718.29	-141.6326	59.7914	13.8	4.8
667	20190313	024225.18	-144.4701	69.5209	12.8	4.3
668	20190315	055836.02	-151.1263	63.2812	9.0	4.2
669	20190318	074641.17	-154.0710	62.0778	8.1	4.2
670	20190326	212718.71	-157.2470	66.3061	8.5	5.2
671	20190327	073839.34	-157.2143	66.3133	8.9	4.4
672	20190328	084004.15	-157.1856	66.2456	5.9	4.1
673	20190407	030001.36	-154.1992	56.2538	15.0	4.6
674	20190408	152414.22	-153.3526	65.3974	11.5	4.6
675	20190411	104245.60	-149.1761	64.7370	18.9	4.4
676	20190416	050746.94	-157.2352	66.3091	9.0	4.7
677	20190423	153243.41	-157.2105	66.2945	7.3	4.5
678	20190501	193645.77	-156.4973	67.3542	7.3	4.1
679	20190509	052958.62	-157.2369	66.2969	7.4	4.4
680	20190607	150138.30	-151.1941	58.2802	3.9	4.1
681	20190607	145731.26	-151.2381	58.2782	29.3	4.9
682	20190615	063135.79	-157.2078	66.2949	6.3	4.5
683	20190702	181707.67	-157.1808	66.2704	7.9	4.5
684	20190703	011319.45	-166.1906	65.8176	23.0	4.1
685	20190703	043822.60	-144.6872	69.1167	13.9	5.0
686	20190703	045855.03	-144.6355	69.1114	12.8	4.6
687	20190704	125136.38	-135.1206	55.4477	0.4	4.3
688	20190707	160332.08	-149.8954	56.1572	21.5	4.3
689	20190708	084409.39	-154.0311	56.2632	0.3	4.1

a/a	YYYYMMDD	HHMMSS.FF	Longitude	Latitude	Depth (km)	Magnitude
690	20190708	232027.20	-144.6222	69.1057	13.4	4.2
691	20190814	010828.30	-137.6707	58.0274	0.0	4.1
692	20190830	043659.58	-136.9493	59.0740	2.4	4.2
693	20190901	043225.11	-136.9323	59.2059	0.0	4.6
694	20190903	053925.11	-159.6189	55.2693	0.0	4.3
695	20190905	180058.95	-146.6318	68.8743	0.0	4.1
696	20190905	090440.01	-151.7711	58.0540	0.0	4.1
697	20190906	233229.74	-152.3297	64.8465	0.0	4.1
698	20190908	040139.86	-140.6265	60.0258	1.2	4.5
699	20190920	165712.84	-151.9053	55.5025	0.0	4.1
700	20191014	121350.20	-153.2600	56.3600	10.0	4.8
701	20191018	005831.90	-156.9900	66.3600	10.0	5.3
702	20191018	130902.40	-157.1800	66.4600	10.0	5.1

Table A-2. Mean V_{SZ} derived from the analysis, topographic slope proxy V_{S30} (Slope V_{S30}), measured V_{S30} and V_{S30} correlated to the mean V_{SZ} for the sites used in the analysis. The station coordinates and the depth extent resolvable z(m) from the analysis are also provided.

Site	Latitude	Longitude	z (m)	Mean V_{SZ} (m/s)	Slope V_{S30} (m/s)	Measured V_{S30} (m/s)	*Estimated* V_{S30} (m/s)	NEHRP	Geologic Description
ACH	-155.3280	58.2100	225	2246	900	-	1779	A	Naknek Formation and Kotsina Congolomerate (Upper Jurassic Tithonian to Oxfordian)
AD09	-149.5050	61.3055	109	1094	575	-	706	C	Unconsolidated surficial deposits undivided (Quaternary)
ALPI	-149.5400	61.2448	227	2265	900	-	1815	A	McHugh and Uyak Complexes (Late Cretaceous)
ANCK	-155.4960	58.1981	220	2203	900	-	1699	A	Naknek Formation and Kotsina Congolomerate (Upper Jurassic Tithonian to Oxfordian)
ARTY	-149.4380	61.3970	222	2218	514	-	1726	A	-
AUL	-153.4380	59.3816	168	1681	900	-	1031	C	Youngest volcanic rocks (Quaternary and latest Tertiary?)
AVAL	-149.3470	60.3755	285	2851	452	-	2673	A	Chugach flysch (Upper Cretaceous)
AWPL	-149.4410	61.5830	186	1859	313	-	1131	C	Unconsolidated surficial deposits undivided (Quaternary)
BAGL	-142.0920	60.4896	204	2037	431	-	1289	B	Volcanic rocks of the Orca Group and Ghost Rocks Formation (Tertiary Eocene to Paleocene)
BAL	-142.3460	61.0360	211	2113	898	-	1462	A	Saint Elias suite of Gordey and Makepeace (2003) and similar rocks (Early Cretaceous and Late Jurassic)
BARK	-142.4930	60.4030	187	1867	900	-	1136	B	Kulthieth Formation (Tertiary Eocene)
BARN	-141.6620	61.0595	235	2350	900	-	1996	A	Strelna Metamorphics and related rocks (early Permian to Middle Pennsylvanian)
BBB	-147.0480	61.1216	208	2077	481	-	1377	-	-
BCP	-139.6370	59.9534	209	2089	900	-	1406	A	Yakutat Group undivided (Lower Cretaceous and Upper Jurassic?)
BERG	-143.7040	60.3923	204	2040	770	-	1296	B	Kulthieth Formation (Tertiary Eocene)
BESE	-134.8560	58.5792	233	2332	-	-	1955	A	Gravina-Nuzotin unit (Lower Cretaceous and Upper Jurassic)
BGLC	-143.2840	60.1205	125	1254	372	-	795	-	-
BIGB	-149.8170	61.5919	135	1349	300	-	842	C	Unconsolidated surficial deposits undivided (Quaternary)
BLAK	-148.4170	60.7746	257	2568	519	-	2287	A	Chugach flysch (Upper Cretaceous)
BMR	-144.6050	60.9677	225	2255	900	-	1796	A	Chugach flysch (Upper Cretaceous)
BPAW	-150.9870	64.0997	228	2283	523	-	1851	A	Granodiorite to quartz monzodiorite (Tertiary Paleocene or Late

Site	Latitude	Longitude	z (m)	Mean V_{SZ} (m/s)	Slope V_{S30} (m/s)	Measured V_{S30} (m/s)	*Estimated* V_{S30} (m/s)	NEHRP	Geologic Description
									Cretaceous Maastrichtian)
BRG1	-145.8700	63.5983	273	2729	531	-	2497	C	Unconsolidated surficial deposits undivided (Quaternary)
BRLK	-150.9060	59.7511	242	2424	745	-	2141	A	McHugh and Uyak Complexes (Late Cretaceous)
BVCY	-140.8610	62.4141	169	1690	306	-	1036	-	-
BWN	-149.2990	64.1732	107	1071	587	-	682	C	Nenana Gravel (Tertiary Pliocene and upper Miocene)
BYR	-150.2320	62.6892	154	1539	715	-	947	C	Unconsolidated surficial deposits undivided (Quaternary)
C23K	-150.6130	69.8360	167	1666	471	-	1022	B	Sagavanirktok Formation (Tertiary Miocene to Paleocene)
C24K	-148.7010	69.7200	147	1469	266	-	906	C	Unconsolidated surficial deposits undivided (Quaternary)
CAPN	-151.1540	60.7683	125	1246	453	-	791	C	Unconsolidated surficial deposits undivided (Quaternary)
CAST	-152.0840	63.4188	242	2425	482	-	2142	A	Felsic granitic rocks (Tertiary Paleocene or Late Cretaceous Maastrichtian)
CASW	-150.0530	62.0056	99	987	310	-	610	C	Unconsolidated surficial deposits undivided (Quaternary)
CCB	-147.8050	64.6453	287	2873	483	-	2706	-	-
CHI	-155.6220	55.8218	205	2049	377	-	1316	B	Sitkinak Formation (Tertiary Oligocene)
CHUM	-152.3150	63.8827	128	1275	487	-	805	-	-
CNP	-151.2370	59.5251	234	2343	870	-	1981	A	McHugh and Uyak Complexes (Late Cretaceous)
COLA	-147.8620	64.8736	181	1811	454	-	1104	C	Unconsolidated surficial deposits undivided (Quaternary)
COLD	-150.2070	67.2269	271	2709	524	-	2469	-	-
CRQ	-143.0930	60.7523	201	2015	565	-	1244	C	Unconsolidated surficial deposits undivided (Quaternary)
CTG	-141.3400	60.9649	218	2177	900	-	1629	C	Unconsolidated surficial deposits undivided (Quaternary)
CUT	-150.2620	62.4058	86	860	358	-	555	C	Unconsolidated surficial deposits undivided (Quaternary)
CYK	-142.4870	60.0823	144	1445	260	-	893	C	Unconsolidated surficial deposits undivided (Quaternary)
D24K	-148.8230	69.1532	196	1955	419	-	1188	C	Unconsolidated surficial deposits undivided (Quaternary)
DCPH	-138.2150	59.0906	232	2321	686	-	1932	A	Me_lange of the Yakutat Group (Cretaceous and Jurassic?)
DEVL	-149.5940	60.5508	229	2292	424	-	1869	C	Unconsolidated surficial deposits undivided (Quaternary)

Site	Latitude	Longitude	z (m)	Mean V_{SZ} (m/s)	Slope V_{S30} (m/s)	Measured V_{S30} (m/s)	*Estimated* V_{S30} (m/s)	NEHRP	Geologic Description
DH1	-148.3830	63.3734	233	2332	710	-	1955	A	Flysch (Upper and Lower? Cretaceous)
DH3	-147.1440	63.0345	201	2006	900	-	1226	C	Unconsolidated surficial deposits undivided (Quaternary)
DH97	-147.8550	63.2667	214	2138	559	-	1526	-	-
DHY	-147.3760	63.0753	213	2134	680	-	1514	-	-
DIV	-145.7750	61.1292	237	2372	900	-	2048	A	Chugach flysch (Upper Cretaceous)
DOT	-144.0700	63.6482	183	1825	792	-	1112	A	Alaska Range melange (Cretaceous)
E17K	-161.8260	67.0820	212	2115	653	-	1468	A	Marble of Tukpahlearik Creek (Devonian to Ordovician)
E23K	-149.6160	68.0584	279	2787	900	-	2579	A	Beaucoup Formation undivided (Devonian)
E24K	-148.4870	68.0748	222	2220	900	-	1730	C	Unconsolidated surficial deposits undivided (Quaternary)
E25K	-145.5680	68.1207	185	1850	180	-	1126	C	Unconsolidated surficial deposits undivided (Quaternary)
EFS	-149.7810	63.5581	132	1318	451	-	826	C	Unconsolidated surficial deposits undivided (Quaternary)
EGAK	-141.1580	64.7774	251	2511	379	-	2230	C	Unconsolidated surficial deposits undivided (Quaternary)
EYAK	-145.7500	60.5487	207	2069	605	-	1361	B	Sedimentary rocks of the Orca Group (Tertiary Eocene to Paleocene)
F18K	-159.6510	66.6001	152	1520	180	-	935	C	Unconsolidated surficial deposits undivided (Quaternary)
F19K	-157.7730	66.8332	175	1747	452	-	1068	A	Andesitic volcanic rocks (Early Cretaceous and Late Jurassic)
FA01	-147.9370	64.8348	179	1794	372	-	1094	C	Unconsolidated surficial deposits undivided (Quaternary)
FA02	-148.0090	64.8456	130	1296	458	-	814	C	Unconsolidated surficial deposits undivided (Quaternary)
FA09	-147.8170	64.8377	135	1348	211	-	842	C	Unconsolidated surficial deposits undivided (Quaternary)
FA10	-147.7780	64.8186	52	518	180	-	407	C	Unconsolidated surficial deposits undivided (Quaternary)
FIB	-150.1780	61.1656	131	1314	391	-	824	C	Unconsolidated surficial deposits undivided (Quaternary)
FID	-146.5990	60.7277	247	2471	900	-	2189	B	Sedimentary rocks of the Orca Group (Tertiary Eocene to Paleocene)
FRB	-148.6990	69.7162	204	2041	266	-	1299	C	Unconsolidated surficial deposits undivided (Quaternary)
FYU	-145.2340	66.5657	97	973	211	-	604	C	Unconsolidated surficial deposits undivided (Quaternary)
G15K	-164.0390	64.9941	301	3010	723	-	2979	A	Marble graphitic rocks and schist (Devonian to Ordovician?)

Site	Latitude	Longitude	z (m)	Mean V_{SZ} (m/s)	Slope V_{S30} (m/s)	Measured V_{S30} (m/s)	*Estimated* V_{S30} (m/s)	NEHRP	Geologic Description
G16K	-162.3550	65.3936	239	2391	513	-	2094	C	Unconsolidated surficial deposits undivided (Quaternary)
G22K	-151.5070	66.9214	143	1431	212	-	885	C	Unconsolidated surficial deposits undivided (Quaternary)
G24K	-147.4750	66.7004	236	2359	515	-	2017	A	Igneous rocks (Angayucham) (Jurassic to Devonian)
G25K	-146.1010	66.7653	269	2688	234	-	2440	C	Unconsolidated surficial deposits undivided (Quaternary)
GAMB	-171.7040	63.7758	225	2250	-	-	1786	C	Unconsolidated surficial deposits undivided (Quaternary)
GCSA	-156.8790	64.7461	116	1163	180	-	748	C	Unconsolidated surficial deposits undivided (Quaternary)
GHO	-148.9260	61.7710	242	2421	900	-	2139	A	Matanuska Formation and correlative rocks (Upper Cretaceous to upper Lower Cretaceous)
GLB	-143.8120	61.4417	235	2346	503	-	1988	-	-
GLI	-147.0960	60.8792	181	1814	900	-	1106	B	Volcanic rocks of the Orca Group and Ghost Rocks Formation (Tertiary Eocene to Paleocene)
GNR	-148.9780	63.8345	181	1810	535	-	1103	-	-
GOAT	-144.7290	60.1369	197	1966	600	-	1194	-	-
GOO	-149.2710	63.2286	38	380	417	-	342	C	Unconsolidated surficial deposits undivided (Quaternary)
GRIN	-143.3210	60.2805	182	1819	900	-	1108	B	Redwood and Poul Creek Formations (Tertiary Miocene to Eocene?)
GRNC	-141.7560	60.7315	270	2696	900	-	2451	-	-
H21K	-152.8050	65.6571	238	2382	501	-	2072	C	Unconsolidated surficial deposits undivided (Quaternary)
H22K	-151.3770	65.8937	202	2021	330	-	1256	A	Pelitic and quartzitic schist of the Ruby terrane (early Paleozoic to Proterozoic?)
H23K	-149.5430	65.8251	224	2243	521	-	1772	C	Unconsolidated surficial deposits undivided (Quaternary)
H24K	-147.8780	65.8371	219	2194	568	-	1677	-	-
H25L	-145.8190	66.2670	146	1460	234	-	901	C	Unconsolidated surficial deposits undivided (Quaternary)
HARP	-145.1570	62.3986	92	916	249	-	579	C	Unconsolidated surficial deposits undivided (Quaternary)
HDA	-146.9480	64.4091	224	2239	525	-	1766	C	Unconsolidated surficial deposits undivided (Quaternary)
HIN	-146.5030	60.3960	180	1803	900	-	1100	B	Sedimentary rocks of the Orca Group (Tertiary Eocene to Paleocene)
HMT	-144.2620	60.3351	168	1677	552	-	1029	B	Kulthieth Formation (Tertiary Eocene)

Site	Latitude	Longitude	z (m)	Mean V_{SZ} (m/s)	Slope V_{S30} (m/s)	Measured V_{S30} (m/s)	*Estimated* V_{S30} (m/s)	NEHRP	Geologic Description
HOM	-151.6520	59.6572	143	1425	693	-	882	B	Kenai Group undivided (Tertiary Miocene to Oligocene)
HOPE	-149.5980	60.8738	260	2603	846	-	2323	C	Unconsolidated surficial deposits undivided (Quaternary)
HYT	-137.5070	60.8267	235	2355	900	-	2007	-	-
I21K	-151.9820	65.1800	206	2062	471	-	1345	B	Coal-bearing sedimentary rocks (Tertiary Pliocene to Eocene?)
I23K	-149.3600	65.1479	137	1375	433	-	855	A	Flysch and quartzite Kandik Group and equivalent (Lower Cretaceous Albian to Valanginian)
ICT	-148.8360	69.0223	212	2123	545	-	1487	A	Torok Formation (Cretaceous Cenomanian to Aptian)
ISLE	-142.3410	60.6020	178	1782	580	-	1088	A	Chugach flysch (Upper Cretaceous)
J19K	-155.6210	63.9940	89	894	547	-	570	B	Cherty tuff and breccia (Angayucham) (Jurassic to Mississippian)
J20K	-154.1470	64.1767	245	2448	522	-	2166	-	-
J25K	-145.3700	64.6130	294	2942	628	-	2811	-	-
JIS	-134.3850	58.2758	294	2941	-	-	2810	A	Gabbro and diorite of southeast Alaska (Cretaceous)
K204	-150.0120	61.1758	75	751	280	-	509	C	Unconsolidated surficial deposits undivided (Quaternary)
K20K	-154.0700	63.3569	218	2183	526	-	1647	-	-
K211	-149.8580	61.1491	28	282	286	394	290	C	Unconsolidated surficial deposits undivided (Quaternary)
K212	-149.7930	61.1556	99	990	318	514	611	C	Unconsolidated surficial deposits undivided (Quaternary)
K213	-149.8590	61.1128	93	930	344	354	585	C	Unconsolidated surficial deposits undivided (Quaternary)
K215	-149.7520	61.0862	49	492	550	412	396	C	Unconsolidated surficial deposits undivided (Quaternary)
K221	-149.9510	61.1525	115	1147	212	-	738	C	Unconsolidated surficial deposits undivided (Quaternary)
K222	-149.8370	61.0876	107	1072	478	-	683	C	Unconsolidated surficial deposits undivided (Quaternary)
K24K	-145.7780	63.8036	136	1359	553	-	847	C	Unconsolidated surficial deposits undivided (Quaternary)
KABU	-155.2840	58.2702	148	1479	801	-	911	A	Naknek Formation and Kotsina Congolomerate (Upper Jurassic Tithonian to Oxfordian)
KAHG	-154.5480	58.4933	248	2477	766	-	2195	A	Naknek Formation and Kotsina Congolomerate (Upper Jurassic Tithonian to Oxfordian)
KAI	-144.4190	59.9268	239	2391	493	-	2093	C	Yakataga and Tugidak Formations (Quaternary and uppermost Tertiary)

Site	Latitude	Longitude	z (m)	Mean V_{SZ} (m/s)	Slope V_{S30} (m/s)	Measured V_{S30} (m/s)	*Estimated* V_{S30} (m/s)	NEHRP	Geologic Description
KAKN	-155.0630	58.2963	233	2332	900	-	1955	A	Naknek Formation and Kotsina Congolomerate (Upper Jurassic Tithonian to Oxfordian)
KASH	-150.0820	61.8636	100	1000	366	-	615	C	Unconsolidated surficial deposits undivided (Quaternary)
KD00	-152.4480	57.4413	152	1518	474	-	934	B	Ghost Rocks sedimentary rocks (Tertiary Paleocene and Upper Cretaceous)
KDAK	-152.5830	57.7828	195	1952	668	-	1186	A	Chugach flysch (Upper Cretaceous)
KHIT	-143.2510	60.4427	148	1484	900	-	914	-	-
KIAG	-142.3610	60.9231	237	2371	900	-	2047	A	McHugh and Uyak Complexes (Late Cretaceous)
KLU	-145.9230	61.4924	197	1970	900	-	1196	C	Unconsolidated surficial deposits undivided (Quaternary)
KNK	-148.4580	61.4131	231	2308	458	-	1903	A	Chugach flysch (Upper Cretaceous)
KOTZ	-162.6000	66.8951	231	2308	302	-	1903	C	Unconsolidated surficial deposits undivided (Quaternary)
KT07	-153.9810	57.5375	257	2568	600	-	2287	A	Chugach flysch (Upper Cretaceous)
KTH	-150.9230	63.5527	205	2049	706	-	1315	-	-
KULT	-142.7230	60.2474	180	1804	900	-	1100	B	Redwood and Poul Creek Formations (Tertiary Miocene to Eocene?)
L19K	-154.8540	62.1816	138	1380	629	-	858	A	Farewell platform facies (Upper Devonian Frasnian to Neoproterozoic)
L20K	-153.8800	62.4787	340	3396	506	-	5598	A	Limestone of the Mystic structural complex (Devonian)
L26K	-143.3480	63.0254	238	2376	459	-	2057	C	Unconsolidated surficial deposits undivided (Quaternary)
L27K	-141.8270	63.0618	242	2423	777	-	2140	-	-
LMW	-148.5110	65.5114	257	2568	522	-	2287	A	Cascaden Ridge and Beaver Bend combined correlative units (Devonian)
LOGN	-141.0050	60.8241	219	2190	900	-	1667	A	Strelna Metamorphics and related rocks (early Permian to Middle Pennsylvanian)
LSUM	-149.4810	60.6717	234	2344	900	-	1983	A	Chugach flysch (Upper Cretaceous)
LVG	-148.5510	65.5220	232	2322	350	-	1933	C	Unconsolidated surficial deposits undivided (Quaternary)
M110	-148.1850	63.3060	232	2317	445	-	1924	C	Unconsolidated surficial deposits undivided (Quaternary)
M19K	-154.3910	61.9037	255	2553	555	-	2272	C	Unconsolidated surficial deposits undivided (Quaternary)
M20K	-153.1320	61.8823	229	2287	900	-	1860	C	Unconsolidated surficial deposits undivided (Quaternary)

Site	Latitude	Longitude	z (m)	Mean V_{SZ} (m/s)	Slope V_{S30} (m/s)	Measured V_{S30} (m/s)	*Estimated* V_{S30} (m/s)	NEHRP	Geologic Description
M22K	-150.1200	61.7531	58	582	257	-	436	C	Unconsolidated surficial deposits undivided (Quaternary)
M26K	-142.9960	62.4013	210	2098	845	-	1427	C	Unconsolidated surficial deposits undivided (Quaternary)
M27K	-141.8780	62.3579	234	2340	715	-	1974	A	Gravina-Nuzotin unit (Lower Cretaceous and Upper Jurassic)
MCAR	-143.0240	61.3836	170	1696	507	-	1039	C	Unconsolidated surficial deposits undivided (Quaternary)
MCK	-148.9370	63.7318	185	1854	742	-	1128	C	Unconsolidated surficial deposits undivided (Quaternary)
MDM	-148.2320	64.9602	214	2139	614	-	1527	A	Quartzite and pelitic schist (Devonian and older)
MEN1	-143.6430	62.9284	177	1769	722	-	1080	C	Unconsolidated surficial deposits undivided (Quaternary)
MENT	-143.7190	62.9380	138	1377	900	-	857	C	Unconsolidated surficial deposits undivided (Quaternary)
MESA	-141.9510	60.1782	165	1653	794	-	1015	-	-
MHR	-149.8650	62.8603	174	1741	357	-	1065	C	Unconsolidated surficial deposits undivided (Quaternary)
MLR	-145.4950	62.8165	220	2200	446	-	1694	C	Unconsolidated surficial deposits undivided (Quaternary)
MLY	-150.7440	65.0304	282	2824	796	-	2633	A	Flysch and quartzite Kandik Group and equivalent (Lower Cretaceous Albian to Valanginian)
MPEN	-150.4820	60.7351	168	1677	293	-	1028	C	Unconsolidated surficial deposits undivided (Quaternary)
N20K	-152.2090	61.2001	227	2270	900	-	1826	A	Granodiorite to quartz monzodiorite (Tertiary Paleocene or Late Cretaceous Maastrichtian)
N31M	-135.7800	61.4862	180	1804	-	-	1100	-	-
NANC	-150.0290	61.6954	45	451	361	-	376	C	Unconsolidated surficial deposits undivided (Quaternary)
NCT	-152.9290	60.5621	218	2178	900	-	1633	A	Trondhjemite (Jurassic)
NEA	-149.0710	64.5922	217	2169	900	-	1608	A	Quartzite and pelitic schist (Devonian and older)
NICH	-143.9690	60.2361	201	2005	479	-	1225	B	Redwood and Poul Creek Formations (Tertiary Miocene to Eocene?)
NNA	-149.0790	64.5797	295	2952	799	-	2826	A	Quartzite and pelitic schist (Devonian and older)
NOTK	-162.9710	67.5795	183	1830	267	-	1115	C	Unconsolidated surficial deposits undivided (Quaternary)
NTW3	-141.9330	62.9622	121	1209	284	-	772	C	Unconsolidated surficial deposits undivided (Quaternary)

Site	Latitude	Longitude	z (m)	Mean V_{SZ} (m/s)	Slope V_{S30} (m/s)	Measured V_{S30} (m/s)	*Estimated* V_{S30} (m/s)	NEHRP	Geologic Description
O20K	-152.6240	60.0815	138	1384	900	-	860	A	Naknek Formation and Kotsina Congolomerate (Upper Jurassic Tithonian to Oxfordian)
O22K	-149.7240	60.4814	102	1025	484	-	638	C	Unconsolidated surficial deposits undivided (Quaternary)
O28M	-140.1910	60.7718	230	2305	700	-	1896	C	Unconsolidated surficial deposits undivided (Quaternary)
O29M	-138.5760	60.3024	199	1990	796	-	1208	C	Unconsolidated surficial deposits undivided (Quaternary)
P17K	-156.4390	59.1953	98	981	394	-	607	C	Unconsolidated surficial deposits undivided (Quaternary)
P18K	-155.2290	59.3922	209	2086	524	-	1398	B	Meshik Volcanics and similar rock units (Tertiary Oligocene to Eocene)
P19K	-153.2320	59.6524	263	2633	900	-	2364	A	Naknek Formation and Kotsina Congolomerate (Upper Jurassic Tithonian to Oxfordian)
P23K	-147.4030	59.9979	234	2337	690	-	1968	B	Sedimentary rocks of the Orca Group (Tertiary Eocene to Paleocene)
P30M	-136.9600	60.1218	185	1854	504	-	1129	-	-
PAX	-145.4700	62.9699	240	2404	609	-	2121	-	-
PERI	-147.9530	60.7098	193	1931	581	-	1173	A	Granite and granodiorite (Tertiary Oligocene)
PIC1	-147.4330	65.1173	208	2078	750	-	1379	-	-
PIC3	-147.4330	65.1173	231	2307	750	-	1902	-	-
PIN	-140.2530	60.0959	188	1883	749	-	1145	A	Yakutat Group undivided (Lower Cretaceous and Upper Jurassic?)
PLBC	-136.3660	59.4550	224	2238	877	-	1764	C	Unconsolidated surficial deposits undivided (Quaternary)
PNL	-139.4010	59.6670	198	1977	900	-	1200	A	Me_lange of the Yakutat Group (Cretaceous and Jurassic?)
POKR	-147.4340	65.1171	222	2220	750	-	1731	-	-
PPD	-145.5250	65.5174	313	3130	775	-	4207	A	Quartzite and pelitic schist (Devonian and older)
PPLA	-152.1890	62.8962	198	1983	900	-	1205	-	-
PRB	-148.4460	70.2036	196	1956	230	-	1188	C	Unconsolidated surficial deposits undivided (Quaternary)
PS1A	-161.7440	55.4201	139	1388	499	-	862	C	Youngest volcanic rocks (Quaternary and latest Tertiary?)
PTPK	-142.4670	61.1870	196	1962	640	-	1191	A	Matanuska Formation and correlative rocks (Upper Cretaceous to upper Lower Cretaceous)
PVW	-150.8040	62.5277	261	2611	810	-	2334	A	Flysch (Upper and Lower? Cretaceous)
PWL	-148.3330	60.8584	258	2582	714	-	2302	A	Chugach flysch (Upper Cretaceous)

Site	Latitude	Longitude	z (m)	Mean V_{SZ} (m/s)	Slope V_{S30} (m/s)	Measured V_{S30} (m/s)	*Estimated* V_{S30} (m/s)	NEHRP	Geologic Description
Q17K	-155.8870	58.2637	243	2425	900	-	2143	A	Jurassic phase Alaska-Aleutian Range batholith undifferentiated (Jurassic)
Q18K	-155.0090	58.6484	254	2538	900	-	2257	A	Naknek Formation and Kotsina Congolomerate (Upper Jurassic Tithonian to Oxfordian)
Q23K	-146.3400	59.4296	143	1426	422	-	882	C	Yakataga and Tugidak Formations (Quaternary and uppermost Tertiary)
R17K	-156.3870	57.6397	206	2055	531	-	1330	A	Naknek Formation and Kotsina Congolomerate (Upper Jurassic Tithonian to Oxfordian)
R18K	-154.4520	57.5665	249	2489	645	-	2207	C	Unconsolidated surficial deposits undivided (Quaternary)
R32K	-134.5180	58.2747	290	2901	-	-	2748	A	Volcanic rocks of the Gravina-Nutzotin belt (Lower Cretaceous or Upper Jurassic?)
RAG	-144.6770	60.3863	172	1720	900	-	1053	B	Sedimentary rocks of the Orca Group (Tertiary Eocene to Paleocene)
RC01	-149.7390	61.0889	211	2106	509	-	1446	A	McHugh and Uyak Complexes (Late Cretaceous)
RDJH	-152.8060	60.5905	136	1358	866	-	847	-	-
RDOG	-162.9080	68.0541	217	2174	702	-	1620	-	-
RDT	-152.4080	60.5726	236	2358	641	-	2016	A	Jurassic phase Alaska-Aleutian Range batholith undifferentiated (Jurassic)
RDWB	-152.8420	60.4875	212	2119	900	-	1476	-	-
RED	-152.7740	60.4196	216	2163	734	-	1590	A	Jurassic phase Alaska-Aleutian Range batholith undifferentiated (Jurassic)
RIDG	-144.8460	63.7399	252	2517	900	-	2236	ABC	BBBBB
RKAV	-141.3480	60.2994	216	2156	788	-	1572	B	Hypabyssal intrusions (Tertiary)
RND	-148.8600	63.4056	217	2169	900	-	1606	A	Alaska Range melange (Cretaceous)
S14K	-159.5530	56.2848	203	2031	438	-	1277	C	Youngest volcanic rocks (Quaternary and latest Tertiary?)
S31K	-136.2320	57.9616	220	2205	600	-	1702	-	-
SAG	-148.6940	69.4240	198	1975	501	-	1200	B	Sagavanirktok Formation (Tertiary Miocene to Paleocene)
SAMH	-140.7830	60.1294	176	1758	900	-	1074	-	-
SAN	-149.4770	63.7231	129	1292	900	-	813	C	Unconsolidated surficial deposits undivided (Quaternary)
SAW	-148.3320	61.8070	175	1753	451	-	1071	B	Hypabyssal intrusions (Tertiary)
SBL	-150.2000	63.4686	170	1703	647	-	1043	C	Unconsolidated surficial deposits undivided (Quaternary)

Site	Latitude	Longitude	z (m)	Mean V_{SZ} (m/s)	Slope V_{S30} (m/s)	Measured V_{S30} (m/s)	*Estimated* V_{S30} (m/s)	NEHRP	Geologic Description
SCM	-147.3290	61.8320	203	2028	216	-	1272	B	Felsic hypabyssal intrusions (Tertiary Eocene)
SCRK	-143.9900	63.9761	272	2722	862	-	2486	A	Plutonic rocks and dikes granite to diorite (Cretaceous?)
SGA	-145.2080	60.5341	186	1865	900	-	1134	A	Granitic rocks (Tertiary early Oligocene and Eocene)
SII	-154.1840	56.5593	157	1575	590	-	970	B	Sitkalidak Formation (Tertiary Oligocene to Eocene)
SIT	-135.3240	57.0569	249	2490	-	-	2209	C	Unconsolidated surficial deposits undivided (Quaternary)
SKN	-151.5320	61.9800	228	2276	900	-	1837	A	Volcanic rocks undivided (Cretaceous)
SPCG	-152.0230	61.2913	179	1790	900	-	1092	A	Undivided granitic rocks (Tertiary late Paleocene)
SPCN	-152.1850	61.2244	122	1222	778	-	779	C	Youngest volcanic rocks (Quaternary and latest Tertiary?)
SPCP	-152.1550	61.2655	172	1718	900	-	1052	C	Youngest volcanic rocks (Quaternary and latest Tertiary?)
SPIA	-170.2480	57.1766	223	2229	-	-	1748	C	Youngest volcanic rocks (Quaternary and latest Tertiary?)
SPNN	-152.7010	61.3662	210	2101	900	-	1433	C	Unconsolidated surficial deposits undivided (Quaternary)
SPU	-152.0570	61.1811	202	2024	900	-	1262	A	Granodiorite to quartz monzodiorite (Tertiary Paleocene or Late Cretaceous Maastrichtian)
SSN	-150.7470	61.4636	154	1538	900	-	946	C	Unconsolidated surficial deposits undivided (Quaternary)
SSP	-142.8390	60.1791	177	1768	900	-	1079	C	Yakataga and Tugidak Formations (Quaternary and uppermost Tertiary)
STLK	-151.8350	61.4982	255	2548	516	-	2267	A	Volcanic rocks undivided (Cretaceous)
SUCK	-143.7790	60.0720	224	2236	757	-	1760	B	Redwood and Poul Creek Formations (Tertiary Miocene to Eocene?)
SVW2	-155.6220	61.1082	179	1795	778	-	1095	A	Nearshore facies (Kuskokwim Group) (Upper Cretaceous Santonian to Cenomanian)
SWD	-149.4530	60.1043	228	2279	900	-	1843	A	Chugach flysch (Upper Cretaceous)
TABL	-141.1440	60.4399	216	2160	566	-	1582	-	-
TCOL	-147.8620	64.8735	123	1230	454	-	783	C	Unconsolidated surficial deposits undivided (Quaternary)
TFS	-149.5900	68.6274	208	2079	378	-	1382	C	Unconsolidated surficial deposits undivided (Quaternary)
THY	-145.7580	63.4159	172	1720	258	-	1053	C	Unconsolidated surficial deposits undivided (Quaternary)

Site	Latitude	Longitude	z (m)	Mean V_{SZ} (m/s)	Slope V_{S30} (m/s)	Measured V_{S30} (m/s)	*Estimated* V_{S30} (m/s)	NEHRP	Geologic Description
TIDE	-139.5460	59.9722	178	1781	600	-	1087	A	Yakutat Group undivided (Lower Cretaceous and Upper Jurassic?)
TNA	-167.9270	65.5598	270	2698	-	-	2453	B	Kogruk Formation (Upper Mississippian)
TOK3	-144.7980	62.5239	67	674	510	-	476	C	Unconsolidated surficial deposits undivided (Quaternary)
TOLK	-149.5720	68.6408	186	1856	365	-	1129	C	Unconsolidated surficial deposits undivided (Quaternary)
TRF	-150.2890	63.4501	188	1879	900	-	1143	B	Tatina River volcanics of Bundtzen and others (1997a) and similar mafic volcanic rocks (Jurassic and Triassic)
TUPA	-149.1870	60.8045	296	2957	900	-	2834	A	Chugach flysch (Upper Cretaceous)
UCM	-148.8860	63.9112	158	1583	443	-	975	-	-
VRDI	-143.4540	61.2275	277	2769	650	-	2554	A	Strelna Metamorphics and related rocks (early Permian to Middle Pennsylvanian)
WACK	-144.3310	61.9858	223	2234	900	-	1756	C	Youngest volcanic rocks (Quaternary and latest Tertiary?)
WAT1	-148.5510	62.8295	240	2399	415	-	2115	C	Unconsolidated surficial deposits undivided (Quaternary)
WAT2	-148.5850	62.9628	227	2271	542	-	1828	A	Undivided granitic rocks (Tertiary late Paleocene)
WAT3	-148.5380	62.6812	266	2664	900	-	2407	A	-
WAT4	-147.9420	62.8349	241	2414	871	-	2132	A	Strelna Metamorphics and related rocks (early Permian to Middle Pennsylvanian)
WAT5	-148.2290	63.0624	257	2569	569	-	2288	A	Granitic rocks (Tertiary early Oligocene and Eocene)
WAT6	-147.7400	62.5808	287	2875	827	-	2708	A	Trondhjemite (Jurassic)
WAT7	-148.8480	62.8331	248	2478	662	-	2197	A	Gneissose granitic rocks (Tertiary or Late Cretaceous)
WAX	-142.8530	60.4480	182	1822	621	-	1110	B	Kulthieth Formation (Tertiary Eocene)
WAZA	-144.1540	62.0746	150	1495	900	-	920	-	-
WHY	-134.8830	60.6597	293	2926	-	-	2786	-	-
WON	-150.8540	63.4621	254	2539	352	-	2258	C	Unconsolidated surficial deposits undivided (Quaternary)
WRAK	-132.3470	56.4191	208	2083	-	-	1391	C	Unconsolidated surficial deposits undivided (Quaternary)
WRH	-148.0920	64.4716	241	2415	543	-	2132	A	Peridotite of dismembered ophiolite of the Yukon-Tanana region (Mesozoic Triassic? or older)
YAH	-141.7510	60.3583	212	2119	900	-	1478	B	Kulthieth Formation (Tertiary Eocene)
YAN	-148.7750	63.6559	229	2287	510	-	1859	B	Cantwell Formation volcanic rocks subunit (Tertiary Paleocene)

Site	Latitude	Longitude	z (m)	Mean V_{SZ} (m/s)	Slope V_{S30} (m/s)	Measured V_{S30} (m/s)	*Estimated* V_{S30} (m/s)	NEHRP	Geologic Description
YAN2	-148.7730	63.6564	189	1888	510	-	1148	B	Cantwell Formation volcanic rocks subunit (Tertiary Paleocene)
YUK4	-138.5460	61.4348	260	2600	900	-	2320	-	-

Appendix B

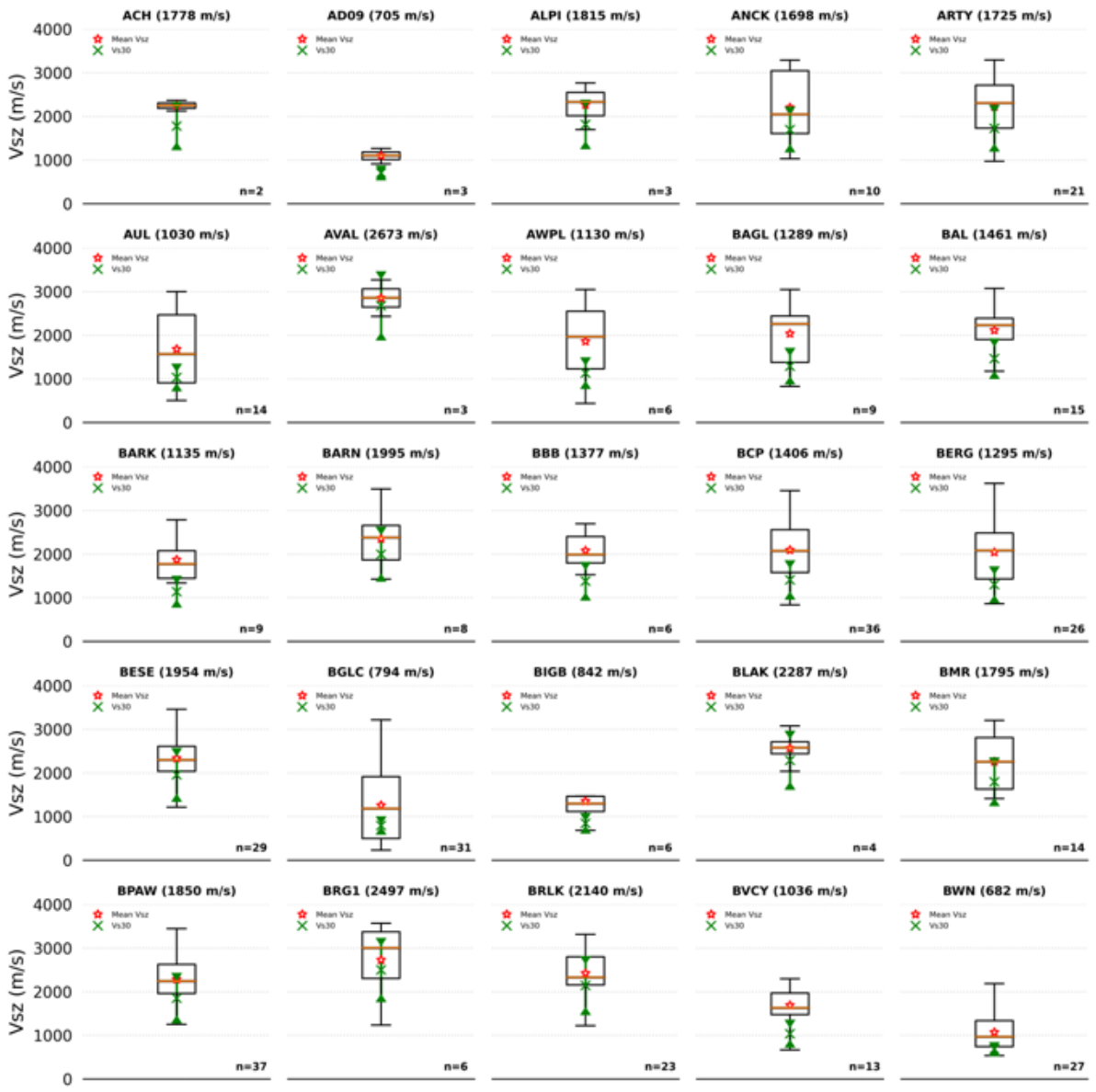

Figure B-1. V_{SZ} results for the recording sites. For each site the box extends from the lower to upper quartile values of the data, with the orange line depicting the median. The whiskers extend from the box to show the range of the data. The mean value is shown with the red star. The mean and the +/- 1 standard deviation values of the estimated V_{S30} are shown with the green x and arrows. The mean value is also listed in the parenthesis next to the station name. The measured V_{S30} values, for those sites that is available, are shown with the open circles.

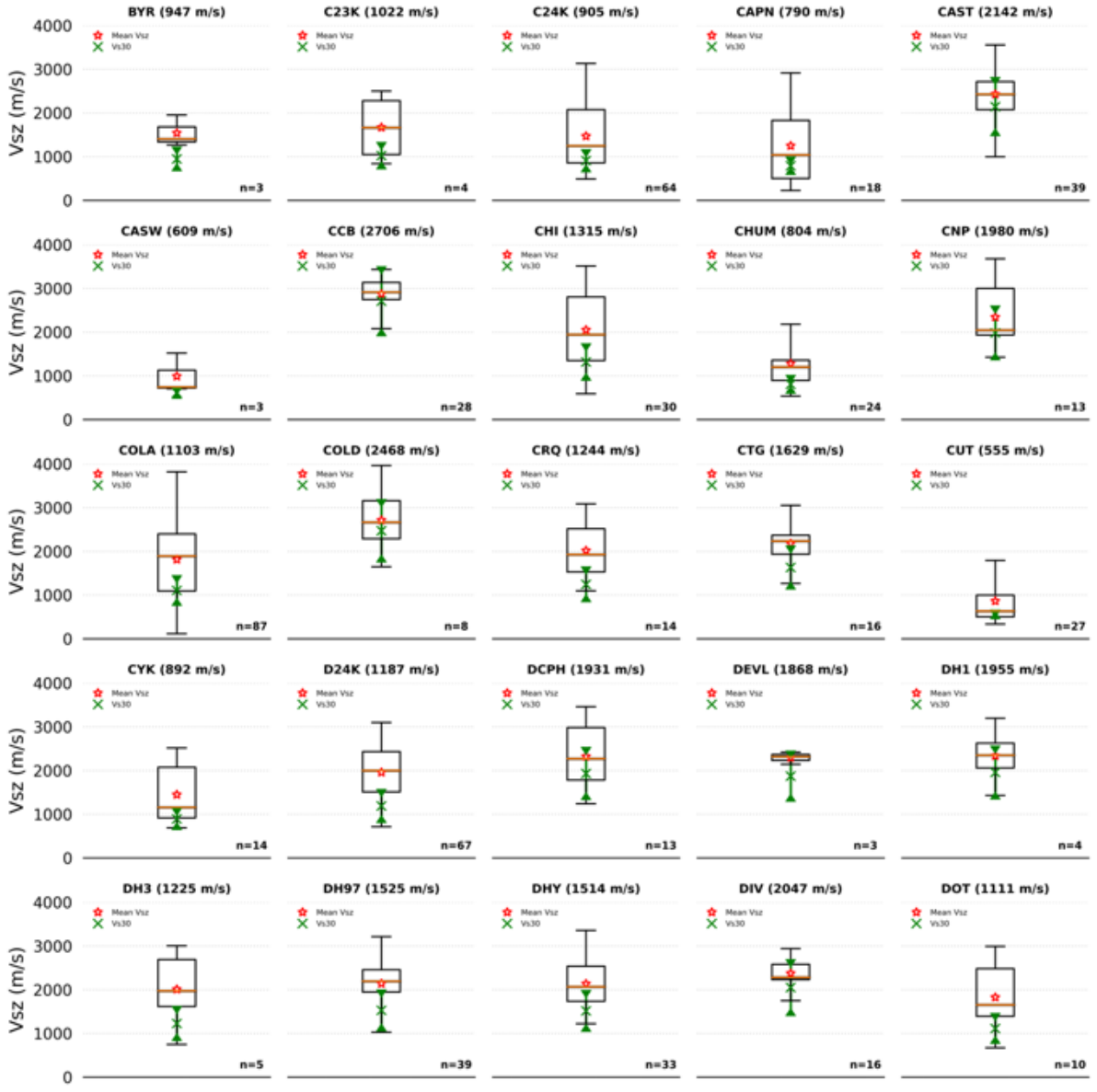

Figure B-1. Continued

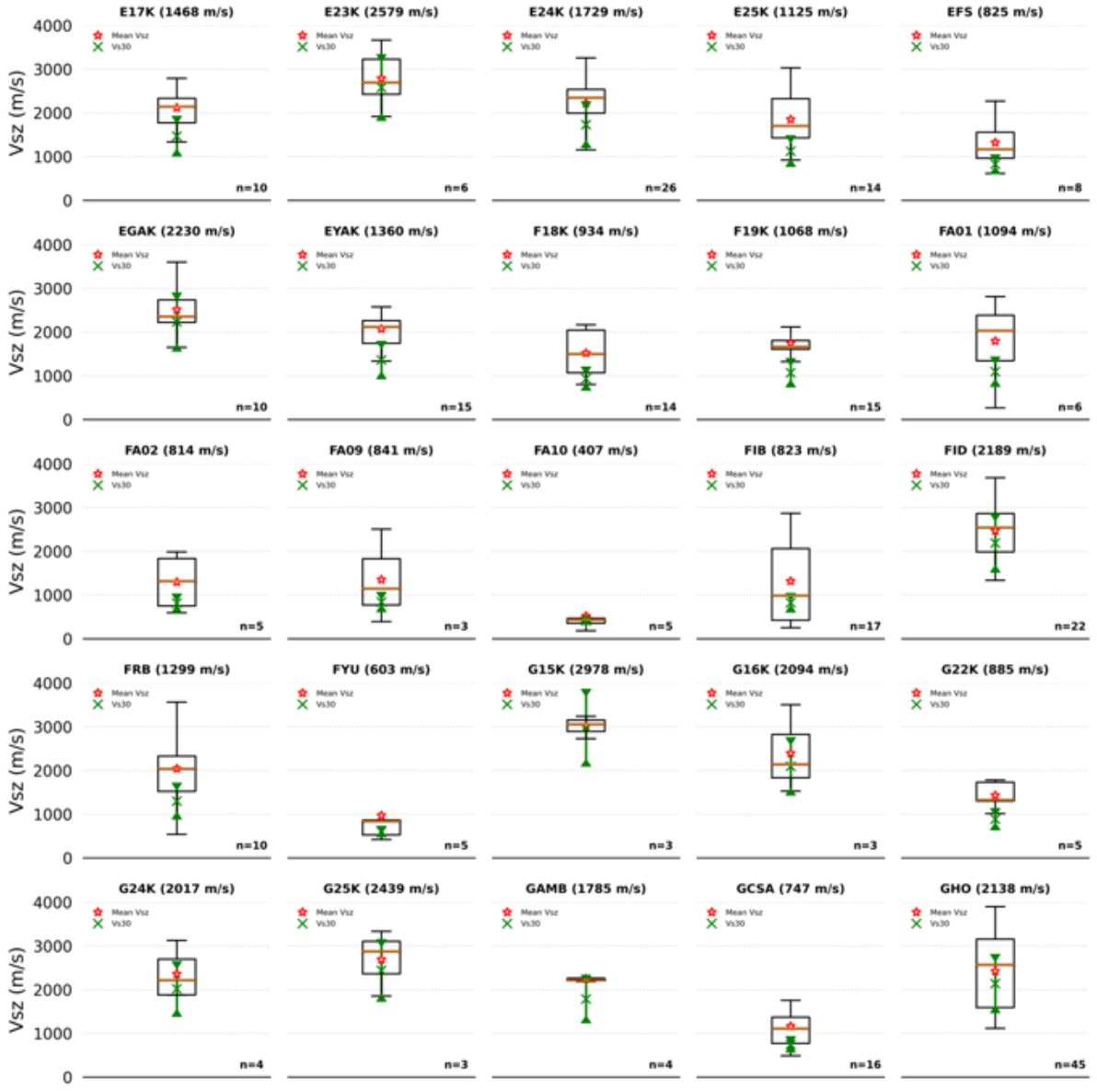

Figure B-1. Continued

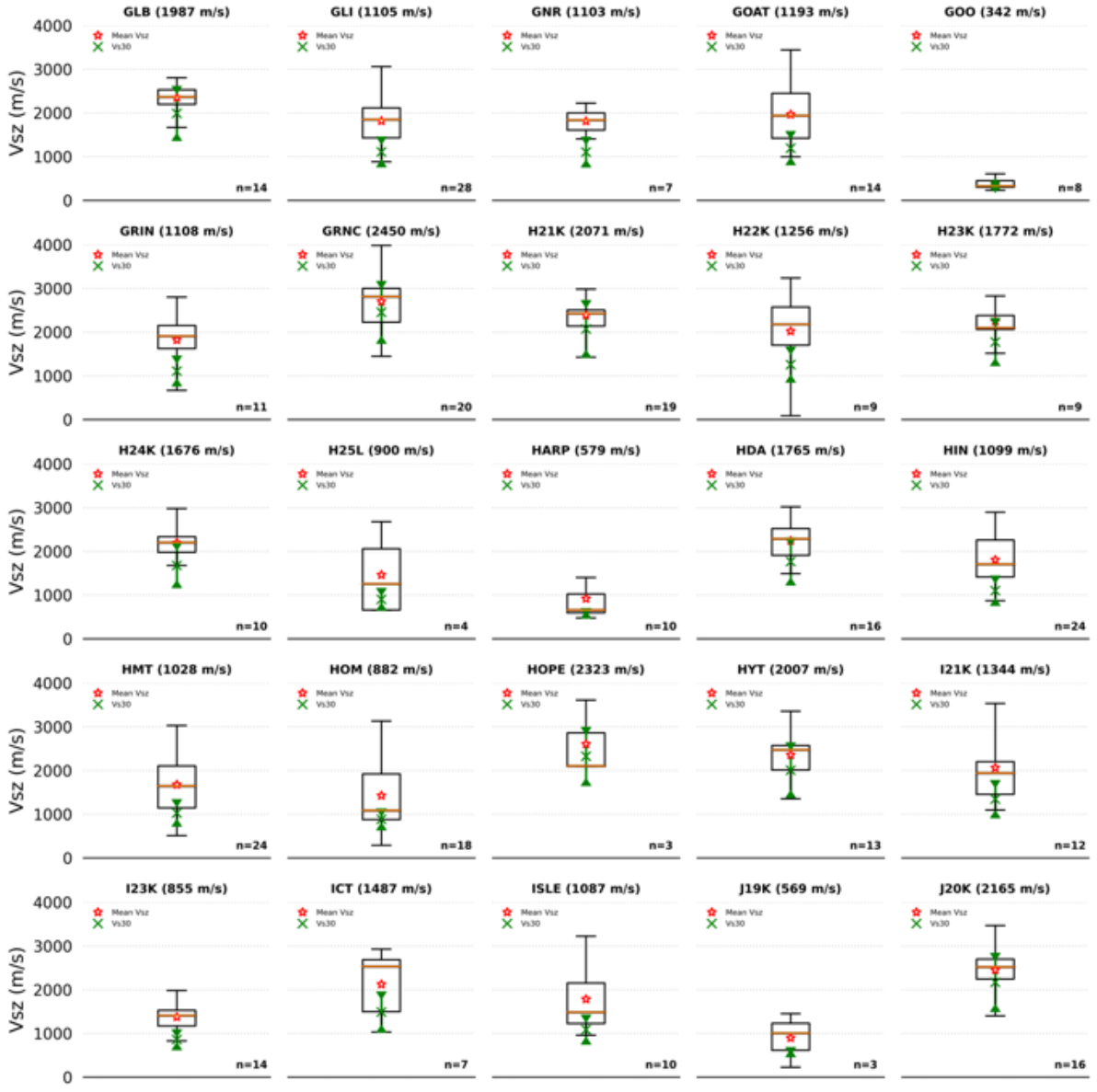

Figure B-1. Continued

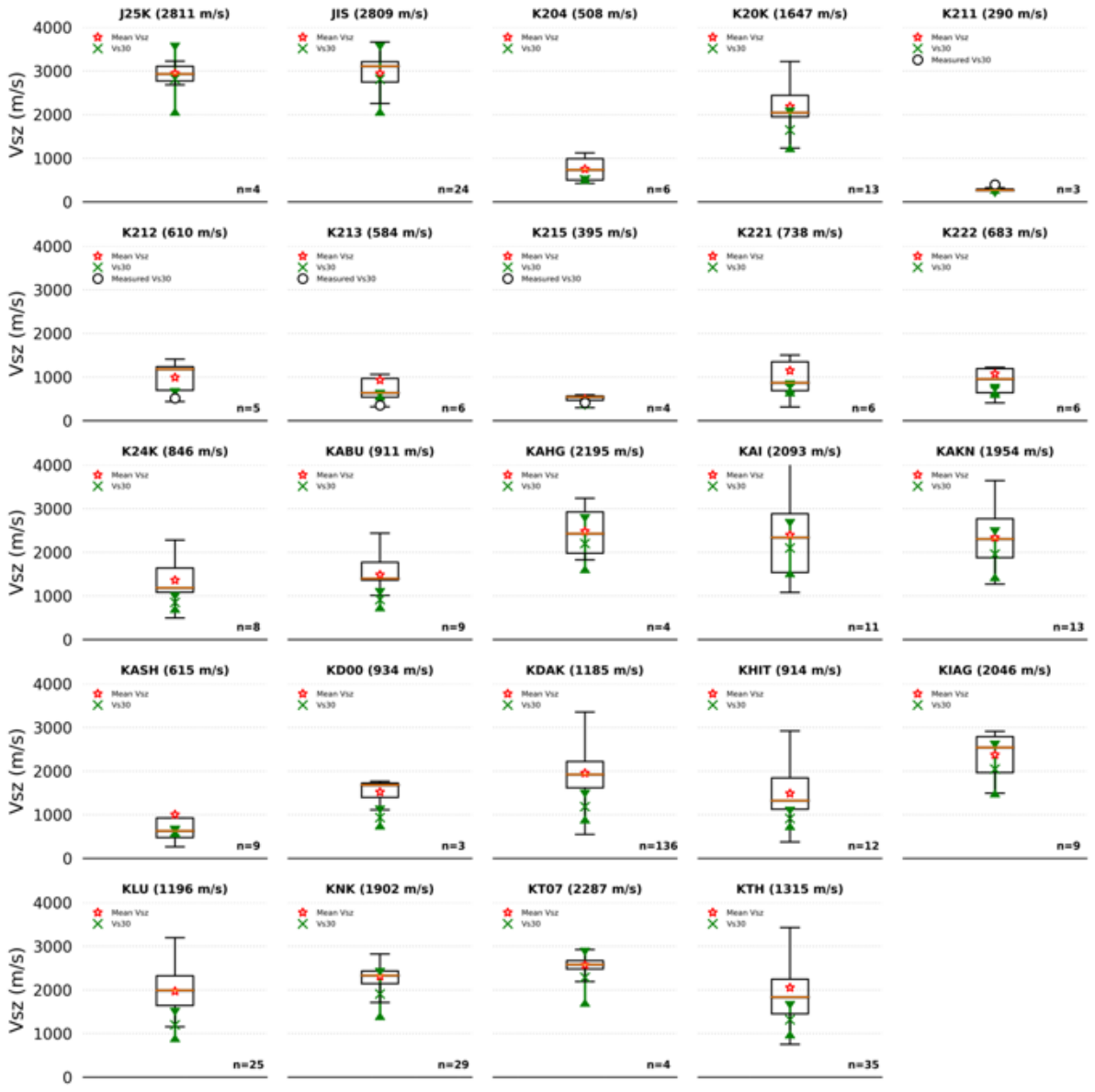

Figure B-1. Continued

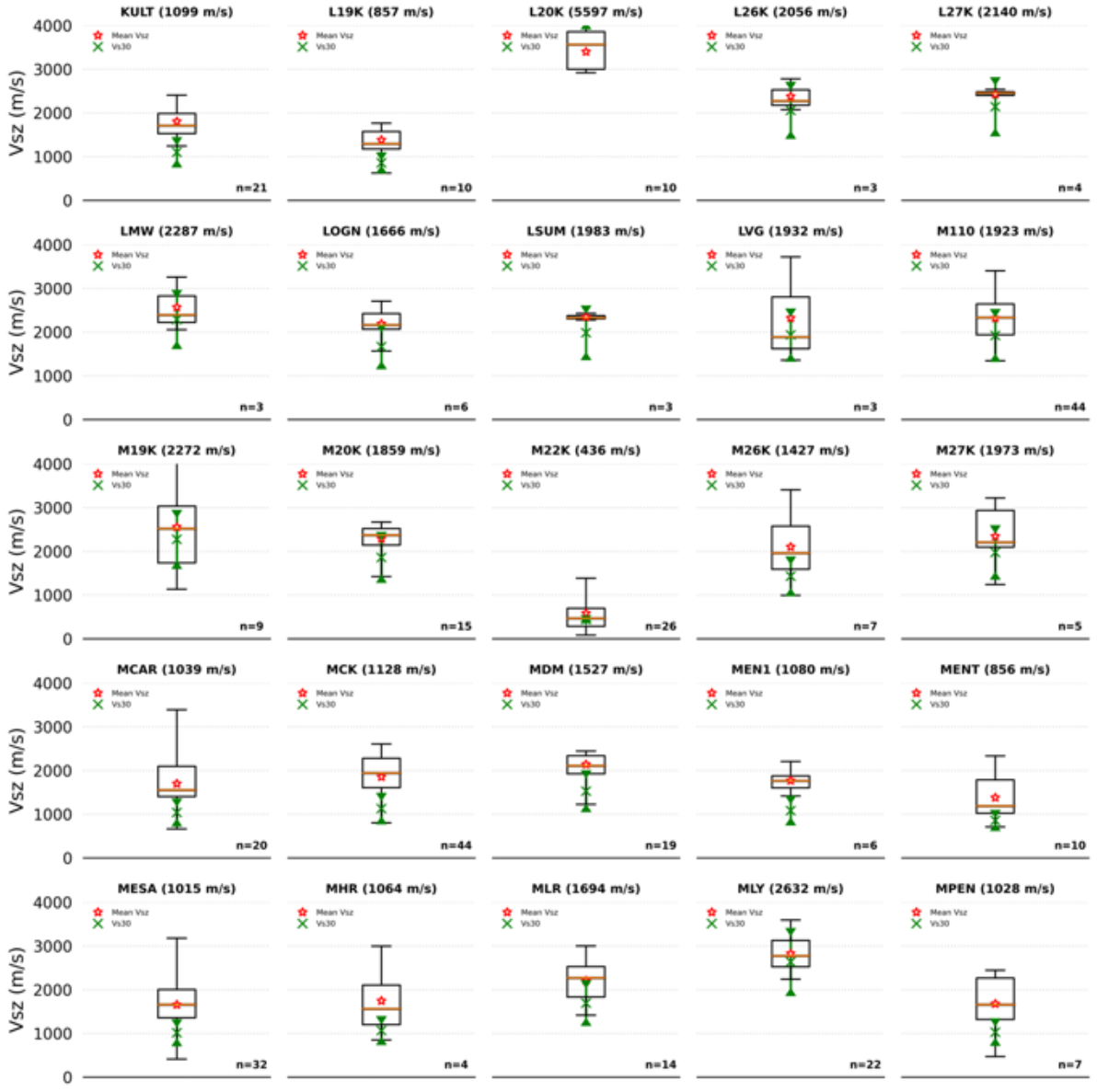

Figure B-1. Continued

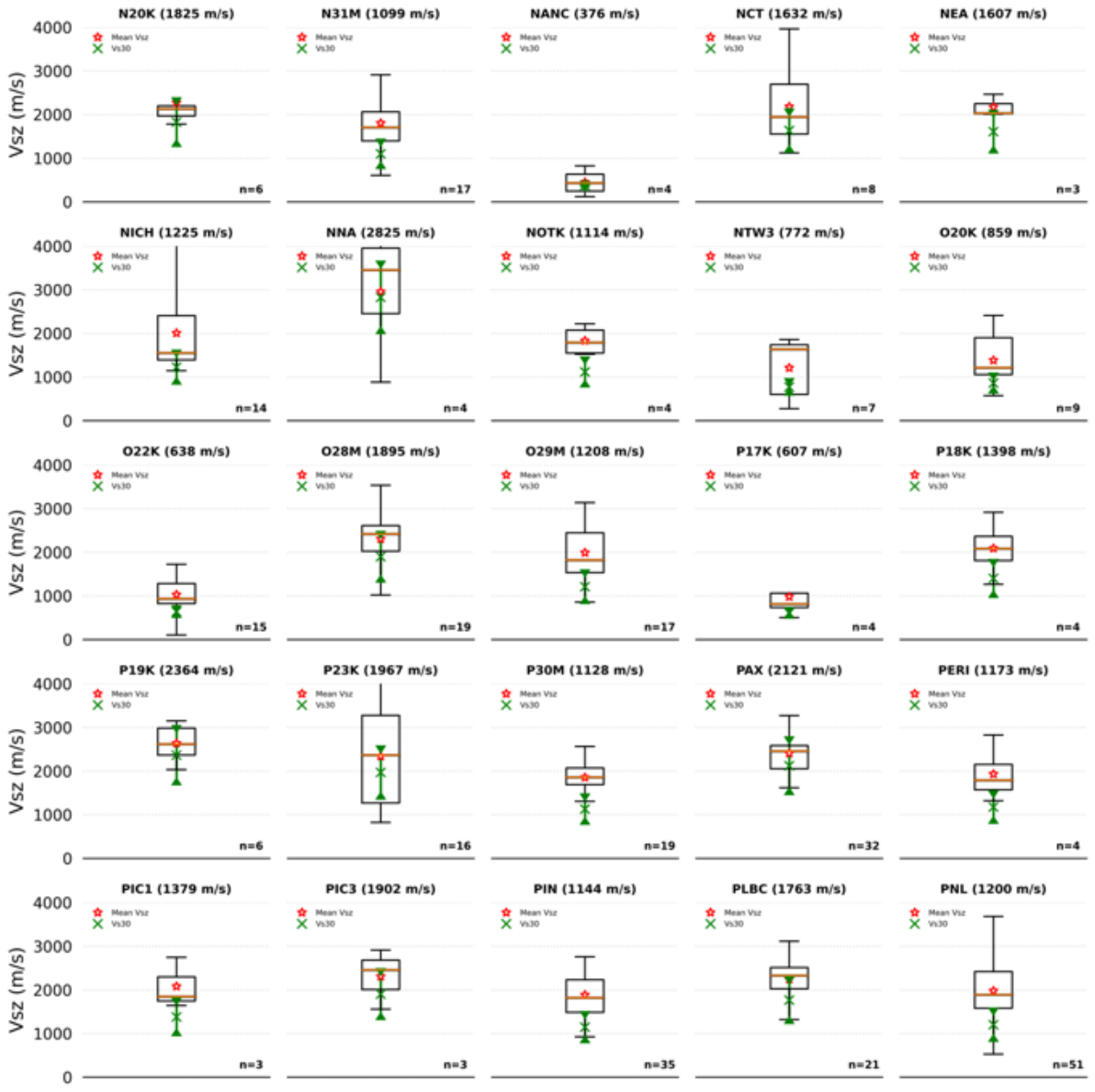

Figure B-1. Continued

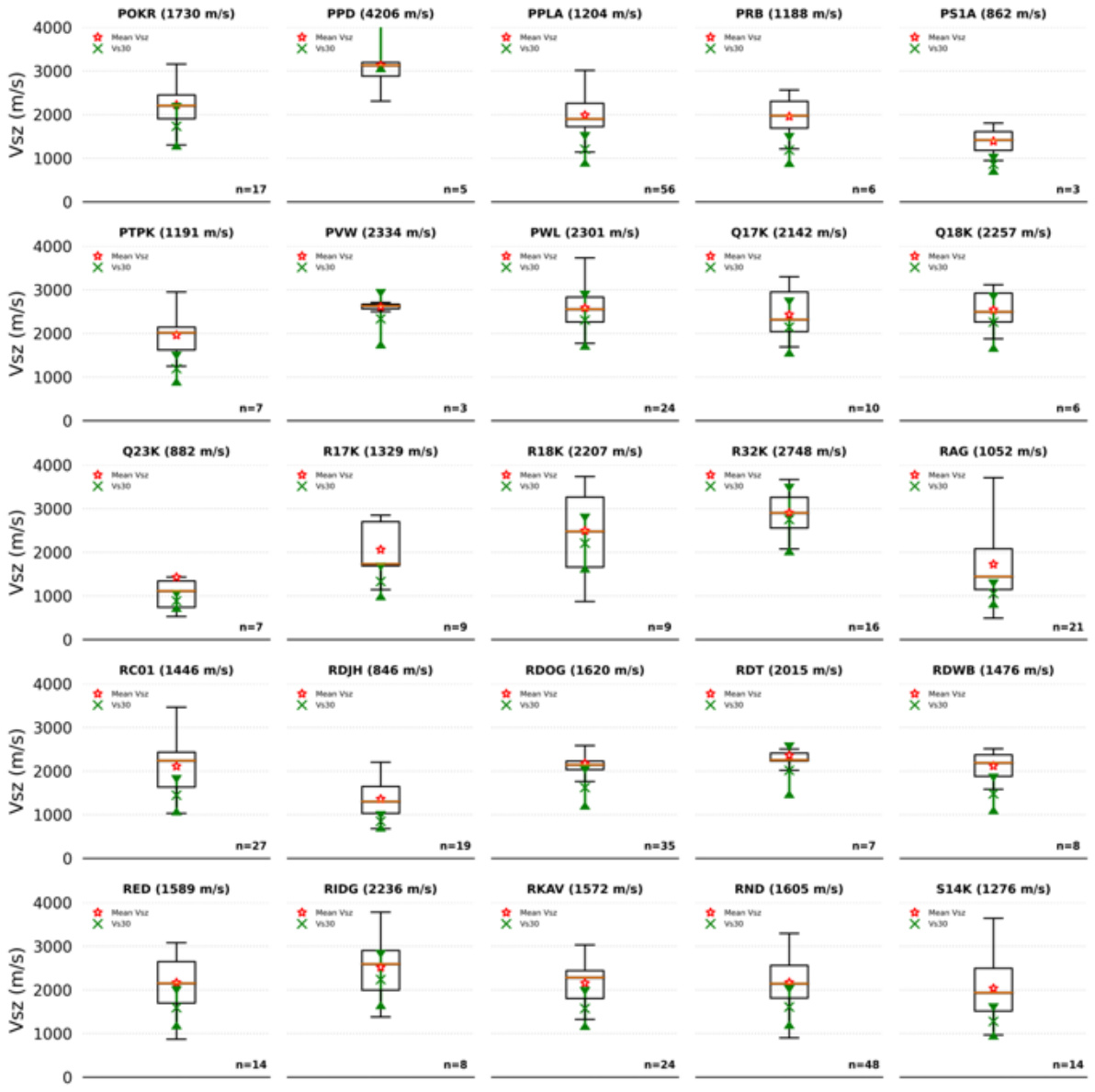

Figure B-1. Continued

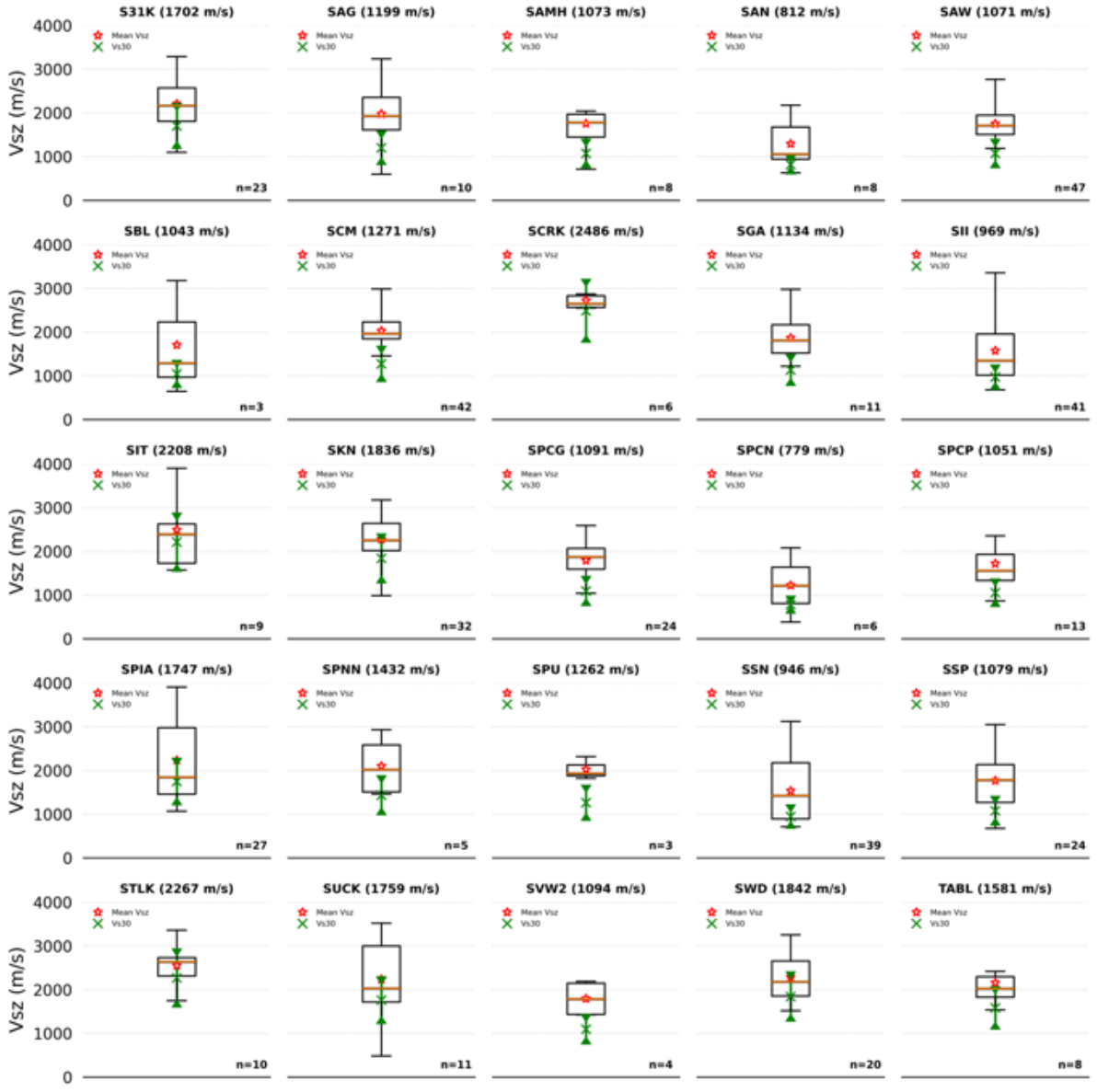

Figure B-1. Continued

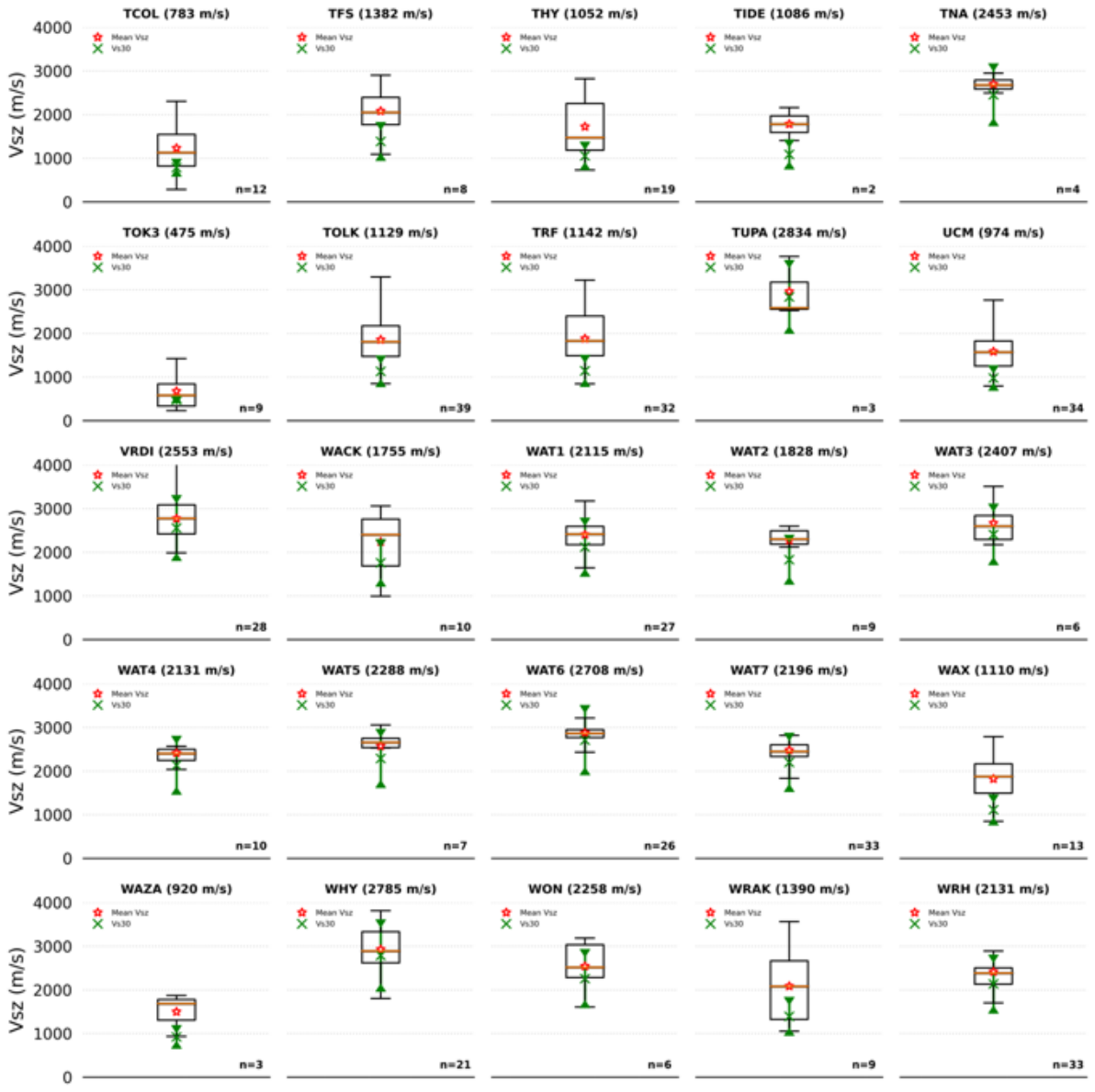

Figure B-1. Continued

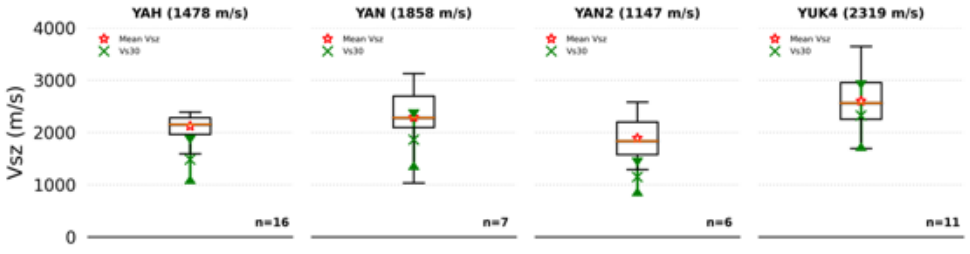

Figure B-1. Continued

FINAL TECHNICAL REPORT

Andreas Skarlatoudis
Seismologist
T: 213.996.2313
E: andreas.skarlatoudis@aecom.com

AECOM
One California Plaza
300 South Grand Avenue
Los Angeles, CA 90071

T: +1 (213) 593 8100
F: +1 (213) 593 8178
www.aecom.com